GEORGIA INSTITUTE OF TECHNOLOGY — OFFICE OF CONTRACT ADMINISTRATION

# PROJECT ADMINISTRATION DATA SHEET

[x] ORIGINAL [ ] REVISION NO. _____

Project No. E-25-694 , GTRI/~~GTI~~ DATE 7 /12 / 84

Project Director: Dr. Winer School/~~XXX~~ Mechanical Engineering

Sponsor: Torrington Company

Type Agreement: Standard Research Agreement dated 7/3/84

Award Period: From 7/1/84 To 12/31/84 (Performance) 12/31/84 (Reports)

| Sponsor Amount: | This Change | Total to Date |
|---|---|---|
| Estimated: | $ 50,000 | $ 50,000 |
| Funded: | $ 50,000 | $ 50,000 |

Cost Sharing Amount: $ _____ Cost Sharing No: _____

Title: Investigation of Roller Follower Skidding on Automotive Camshafts

ADMINISTRATIVE DATA — OCA Contact Brian J. Lindberg x-4820

1) Sponsor Technical Contact:

Dr. Michael J. Hartnett
The Torrington Company
59 Field Street
Torrington, Connecticut 06790
(203) 482-9511

2) Sponsor Admin/Contractual Matters:

Frank S. Troidl
Senior Patent Attorney
Ingersoll-Rand Company
P. O. Box 301
Princeton, N. J. 08540
(609) 921-9103

Defense Priority Rating: N/A — Military Security Classification: N/A

(or) Company/Industrial Proprietary: See Articles 11-14

RESTRICTIONS

See Attached N/A Supplemental Information Sheet for Additional Requirements.

Travel: Foreign travel must have prior approval – Contact OCA in each case. Domestic travel requires sponsor approval where total will exceed greater of $500 or 125% of approved proposal budget category.

Equipment: Title vests with Sponsor

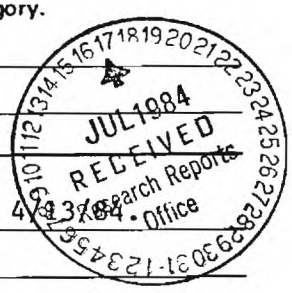


COMMENTS:

Advanced payment of $12,500 received by check No. 2-209839 dated 4/13/84.

Sponsor I.D. #02.219.000.84.003

COPIES TO:

Project Director
Research Administrative Network
Research Property Management
Accounting
Procurement/EES Supply Services
Research Security Services
Reports Coordinator (OCA)
Research Communications (2)
GTRI
Library
Project File
Other I. Newton

FORM OCA 4:383

)RGIA INSTITUTE OF TECHNOLOGY OFFICE OF CONTRACT ADMINISTRATION

## SPONSORED PROJECT TERMINATION/CLOSEOUT SHEET

Date 3/26/86

ct No. E-25-694 School ~~XXXX~~ ME

ides Subproject No.(s)

ct Director(s) Dr. Ward Winer GTRC / ~~XXX~~

sor Torrington Company

Investigation of Roller Follower Skidding on Automotive Camshafts

ctive Completion Date: 12/31/84 (Performance) 12/31/84 (Reports)

t/Contract Closeout Actions Remaining:

- [ ] None
- [X] Final Invoice or Final Fiscal Report
- [ ] Closing Documents
- [ ] Final Report of Inventions
- [ ] Govt. Property Inventory & Related Certificate
- [ ] Classified Material Certificate
- [ ] Other

inues Project No. Continued by Project No.

ES TO:

ct Director
arch Administrative Network
arch Property Management
unting
urement/GTRI Supply Services
arch Security Services
orts Coordinator (OCA)
l Services

Library
GTRC
Research Communications (2)
Project File
Other R. Embry

A. Jones

M. Heyser

M OCA 69.285

SECOND PHASE REPORT

# INVESTIGATION OF ROLLER FOLLOWER SKIDDING ON AUTOMOTIVE CAMSHAFTS

Prepared by
SCOTT BAIR
Senior Research Engineer

WARD O. WINER
Regents' Professor

Prepared for
THE TORRINGTON COMPANY
59 Field Street
Torrington, Connecticut 06790

December 1985

**GEORGIA INSTITUTE OF TECHNOLOGY**
**A UNIT OF THE UNIVERSITY SYSTEM OF GEORGIA**
**SCHOOL OF MECHANICAL ENGINEERING**
**ATLANTA, GEORGIA 30332**

1986

# Investigation of Roller Follower Skidding on Automotive Camshafts

## Second Phase Report

S. Bair
Senior Research Engineer

W. O. Winer
Regents' Professor

Co-principal Investigators

The Torrington Company
59 Field Street
Torrington, Connecticut 06790

December 1985

## INTRODUCTION

To reduce mechanical losses in automotive engines and thereby improve fuel economy the conventional flat tappet is being replaced by a roller tappet in which a roller follower is supported by a needle bearing. Engine tests have demonstrated that roller surface finish can affect the resistance to roller surface distress in an engine operating at high speed (5300 rpm crankshaft). It was suspected that skidding of the roller against the cam may be responsible. To investigate the role of surface finish in roller/cam skidding, a Tappet Roller Skid Test Machine was constructed and experiments were performed with two surface finishes in the first phase (Ref. [1]) of this program. In that phase, the roller rotational velocity was determined by observing the passage of grooves on the roller side chamfer. Initially, the cam rotational velocity was assumed constant as found from the time between lift profiles. Separate measurements of cam rotational velocity were used to correct the data suggesting that the cam velocity be measured concurrently with that of the roller for the second phase.

## EQUIPMENT

### Apparatus

A Tappet Roller Skid Test Machine (Figure 1) was constructed by the Torrington Company for this program from a previous design (Ref. [2]) by the Georgia Tech Tribology and Rheology Research Laboratory. The device (Torrington Drawing #1915) simulates the tribological contact between the tappet roller and cam in an automotive engine. Features

include the measurement of three components of force at the contact, the lift, and the roller follower rotational velocity. A sixty tooth gear was added to the cam shaft and a bracket was attached to the flex frame to accommodate an optical probe for detecting the passage of the gear teeth. The number of roller grooves was increased from 30 to 60 for the second phase.

The contact position is maintained at a nearly constant elevation by allowing the cam to move vertically through the lift curve. This is accomplished by mounting the cam on bearings in one end of a flexible frame. The frame forms two identical four bar linkages which move the cam through a 100 mm radius arc. This circular motion produces a lateral displacement of 40 $\mu$m from the vertical. The cam is driven in rotation by a pair of roller chains whose sprockets are at 100 mm centers, providing a constant chain length through the arc. The chains are located at either side of the cam between the frame flex points.

The roller tappet is retained in a measurement frame containing three piezoelectric force transducers to measure the vertical contact force, the contact force parallel to the cam axis and, the force orthogonal to the previous two. The frame design minimizes mechanical coupling of the three force measurements. The frame can accommodate up to $\pm$ 8 degrees of skew of the roller axis with respect to the cam axis. However, edge loading of the roller occurs at less than 8 degrees of skew.

The automotive valve spring rate is simulated by three compression springs of 131 kN/m combined rate pushing against the bottom of the end of the flexible frame which holds the cam. A stop on the primary spring assembly limits this spring extension (at 400 N) to prevent the primary spring from loading the base circle of the cam. The two smaller loading springs apply an adjustable force during the cam dwell and simulate the base circle load due to the oil pressure supplied to the inside of the automotive lifter. (Each turn of the adjusting screw is equivalent to 7 psi [50 kPa] oil pressure.) Nominal zero clearance on the base circle is provided by a hydraulic lash adjuster taken from an automotive hydraulic lifter in series with and between the primary loading spring and the simulator housing. The effective reciprocating mass is 0.531 kg which is approximately equivalent to the reciprocating mass in a Pontiac L4 engine. The effective mass of the moving end of the flexible frame was determined from its stiffness and natural frequency.

An oil reservoir of 1.5 liter capacity is located in the bottom of the housing which is heated by two 200 W cartridge heaters. An oil drain is provided. A oil slinger in the reservoir simulates oil sling from an engine crankshaft. Commercial 10W-30 motor oil was used.

The simulator is driven by a 750 W gear motor with variable speed drive. A thermocouple measures bulk oil temperature and an LVDT measures displacement (lift) of the cam relative to the roller support. All instrumentation was provided by Georgia Tech.

Rollers were supplied by Torrington and are characterized in Table I. They are designated in the tests as R and S for rough and smooth, respectively.

**Instrumentation**

A Gould Waveform Recorder, Operating System, Plotter, and Interface were acquired during the second phase and used to sample all data. The recorder samples up to eight channels concurrently, eliminating the time skew present with the two recorders that were used in Phase I.

Charge signals from the three piezoelectric force transducers were conditioned by three Kistler charge amplifiers whose voltage outputs were sampled at the same time, the LVDT lift signal and velocity waveforms were being sampled. A 1.1 ms delay was found to occur between a motion of the LVDT core and output from the LVDT signal conditioner. This delay has been accounted for in the software.

Two MTI Fotonic Sensors with fiber optic probes were used to record the passage of notches on the specimen roller and, concurrently, the passage of gear teeth on the shaft holding the cam. Outputs from the Fotonic Sensor and the lift LVDT and force signals were sampled by the Gould Waveform Recorder at 20 kHz or 50 kHz sample rate depending on cam speed to be transferred later by an IEE 488 interface to the IBM PC. An analog filter was not used between transducers and the recorder as it was found to change the phase relationship between signals.

## EXPERIMENTAL PROCEDURE

Lateral force transducers, for $F_x$ and $F_y$, were calibrated in the simulator by applying a known force with a mechanical force guage to the tappet thrust bearing. The normal force transducer, for $F_z$, was calibrated in place by dead weight applied to the lifter thrust bearing. The forces on the lifter $F_x$, $F_y$ and $F_z$ are defined in Figure 2.

The lift measuring LVDT was calibrated apart from the simulator by moving the core with a micrometer while reading output signal.

The relative skew angle is indicated on the scale provided on the apparatus. However, assembly tolerances could produce an error in skew of one or two degrees. For all measurements, zero skew angle was determined by minimizing the amplitude of the roller end thrust $F_y$. Skew is defined in Figure 2.

The same shaft and needle rollers (from Phase I) were used for all tests. The tests of the rough roller were done first.

Prior to a test, the apparatus was brought to temperature for about two hours. About three seconds after the start of rotation the recorder was armed manually. The recorder triggered from the lift channel. All channels recorded 8192 samples which included four to six cam revolutions. The voltage data was transferred to the IBM PC

microcomputer and then the floppy disc using the Gould IOS programs. A summary of test conditions is given in Table II.

## DATA REDUCTION

Several programs were written in Basic for data reduction. The most useful are listed in Table III. The Gould IOS (Instrument Operating System) created a disc file for each channel in which voltages are represented as integers and the time between samples is recorded.

The program, REDUCE, reads the six disc files created by IOS. The waveforms from the velocity probes are analyzed to find the average angular velocity for the cam or roller during one wave cycle. (One cycle of the velocity waveform corresponds to the passage of a tooth or groove.) The waveform is approximately sinusoidal. The cam signal is analyzed first. An estimate is made of the period of the waveform from the cam test rpm. A segment of data for a time span of 1.7 of the estimated period is averaged and the standard deviation found. A level is assigned by adding to the mean the standard deviation multiplied by a factor, FSD. The times at which interpolated values of the waveform first crossed the level in ascending and descending fashions are averaged and this time is saved as a cam angle marker. The data was shifted 40% of the estimated period and the process repeated. These markers represent cam angular displacements of $6^{\circ}$ in this work. The time between markers yields the angular velocity. The roller waveform is analyzed similarly.

From the lift signal, the interpolated times at which peak lift occurred were determined and assigned cam angle equal to zero. From the cam angle markers the times for cam angles $-180^{o}$ to $180^{o}$ in $2^{o}$ steps were assigned and all velocities, lift signal, and force signals were interpolated and averaged at these times. Calibration factors were applied to the lift and force signals. The force transducers are dynamic devices and their zero level cannot easily be determined from a condition prior to the test. The base circle load was calculated from the lifter internal spring rate and the simulated oil pressure acting on the hydraulic lifter piston. The average of the force $F_z$ is set equal to this base circle load for cam angle $-180^{o}$ to $-150^{o}$. Since this load is small (less than 5% of peak load), $F_x$ and $F_y$ are set to average zero on this interval.

In Figure 3 are defined the contact force $F_T$ acting on the cam as well as the force $F_N$ normal to the contact and $F_o$ a component of force normal to a line passing through the contact and the axis of cam rotation. ($F_o$ is used for calculation of cam driving torque.) Also shown are the follower pressure angle $\Phi_f$ and the cam pressure angle $\Phi_c$.

Surface velocities are defined in Figure 4. The kinematics calculations developed in the previous program (Ref. [1]) were applied to yield surface velocities, torque, the contact forces, mechanical losses and cam/roller traction coefficient. These reduced data were written on disc.

The reduced data contains noise at the highest rotation speed. To investigate possible sources of the noise, the measured forces were sampled after striking the side of the test rig. An FFT routine (Ref. [3]) gave the power spectral density function for each force. Peaks were noted for all measured forces near the calculated (Ref. [1]) natural frequency of the primary load spring. A software filter was written using the FFT algorithm to pass only those components of a frequency less than $J_{cut}$ (see Table IV) times the fundamental frequency. The filtered data from the program, FILTER 2, was written on disc with the filename prefixed by "F". Cam lift was not filtered. (Since the FFT requires an integer power of 2 data points, the last (180th) entry was repeated for a total of 256. Therefore, the fundamental frequency was 180/256 x rotational frequency.)

## RESULTS

### Forces and Lift

With the new data acquisition system, lift and forces were measured for each test. Typical curves of lift versus cam angle are presented in Figures 5a and 5b for the lowest and highest cam speeds respectively. It can be noted that as speed increases an overshoot on the lift measurement occurs at the peak lift and at the end of the lift event. To determine whether this overshoot resulted from the instrumentation or was the true displacement of the cam, the LVDT was removed from the simulator. The LVDT core was pushed through the LVDT to impact against a plastic stop. For a velocity of 300 mm/s, no overshoot was observed in the signal. At 1250 mm/s there was overshoot equivalent to 0.5 mm which is in fair agreement with the overshoot noted on the high speed lift curve where the maximum

velocity is about 2000 mm/s. Cam toss should be ruled out as there is a normal contact force on the follower (figure 8c) at even the highest speed.

To investigate the effect of lift signal overshoot on the calculated velocities, the program DATASWAP was utilized. The lift data from a low speed run was inserted in place of the lift data for run R0138. No significant difference in surface velocities could be seen from the plots.

Axial contact force is shown in Figures 6a-6c for the three cam speeds and three skews angles of $0^{o}$, $1.5^{o}$ and $3^{o}$. This is the force between the tire and cam in the direction of the cam axis and is reacted by the needle bearing axial thrust and (when the tire is in contact with the lifter body) the tire thrust force against the inside face of the lifter body. The plots are the average of from four to six cam revolutions. It has been shown, Ref. [4] that the axial force may vary greatly - even change sign - between consecutive cam revolutions at low skew angle. The increase in negative axial force for increasing skew angle is expected from the kinematics.

In Figures 7a-7c are plotted the roller/cam traction forces for three cam speeds. The variation of contact normal force with speed is illustrated by Figures 8a-8c. If traction is divided by normal force the traction coefficient plots of Figures 9a-9c result. The torque required to rotate the cam separate from cam support bearing losses

was calculated from the contact forces and pressure angles and is shown in Figures 10a-10c.

Cam rpm is shown as a function of cam angle in Figures 11a-11c. The low speed (900 rpm) cam rpm agrees well with the intermediate shaft rpm reported in Ref. [1]. However at high speed (2500 rpm) the cam rpm (Figure 11c) has an oscillatory component at the initiation of the dwell period not present on the intermediate shaft rpm. This oscillation may be due to elasticity of the drive chains.

The total cam/roller energy loss was calculated by integrating the cam torque information and is plotted in figure 12 for rough and smooth rollers and oil temperature of 30 $^{o}$C. No effect was obvious from the data for oil temperature or oil pressure. However, the smooth tire produced less mechanical loss per revolution than did the rough version. Since the greatest skidding obtained was 15% of the total rolling distance and usually was much less than that it would be difficult to explain such a large (up to 100%) variation in mechanical loss on the basis of surface texture alone. Internal dimensional differences between rollers and differences in simulator set-up may play a part. The roller tappet losses in Figure 12 display an unusual variation with cam speed in that the loss per revolution is minimized at 1700 rpm but were it not for the data at that speed it would appear that the loss would be monotonically increasing with speed. When one test (R0132) was repeated, the loss was reproduced within 3%.

In addition to the roller tappet data some flat follower data at 100 $^{o}$C from Ref. [2] is shown in Figure 12. The flat follower loss should be slightly reduced at 30 $^{o}$C. There is a rapid rise in loss for both rollers from 1700 to 2400 rpm, at which the loss is greater than that measured earlier in a different rig [2] with flat tappets. The trend is qualitatively in agreement with the engine tests by Staron and Willermet [5] in which above 3000 cam rpm the roller tappet no longer offerred a reduction in loss.

**Surface Velocities**

Surface velocities are reported in Appendix A as plots of roller and cam velocity on the same graph for each of the tests listed in Table II except S0130 and S0133. Here, sliding is represented by the vertical difference between roller and cam velocity curves when there is no skew. The greatest sliding, when present, occurs on the base circle ($-180^{o}$ to $-60^{o}$ and $60^{o}$ to $180^{o}$ cam angle) at low temperature and low oil pressure (an unlikely combination of conditions). Base circle sliding tended to increase with time on the base circle ( as should be expected) for all runs but R0132 where the base circle sliding was reduced at $\pm 180^{o}$ cam angle. A repeat of R0132 showed the same behavior. Eccentricity of the cam base circle could cause this.

The oscillations in cam rotational speed seen in Figure 11c, at the end of the lift event and the beginning of the base circle ($40^{o}$ to $140^{o}$ cam angle) at high speed are reflected in the cam surface velocity for high speed. The roller velocity tends to follow these oscillations well.

The roller surface velocity was subtracted vectorially from the cam velocity to arrive at the sliding velocity plots in Appendix B. Sliding velocity can exceed 1 m/s on the base circle. For tests of skewed elements, a sliding velocity exists even when the surface velocities are of equal magnitude.

Integrating the sliding velocity with respect to time over one revolution yields the difference between cam surface displacement and roller surface displacement per revolution which we call here sliding displacement. A sliding distance could be defined as the time integral of the absolute value of sliding velocity which would yield the total distance that the roller slid on the cam. However, signal noise and time skew would have a significant effect on such a quantity. Filtering was found to have negligible effect on sliding displacement. Sliding displacement was calculated for two intervals: $-180^{o}$ to $180^{o}$ cam angle (one cam revolution) and $-80^{o}$ to $80^{o}$ (loaded regime or lift event).

Under those conditions where sliding was minimized (i.e., low speed, high temperature) a sliding displacement of -0.5 mm was consistently calculated for both total sliding and loaded sliding. (This is 0.4% of the total cam surface displacement of 118 mm per revolution.) Since no plausible physical explanation was found for a negative sliding displacement, it was attributed to a consistent error or bias and was added to the sliding displacements to give relative values. These relative sliding displacements are listed in Table V.

Both total and loaded sliding displacements show the following trends: Increasing oil pressure (i.e., base circle load) and temperature reduce sliding. Since lubricant film thickness decreases with load and temperature this was expected. Increasing skew angle increases sliding due mainly to the misalignment of the roller and cam velocity directions. At high temperature, increasing cam speed increases sliding which can be explained by the increase in film thickness with speed.

At low temperature and low oil pressure sliding on the base circle (total sliding minus loaded sliding) is reduced at the highest cam speed. (There is reduced time available for the roller tire to decelerate.) For 1700 and 2500 cam rpm the smooth roller, S, gave increased or equal sliding compared to R. However, for the lowest speed the trend was reversed. Due to a reduced Lambda ratio (film thickness to composite roughness ratio), the rough roller would always be expected to reduce sliding. The increased mechanical loss (Figure 12), which is probably not related to surface finish, found with roller R may explain this anomaly at low speed.

The instantaneous power dissipated at the cam/tire contact can be obtained from the dot product of the force in the contact plane and the sliding velocity. Representative plots of contact power loss are shown in Figures 13a-c for roller R, high temperature, and low oil pressure. Negative power implies mechanical power generation at the contact which is unlikely so those plotted oscillations that take on

negative values should be regarded as noise. The power peak shown at $55^{o}$ cam angle at high speed appears to be significant and appears on all high speed data with peak values of about 50 to 100 W. However, roller roughness does not affect this peak. The contact power for $3^{o}$ skew is shown in Figure 13d to exhibit a high level (approx. 15W) throughout the loaded cam angles.

## CONCLUSIONS

The minimum sliding was observed between cam and roller follower for conditions of high oil temperature (90 $^{o}$C) and low speed (900 cam rpm) in combination. Sliding decreases with oil temperature and oil pressure. Skew angle increases sliding and the effect of rotational speed is to increase sliding at high temperature.

Reducing the roller follower surface roughness increases sliding at 1700 and 2500 rpm but had the counter effect at 900 cam rpm. The roughness effect was strongest at low temperatures. However, at low temperature the majority of the sliding occurs on the cam base circle where the load is light, oil film is thick and little damage would be expected from the sliding. Sliding which occurs under conditions of high traction (i.e., high load) should be the most damaging to running surfaces. Therefore, contact power dissipation should be an indicator of the severity of sliding related to surface damage. Sustained power dissipation was seen throughout the lift event with skewed elements. However, no trend could be seen in the high speed peak contact power

dissipation with respect to roller roughness. The greatest sliding displacements during the loaded cam angles occurred with skewing of the elements. If sliding produces surface distress, one would expect skewing to have a greater influence than surface finishes used in this study.

## REFERENCES


1. Bair, S., Winer, W. O., "First Phase Report: Investigation of Roller Follower Skidding on Automotive Camshafts", The Torrington Company, January 1, 1985.

2. Bair, S., Winer, W. O., Griffieon, J. A., "The Tribological Response of an Automotive Cam and Lifter System", ASME Paper No. 85-TRIB-4, to be published Journal of Tribology 1986.

3. Robinson, Enders, Multichannel Time Series Analysis with Digital Computer Systems, Holden-Day, 1967.

4. "Cam Follower Shuttling Investigation", Letter Report to Marv Knauf, Rochester Products Division of General Motors dated Nov. 13, 1985, with copy to Y. P. Chiu, Torrington.

5. Staron, Willermet, "An Analysis of Valve Train Friction in Terms of Lubrication Principles, "SAE Technical Paper 830165, 1983.

**Table I**
**Roller Specimens**

| Ga. Tech Sample | Torrington Sample | O. D. Roughness $\mu$ in. $R_a$ | Crown Radius in. | O. O. R. $\mu$ in. | Finish |
|---|---|---|---|---|---|
| S | #8 | 6.2 | 20 | 44 | Crowned and superfinished on Nagel |
| R | #5 | 14.4 | 19 | 40 | O. D. tumbled |

Table II
Test Program in Chronological Order
Phase II

| TEST NAME | SPEED RPM | TEMP C | OIL PRESS. PSI | SKEW ANGLE DEGREE |
|---|---|---|---|---|
| R0132 | 900 | 30 | 10 | 0 |
| R0135 | 1800 | 30 | 10 | 0 |
| R0138 | 2500 | 30 | 10 | 0 |
| R0192 | 900 | 90 | 10 | 0 |
| R0195 | 1800 | 90 | 10 | 0 |
| R0198 | 2500 | 90 | 10 | 0 |
| R0532 | 900 | 30 | 50 | 0 |
| R0535 | 1800 | 30 | 50 | 0 |
| R0538 | 2500 | 30 | 50 | 0 |
| R0592 | 900 | 90 | 50 | 0 |
| R0595 | 1800 | 90 | 50 | 0 |
| R0598 | 2500 | 90 | 50 | 0 |
| R1195 | 1800 | 90 | 10 | 1.5 |
| R3195 | 1800 | 90 | 10 | 3 |
| S---- | Repeat all above for roller S | | | |
| S0130 | 400 | 30 | 10 | 0 |
| S0133 | 1400 | 30 | 10 | 0 |

**Table III**
**Computer Programs**

| NAME | INPUT | OUTPUT | TASK |
|---|---|---|---|
| REDUCE | Disc Files created by Gould IOS....1-....6 | 1) Disc File<br>2) Graphics Display | Produces file of forces, velocities, etc., from voltages. |
| FILTER 2 | Disc Files created by REDUCE | 1) Disc File F....<br>2) Print out | Removes high frequency noise from data. |
| PLOTTER | Disc File created by REDUCE or FILTER or DATA SWAP | 1) Graphs<br>2) Display | Plots graphs displays skid distance. |
| DATA SWAP | Disc Files created by REDUCE or FILTER 2 | Disc File L..... | Recalculates kinematics for lift data from another file. |

**Table IV**
**Cutoff Frequencies for Low-Pass Filter - FILTER 2**

$$\text{Cutoff Frequency} = J_{cut} \times \text{Fundamental Frequency}$$

$$\text{Fundamental Freq.} = \frac{180}{256} \times \frac{\text{CAM RPM}}{60}$$

| Quantity | Jcut |
|---|---|
| $F_x$ | 24 |
| $F_y$ | 16 |
| $F_z$ | 24 |
| Roller Velocity | 48 |
| Cam Velocity | 48 |
| $F_t$ | 24 |
| $F_N$ | 24 |
| Torque | 16 |

## Table V
## Relative Sliding Displacement in Milimeters

A. For one revolution of cam (118 mm cam surface)

CAM SPEED/RPM

| Oil Temp °C | Oil Press PSIG | Skew Angle Deg | Roller | 900 | | 1700 | | 2500 | |
|---|---|---|---|---|---|---|---|---|---|
| | | | | R | S | R | S | R | S |
| 30 | 10 | 0 | | 19.1 | 3.4 | 13.9 | 18.0 | 6.4 | 7.5 |
| 30 | 50 | 0 | | .3 | .1 | 2.6 | 4.0 | 1.9 | 2.4 |
| 90 | 10 | 0 | | 0.0 | 0.0 | .2 | .4 | .7 | .8 |
| 90 | 50 | 0 | | 0.0 | 0.0 | .1 | .2 | .1 | .5 |
| 90 | 10 | 1.5 | | | | 4.0 | 4.2 | | |
| 90 | 10 | 3 | | | | 7.0 | 7.2 | | |

B. For the 160° loaded portion of cam revolution (57 mm cam surface)

CAM SPEED/RPM

| Oil Temp °C | Oil Press PSIG | Skew Angle Deg | Roller | 900 | | 1700 | | 2500 | |
|---|---|---|---|---|---|---|---|---|---|
| | | | | R | S | R | S | R | S |
| 30 | 10 | 0 | | 1.4 | .6 | 1.5 | 2.0 | 1.0 | 1.5 |
| 30 | 50 | 0 | | .2 | .1 | .4 | .3 | .6 | .6 |
| 90 | 10 | 0 | | 0.0 | 0.0 | .1 | .1 | .2 | .3 |
| 90 | 50 | 0 | | 0.0 | 0.0 | .1 | .1 | .3 | .4 |
| 90 | 10 | 1.5 | | | | 2.3 | 2.3 | | |
| 90 | 10 | 3 | | | | 3.7 | 3.7 | | |

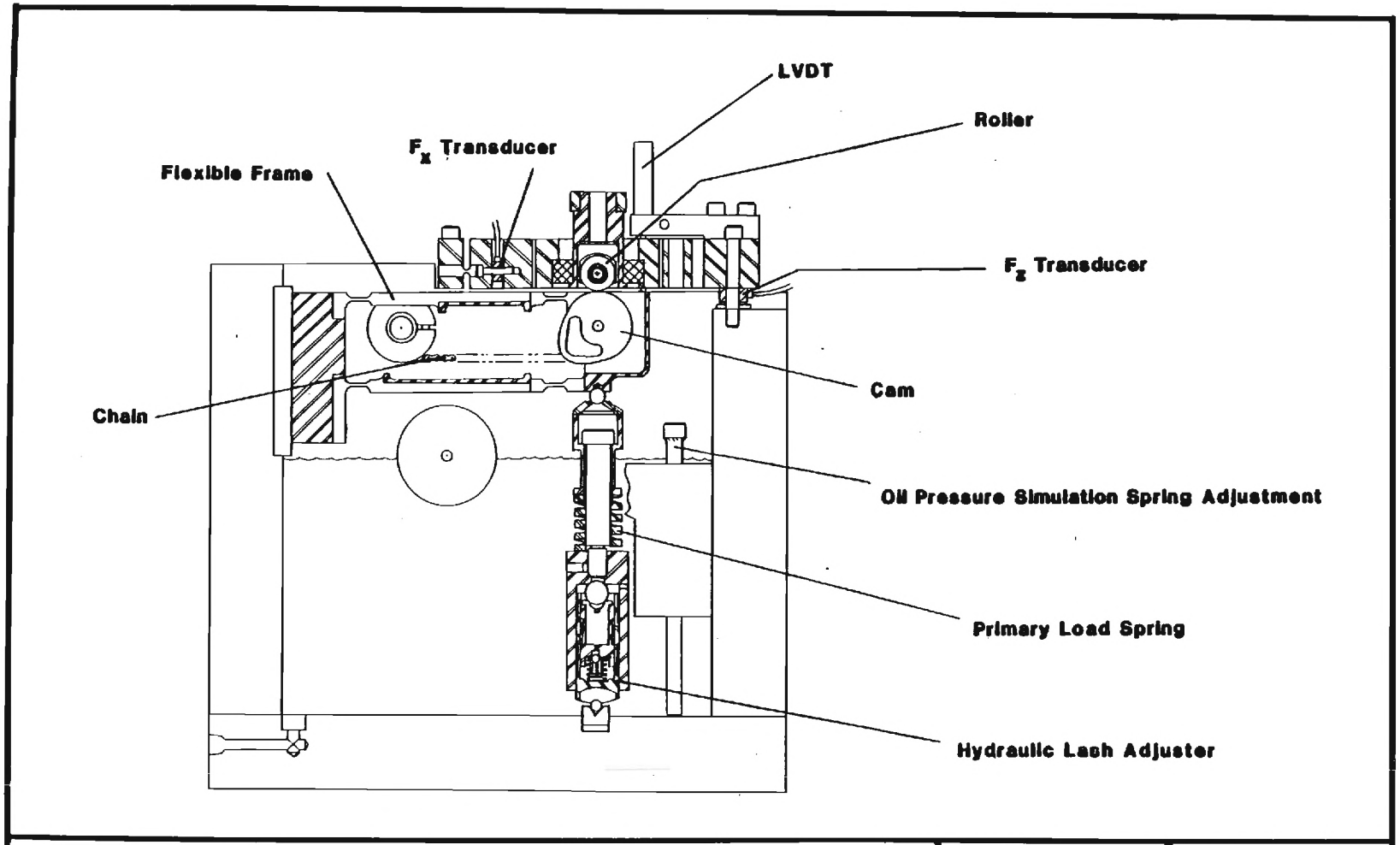


Figure 1a. Tappet Roller Skid Test Machine - Side View

| INITIALS | DATE |
|---|---|
| | |

**TRIBOLOGY & RHEOLOGY LABORATORY**
SCHOOL OF MECHANICAL ENGINEERING
GEORGIA INSTITUTE OF TECHNOLOGY

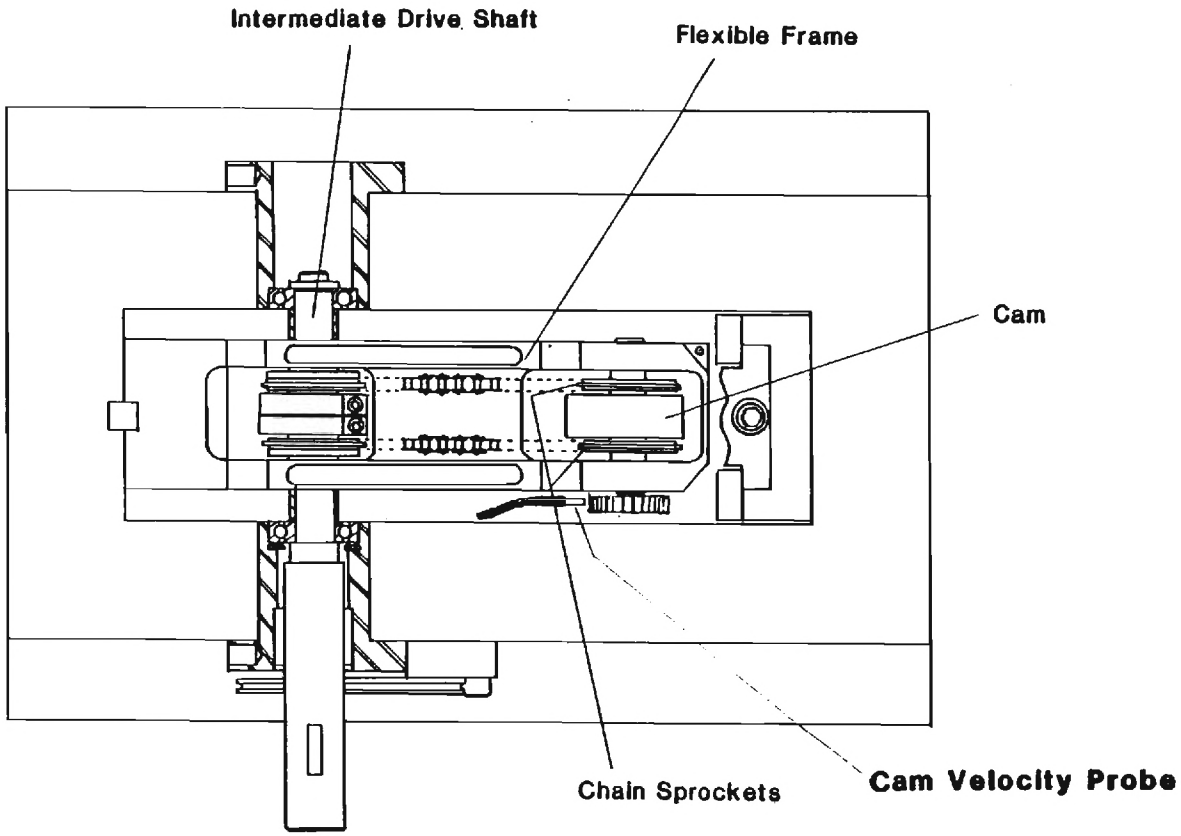


Figure 1b. Tappet Roller Skid Test Machine - Top View
(with measurement frame removed)

| INITIALS | DATE |
|---|---|
| | |

**TRIBOLOGY & RHEOLOGY LABORATORY**
SCHOOL OF MECHANICAL ENGINEERING
GEORGIA INSTITUTE OF TECHNOLOGY

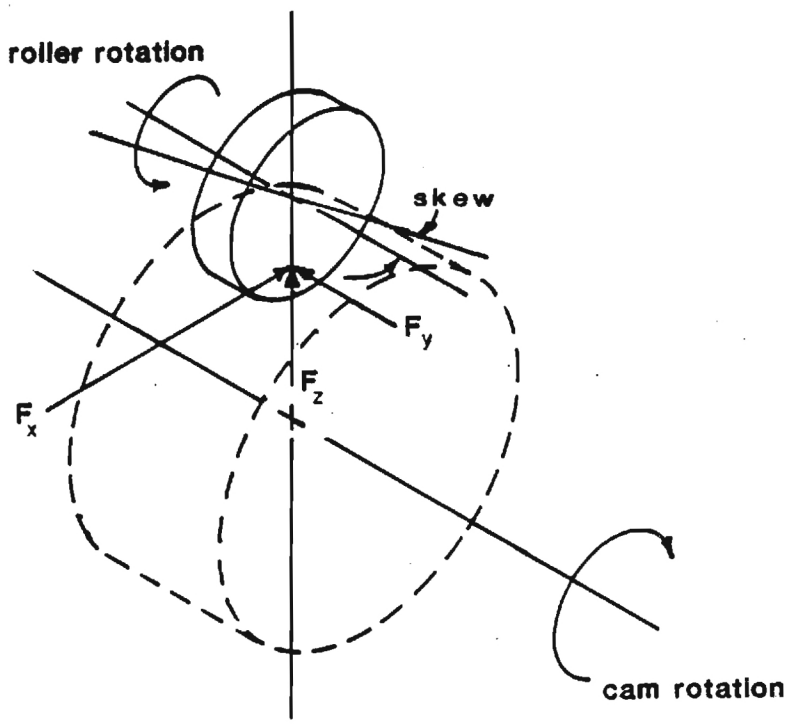


**Figure 2. Definition of forces on roller that are directly measured**

| INITIALS | DATE | **TRIBOLOGY & RHEOLOGY LABORATORY**<br>SCHOOL OF MECHANICAL ENGINEERING<br>GEORGIA INSTITUTE OF TECHNOLOGY |
|---|---|---|

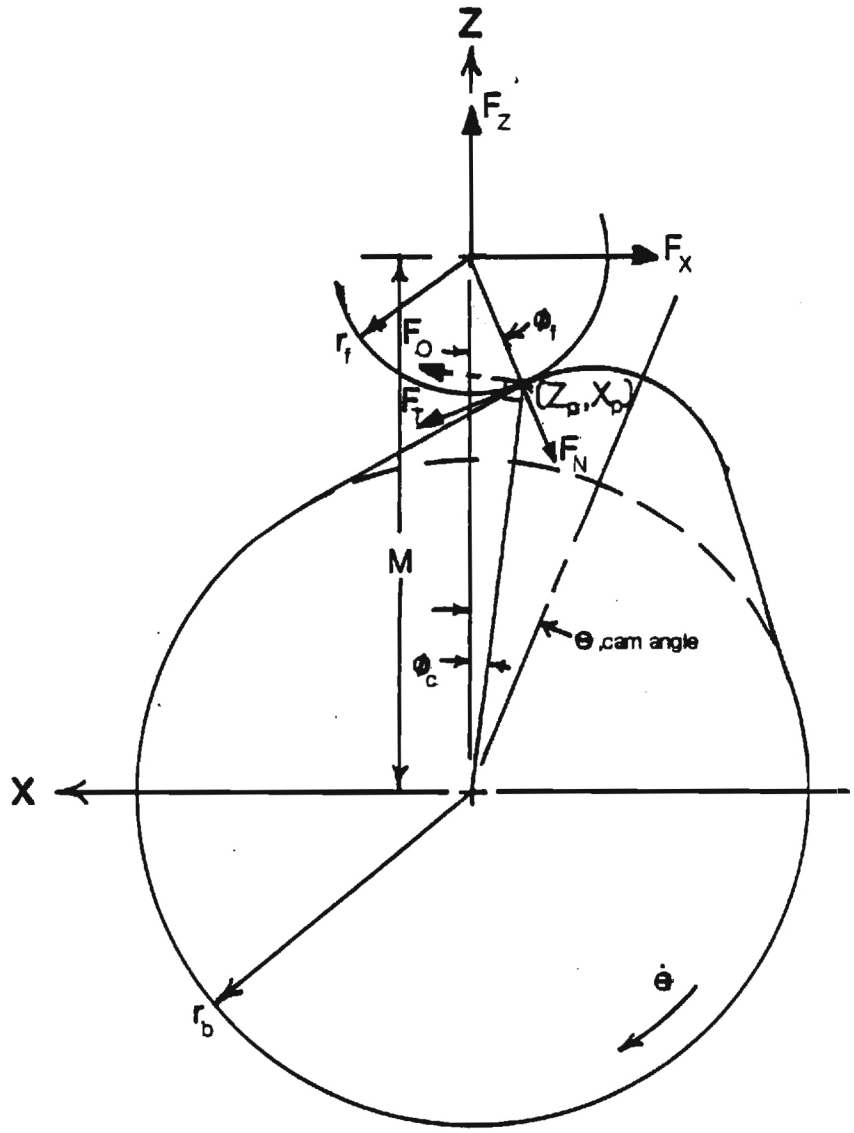


**Figure 3. Definitions of angles and forces at the contact calculated from data**

| INITIALS | DATE | **TRIBOLOGY & RHEOLOGY LABORATORY**<br>SCHOOL OF MECHANICAL ENGINEERING<br>GEORGIA INSTITUTE OF TECHNOLOGY |
|---|---|---|

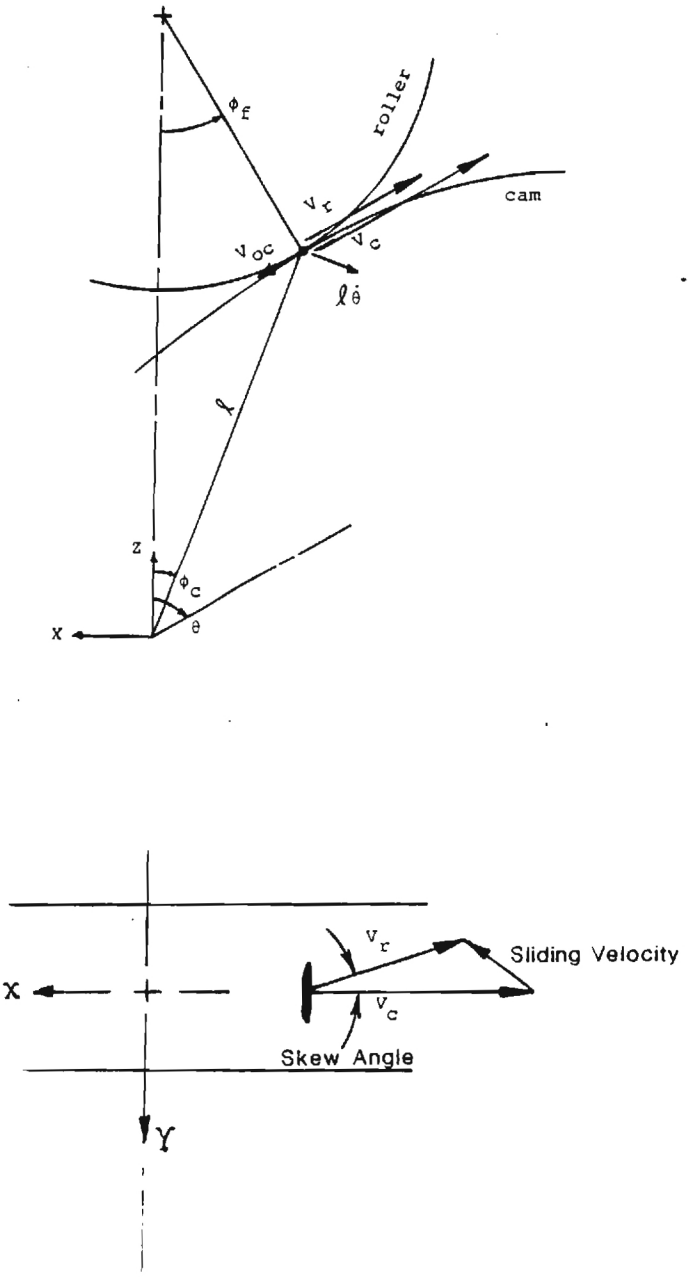





**Figure 4. Definitions of velocities**

| INITIALS | DATE | **TRIBOLOGY & RHEOLOGY LABORATORY**<br>SCHOOL OF MECHANICAL ENGINEERING<br>GEORGIA INSTITUTE OF TECHNOLOGY |
|---|---|---|

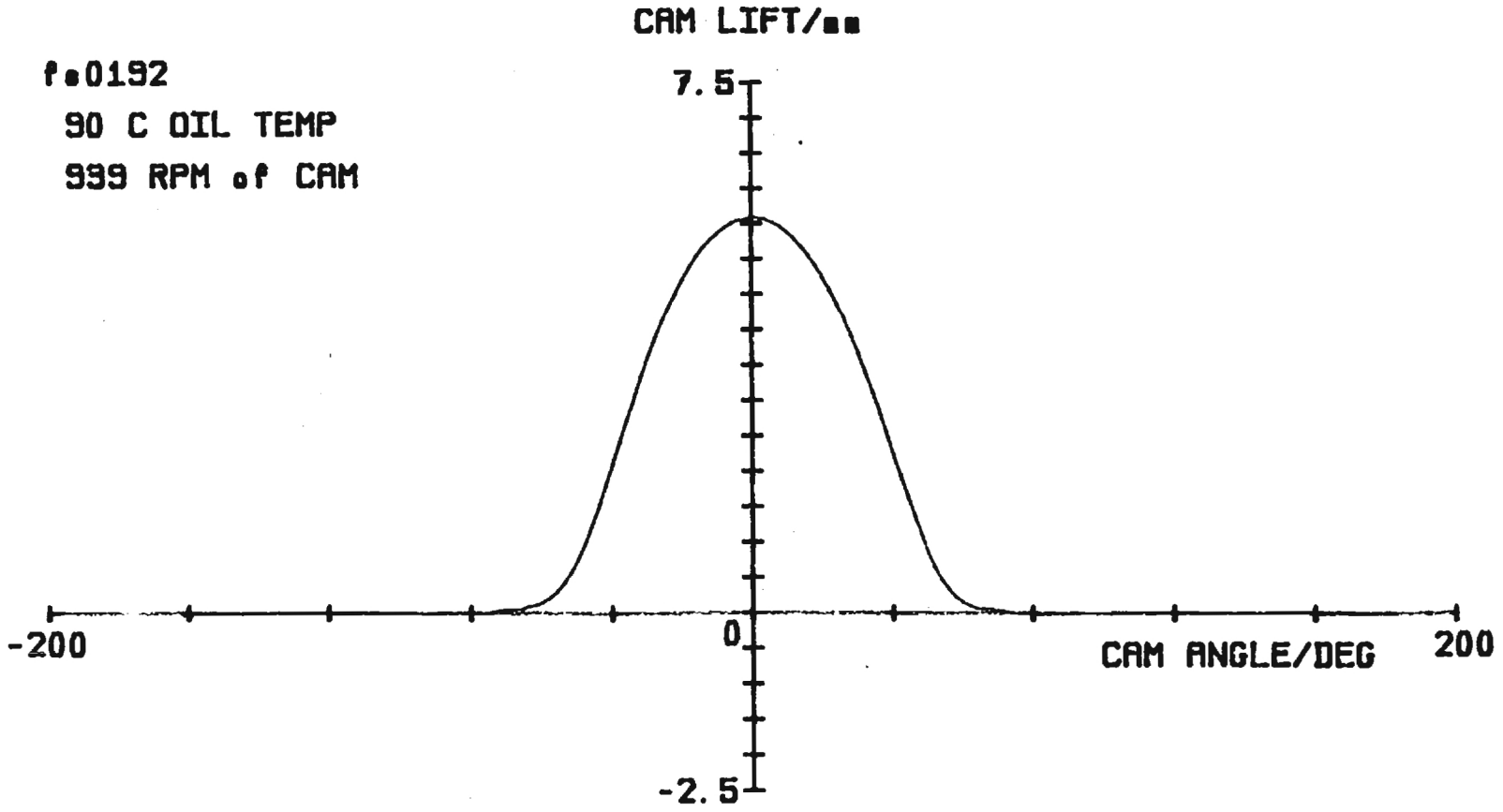


FIGURE 5a: Cam Lift

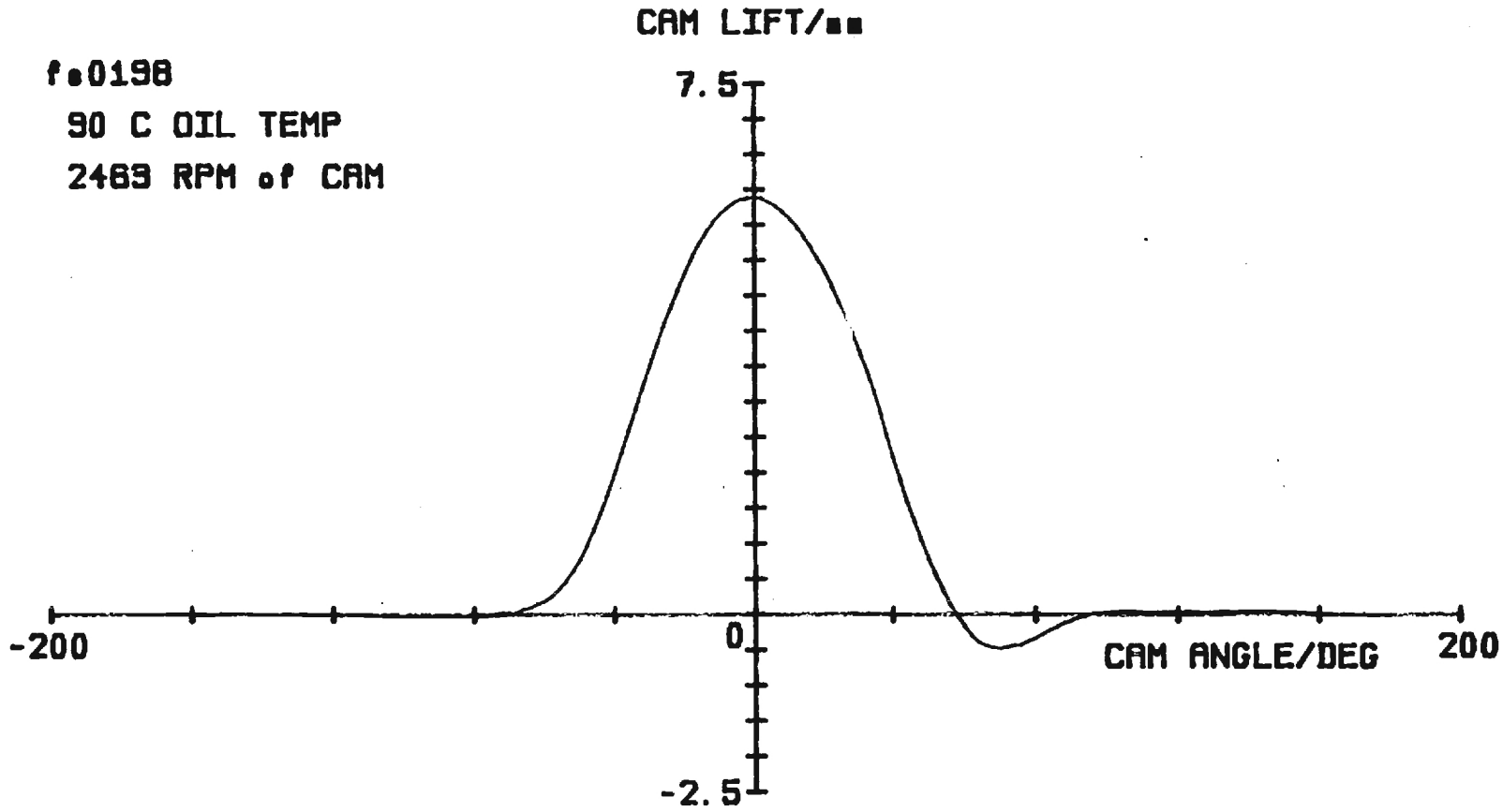


FIGURE 5.6: Cam Lift

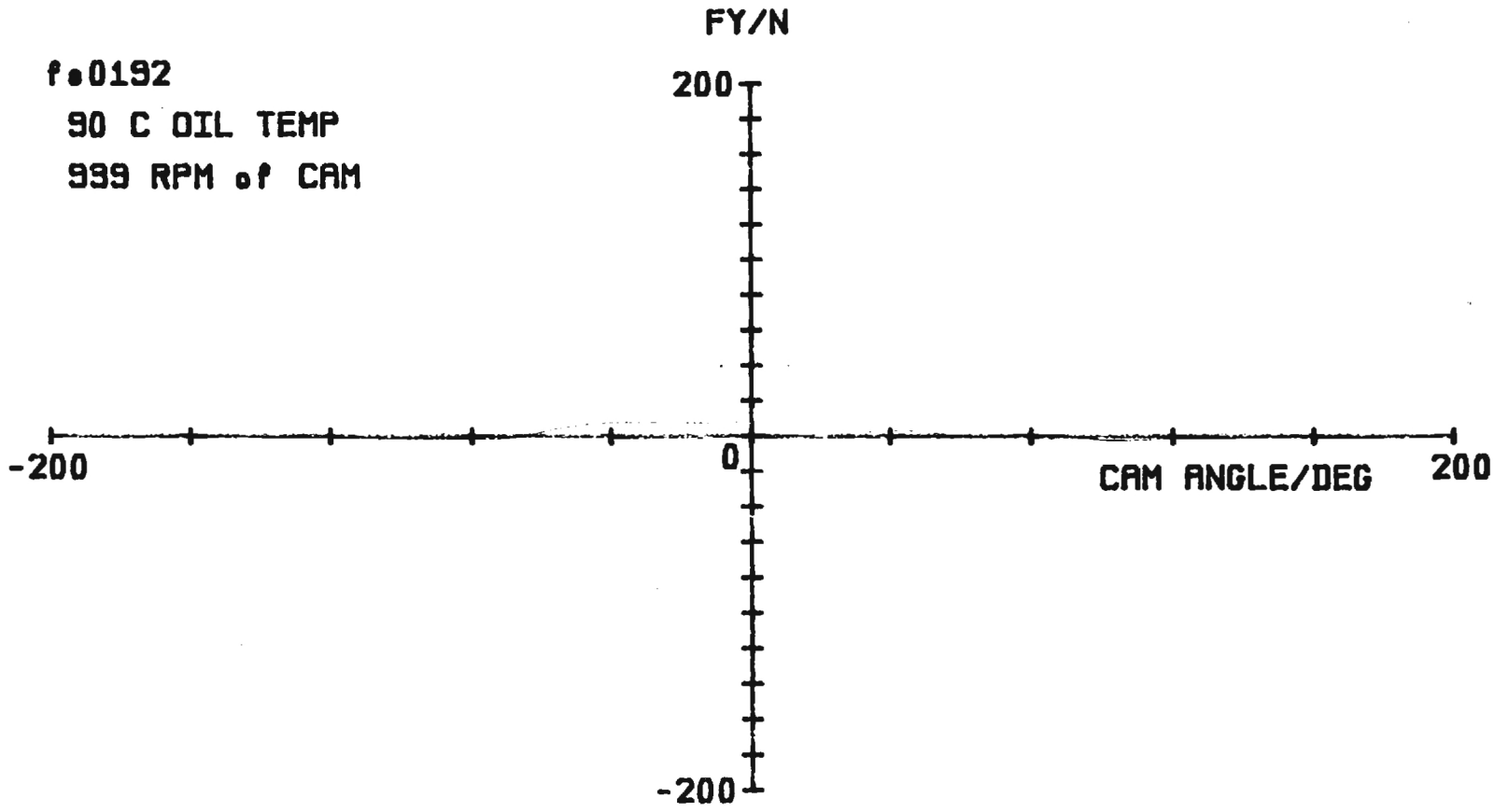


FIGURE 6a: Axial Contact Force - $0^{o}$ Skew

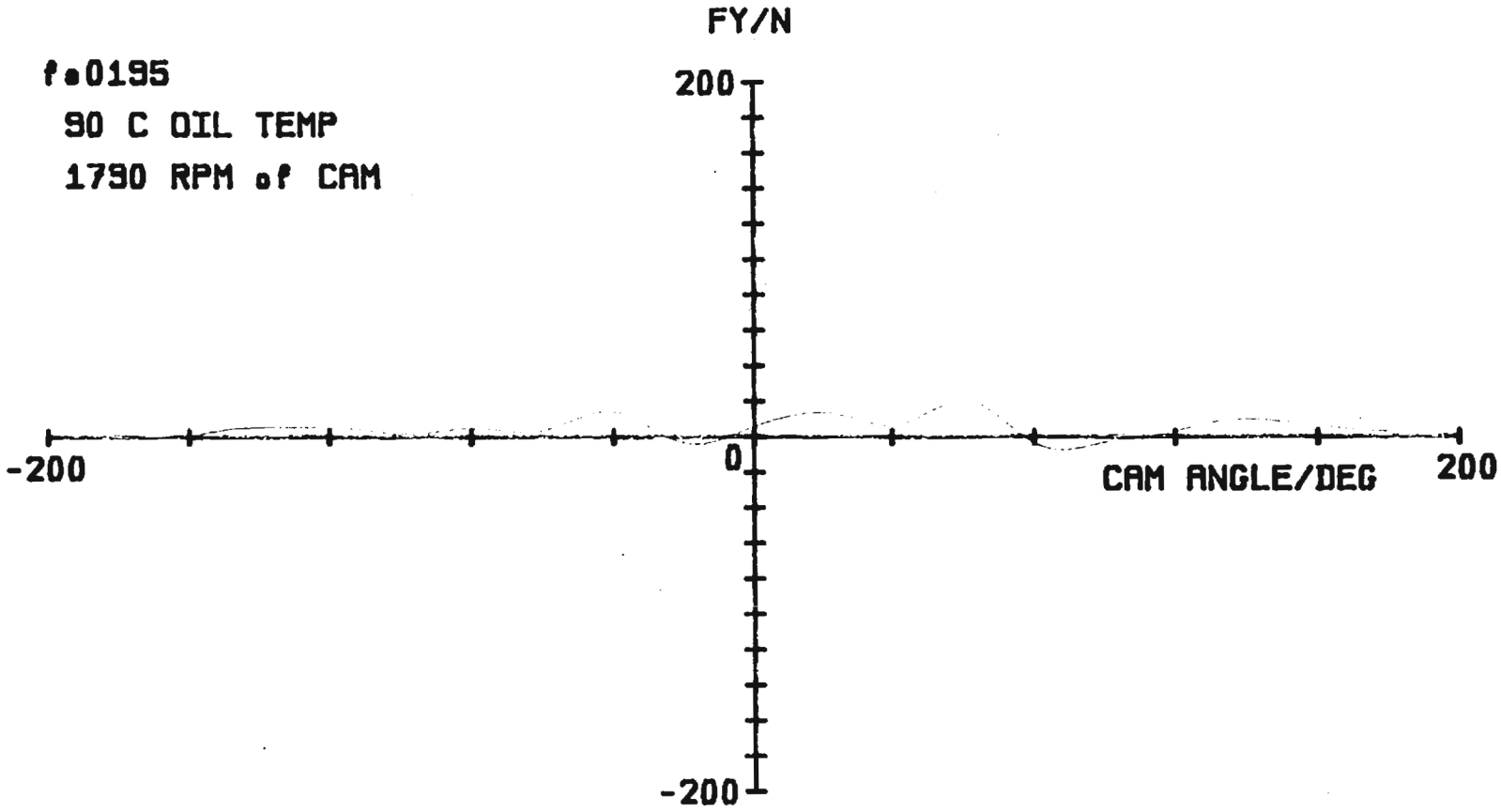


FIGURE 6.6: Axial Contact Force - $0^{o}$ Skew

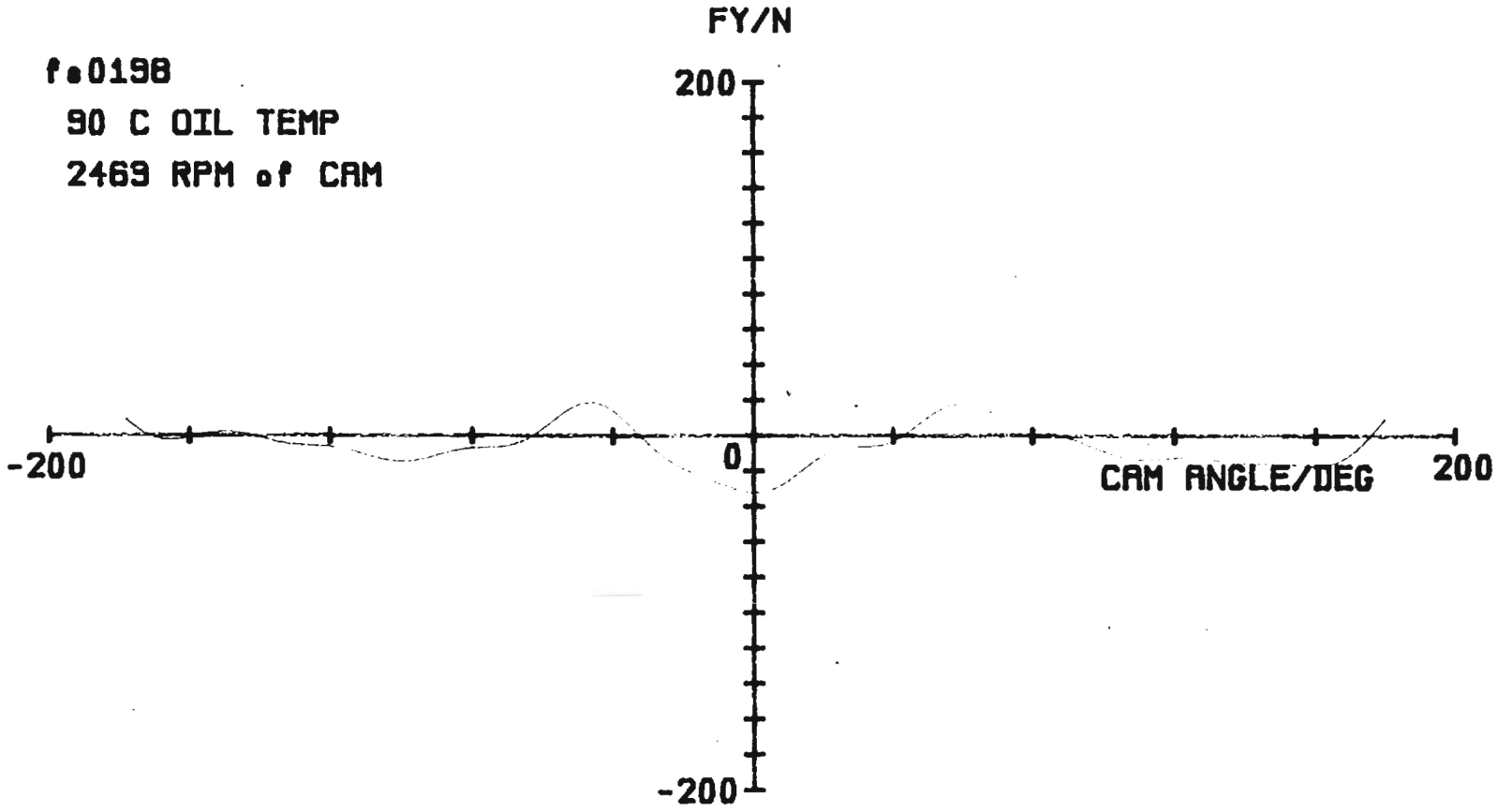


FIGURE 6c: Axial Contact Force - $0^{o}$ Skew

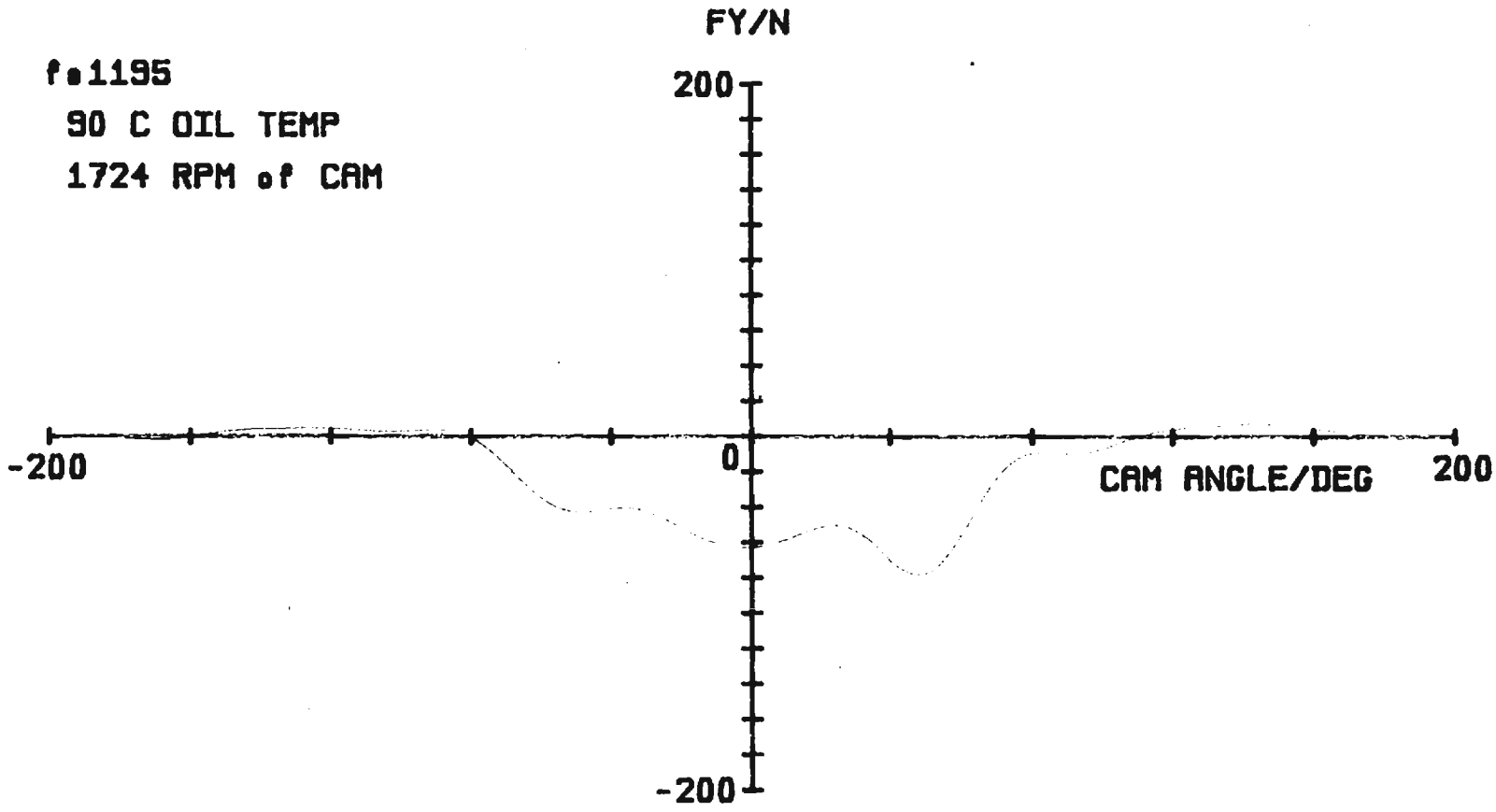


FIGURE 6d: Axial Contact Force - 1.5° Skew

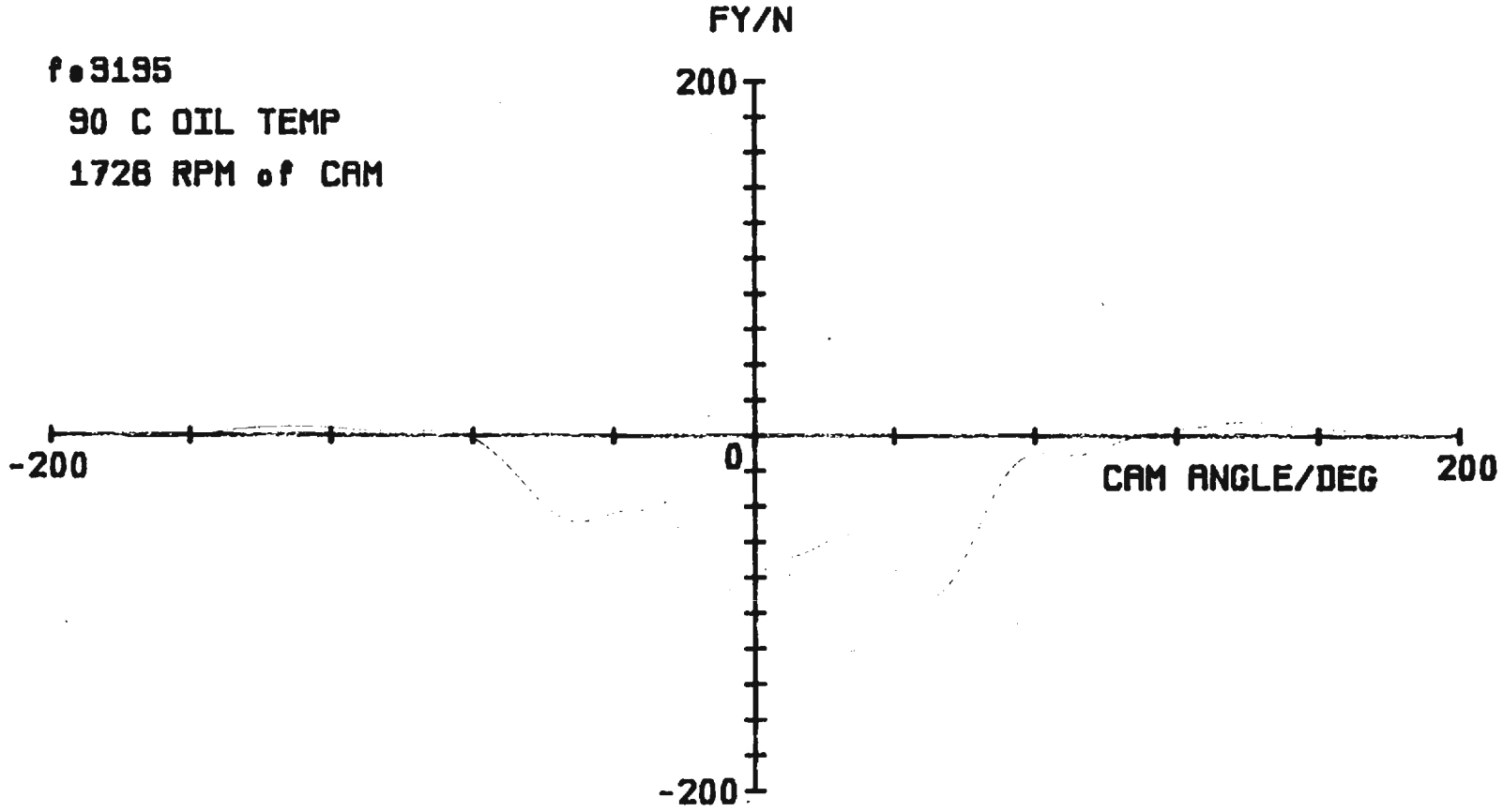


FIGURE 6e: Axial Contact Force for $3^{o}$ Skew

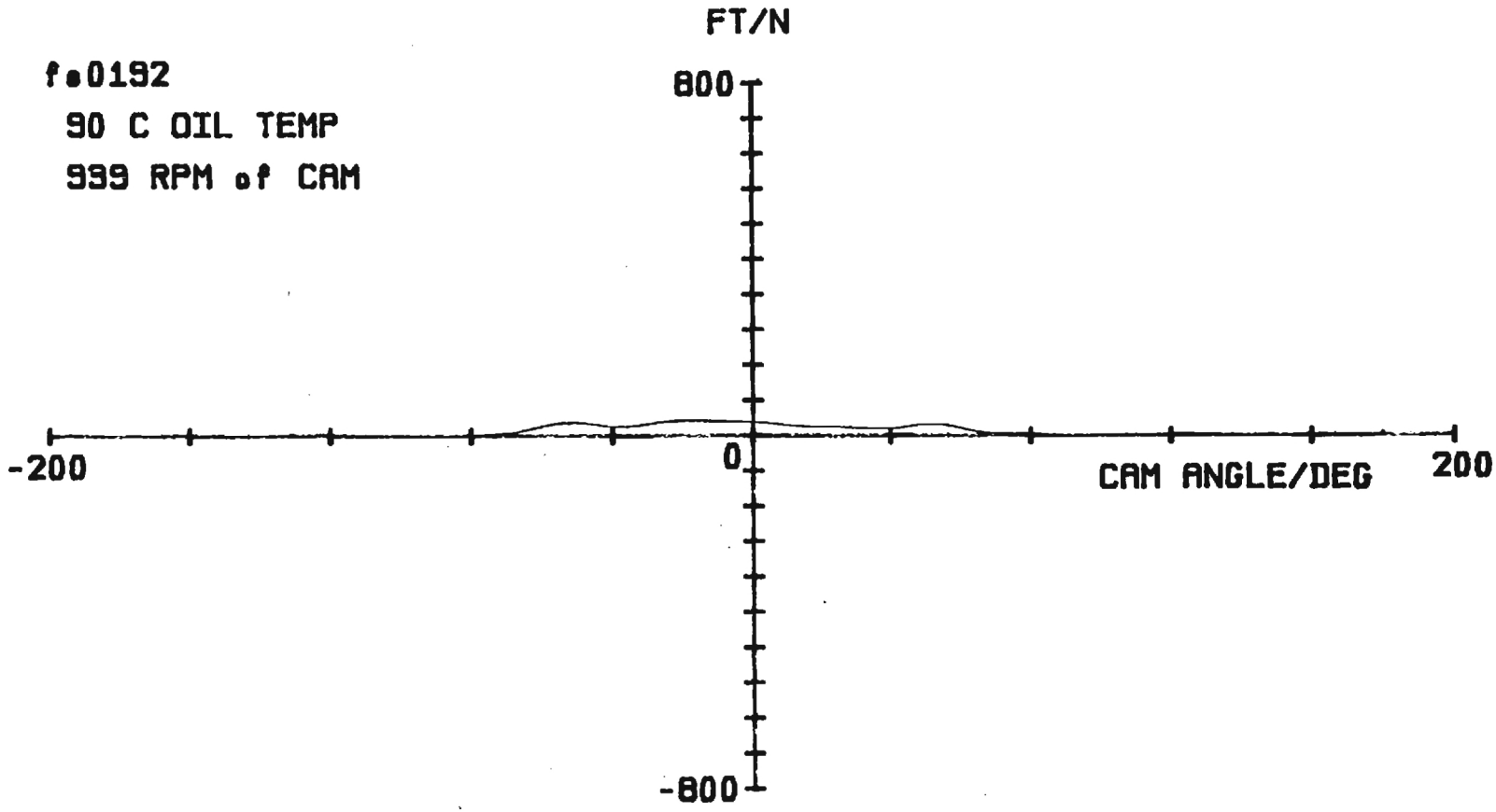


FIGURE 7a: Traction

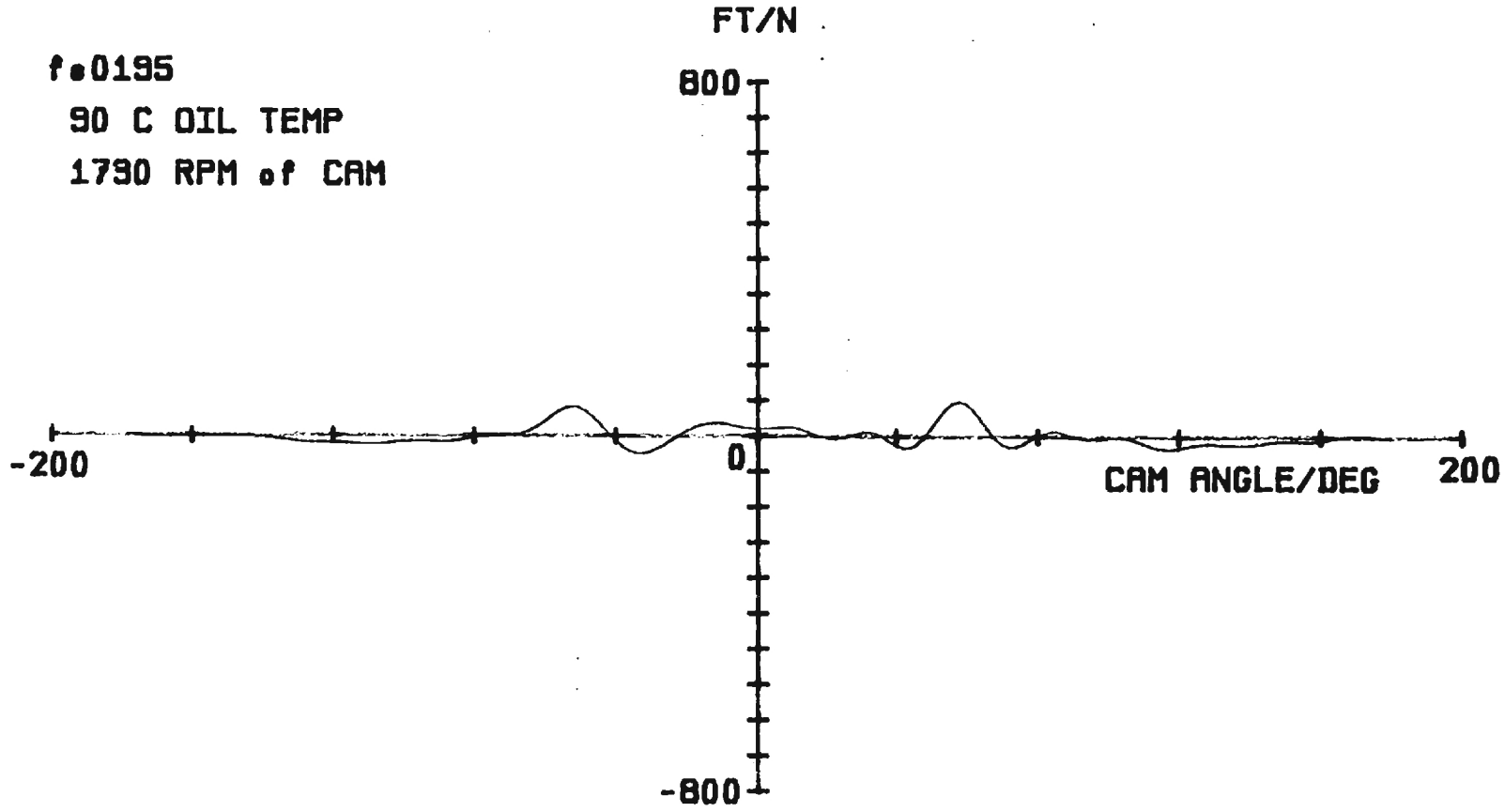


FIGURE 7b: Traction

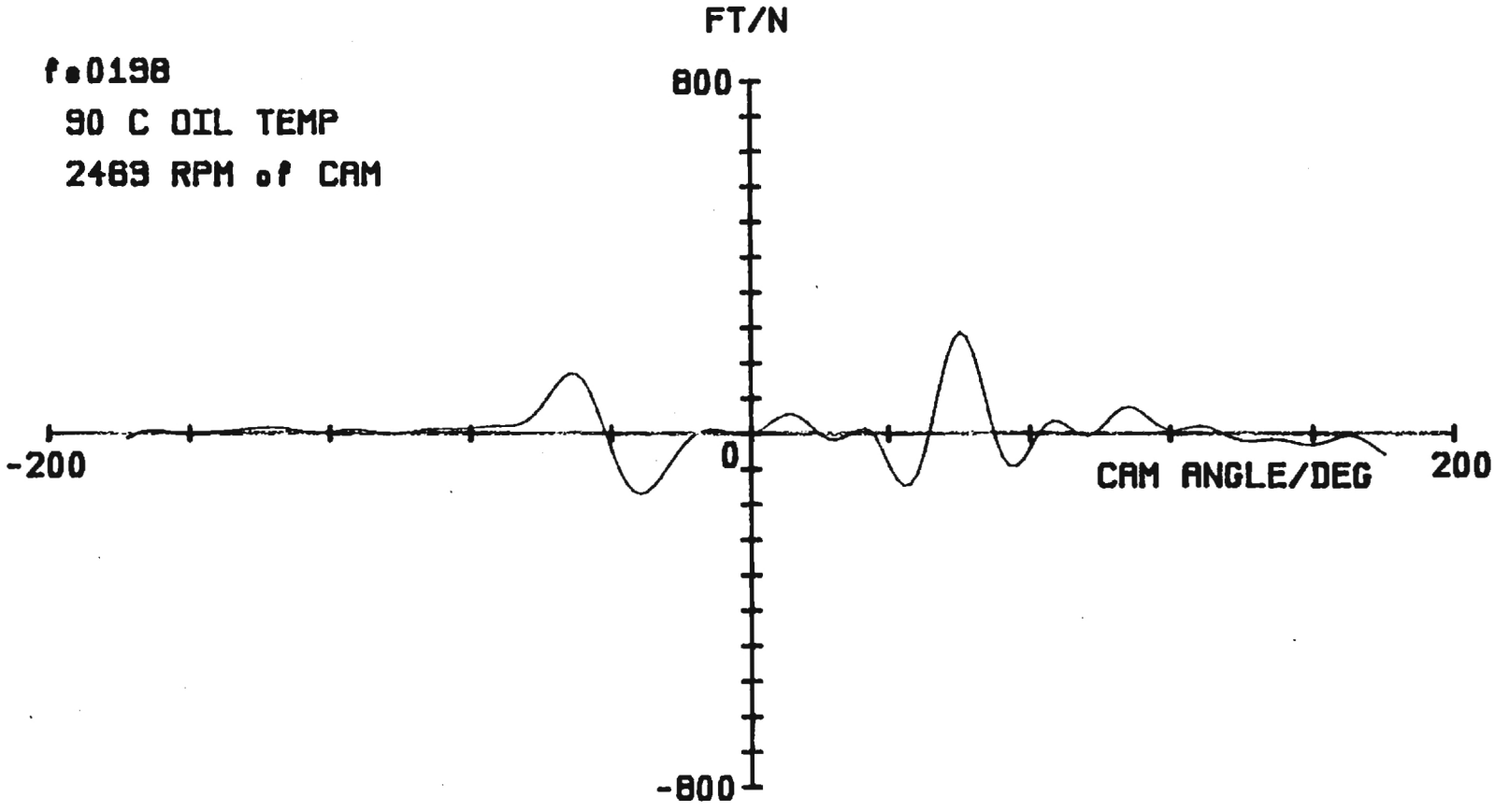


FIGURE 7c: Traction

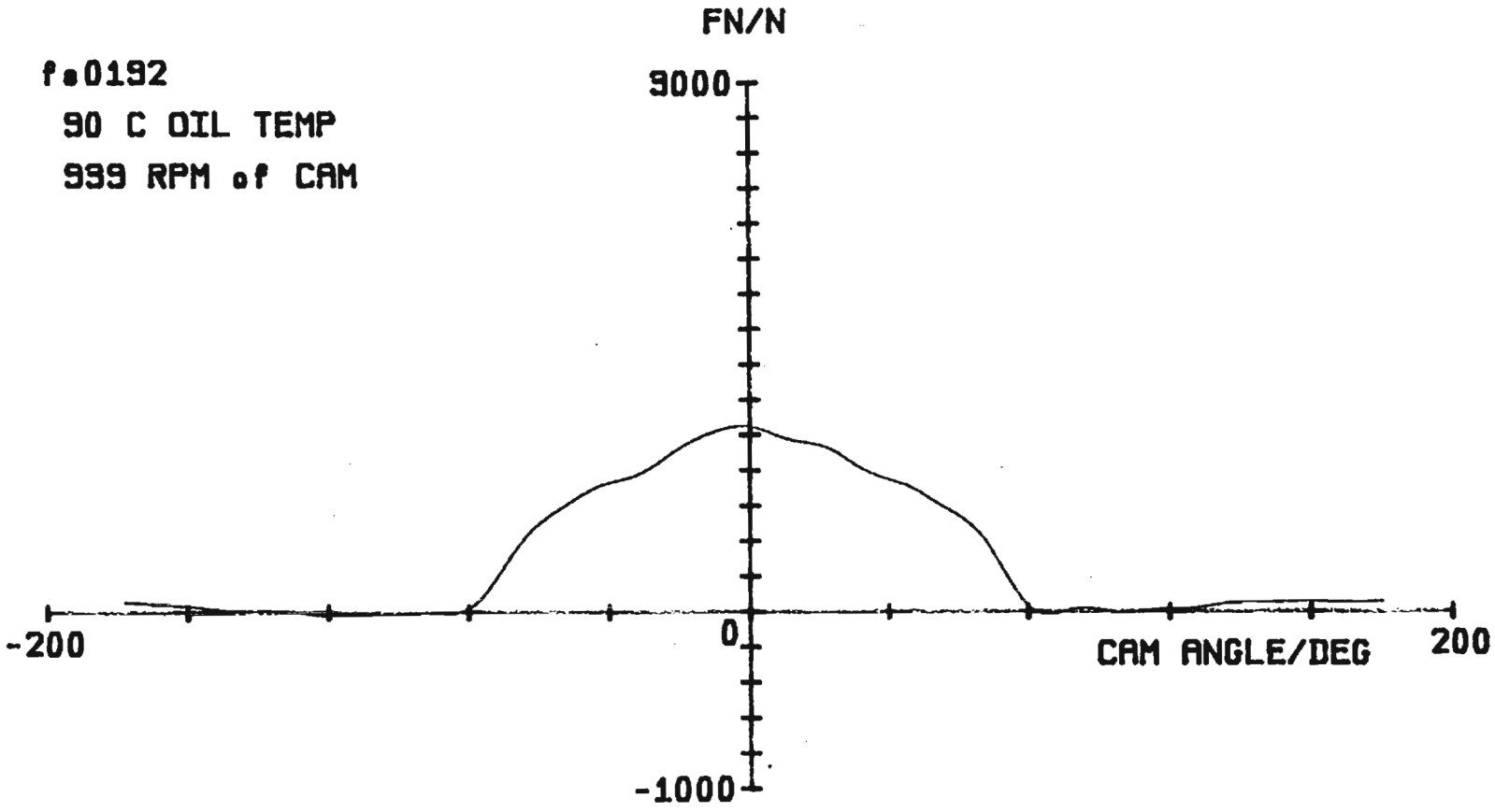


FIGURE 8a: Contact Normal Force

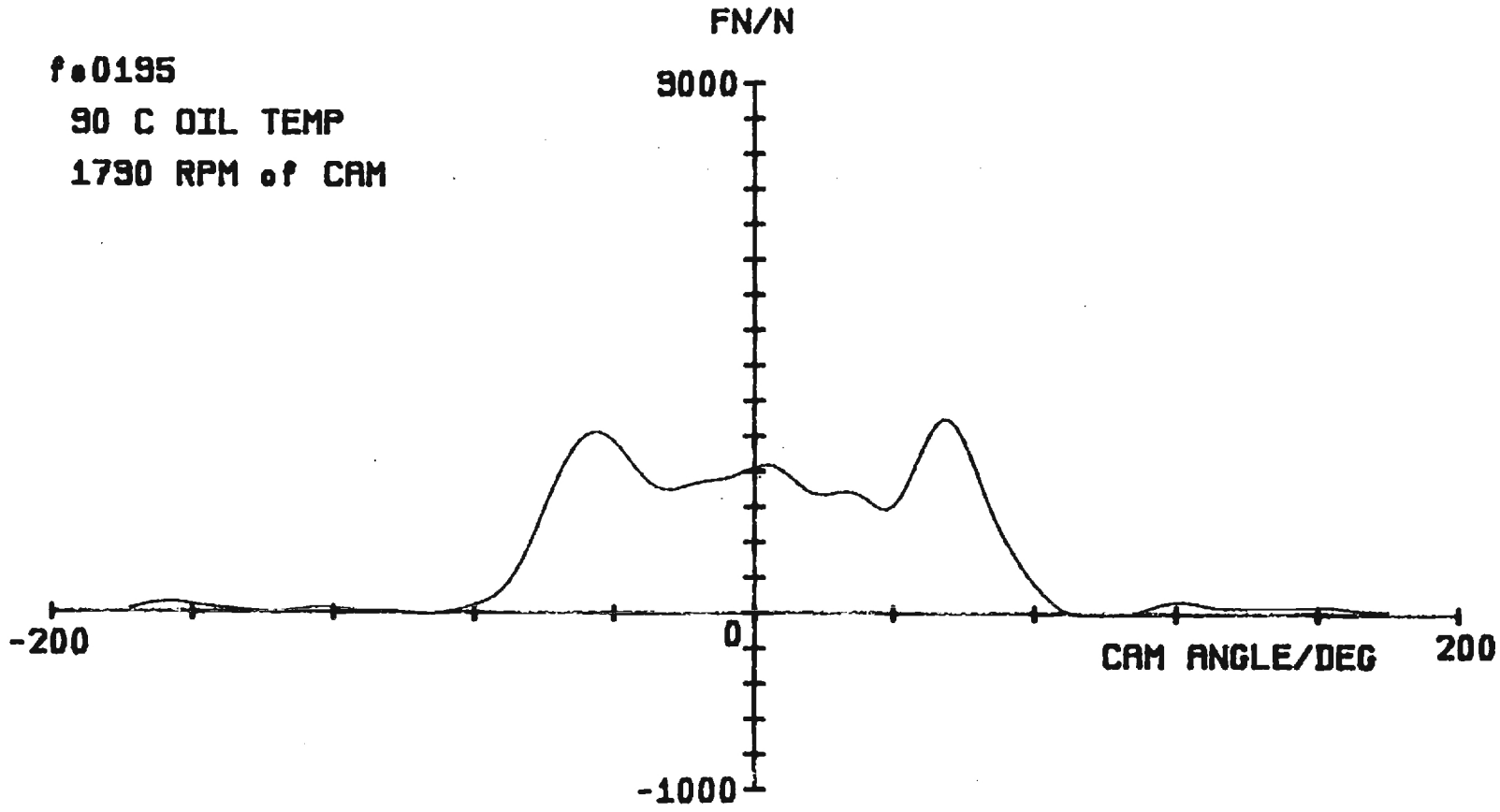


FIGURE 8b: Contact Normal Force

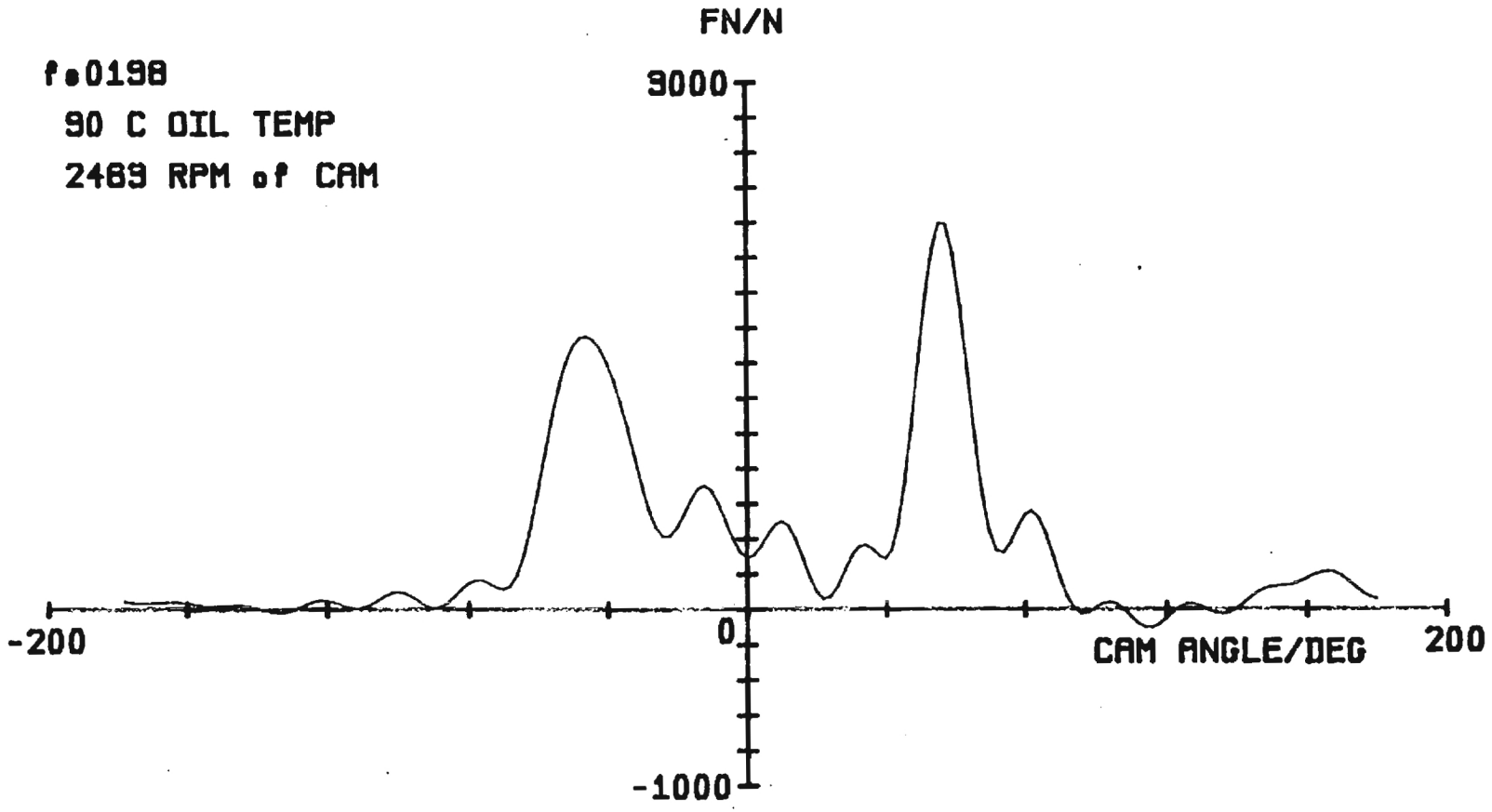


FIGURE 8c: Contact Normal Force

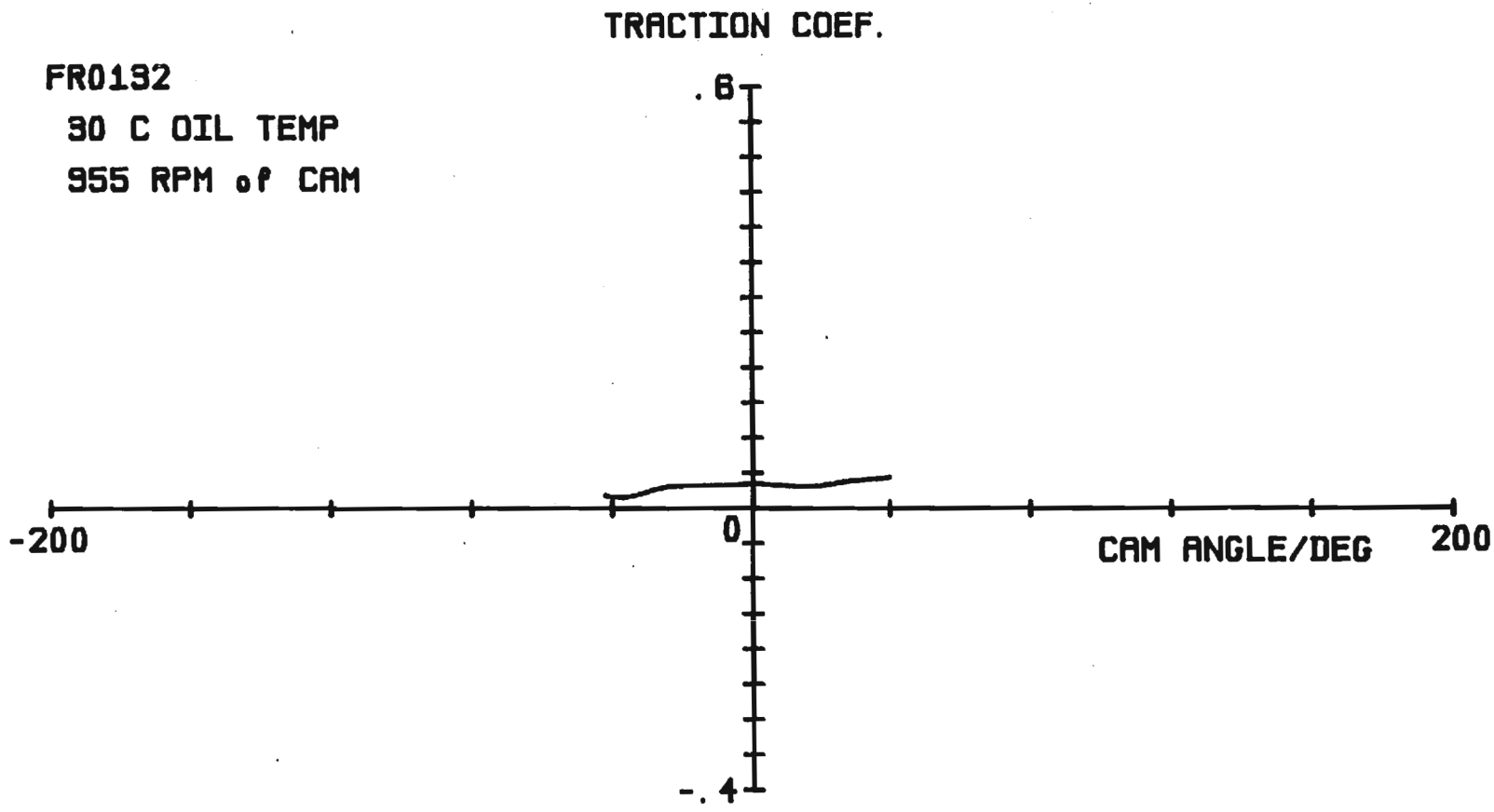


FIGURE 9a. Contact Traction Coefficient

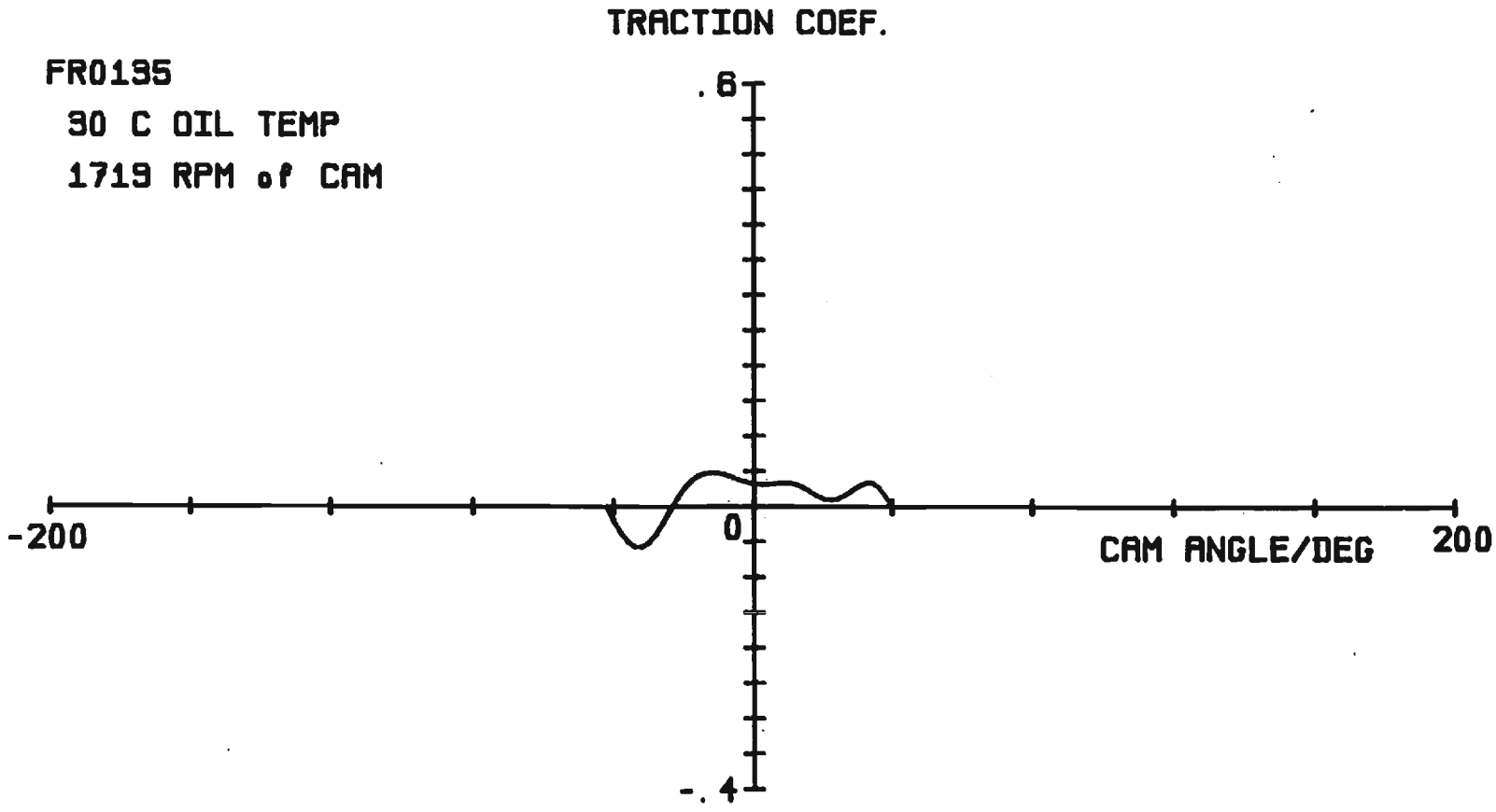


FIGURE 9b: Contact Traction Coefficient

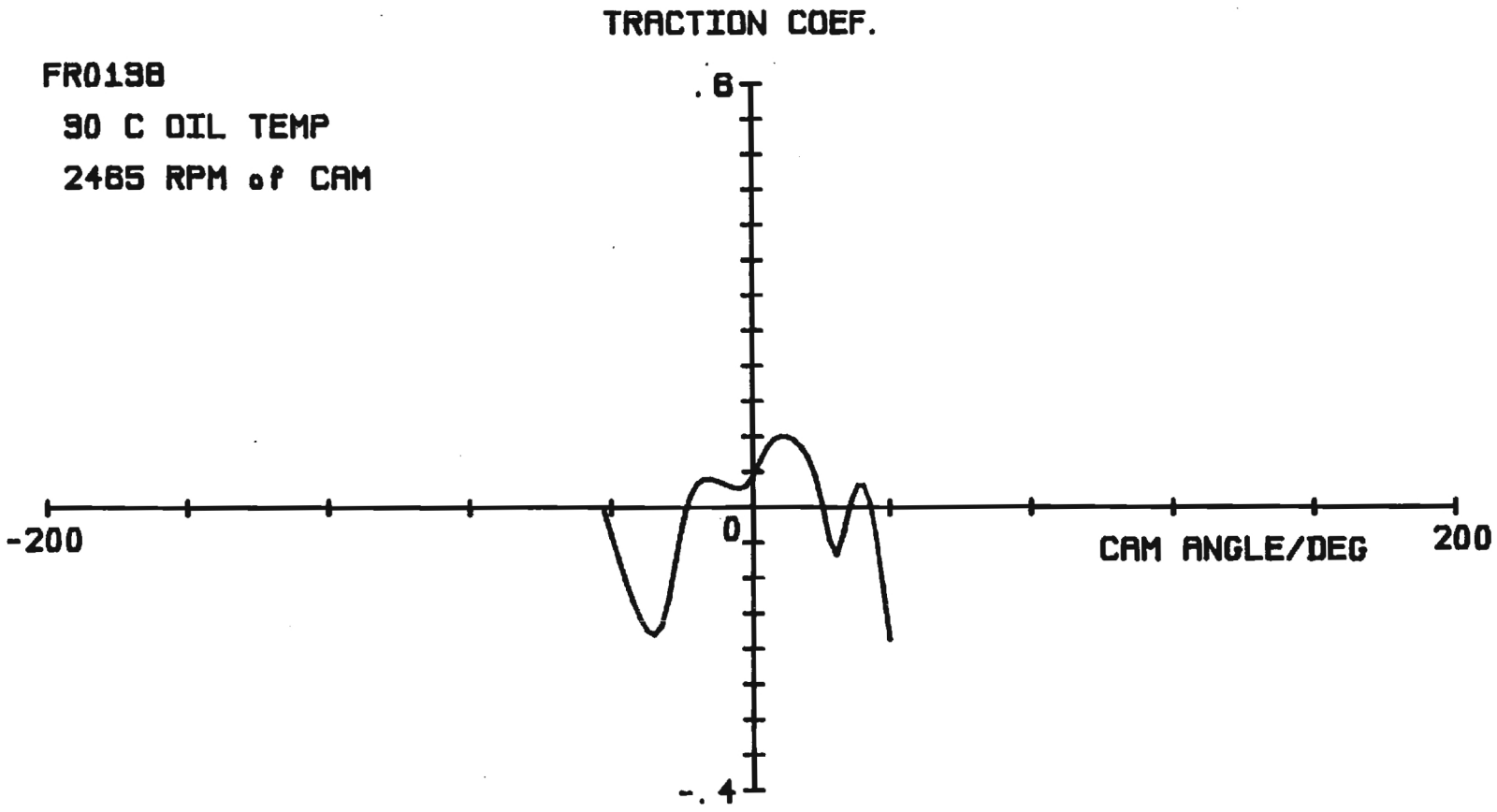


FIGURE 9c: Contact Traction Coefficient

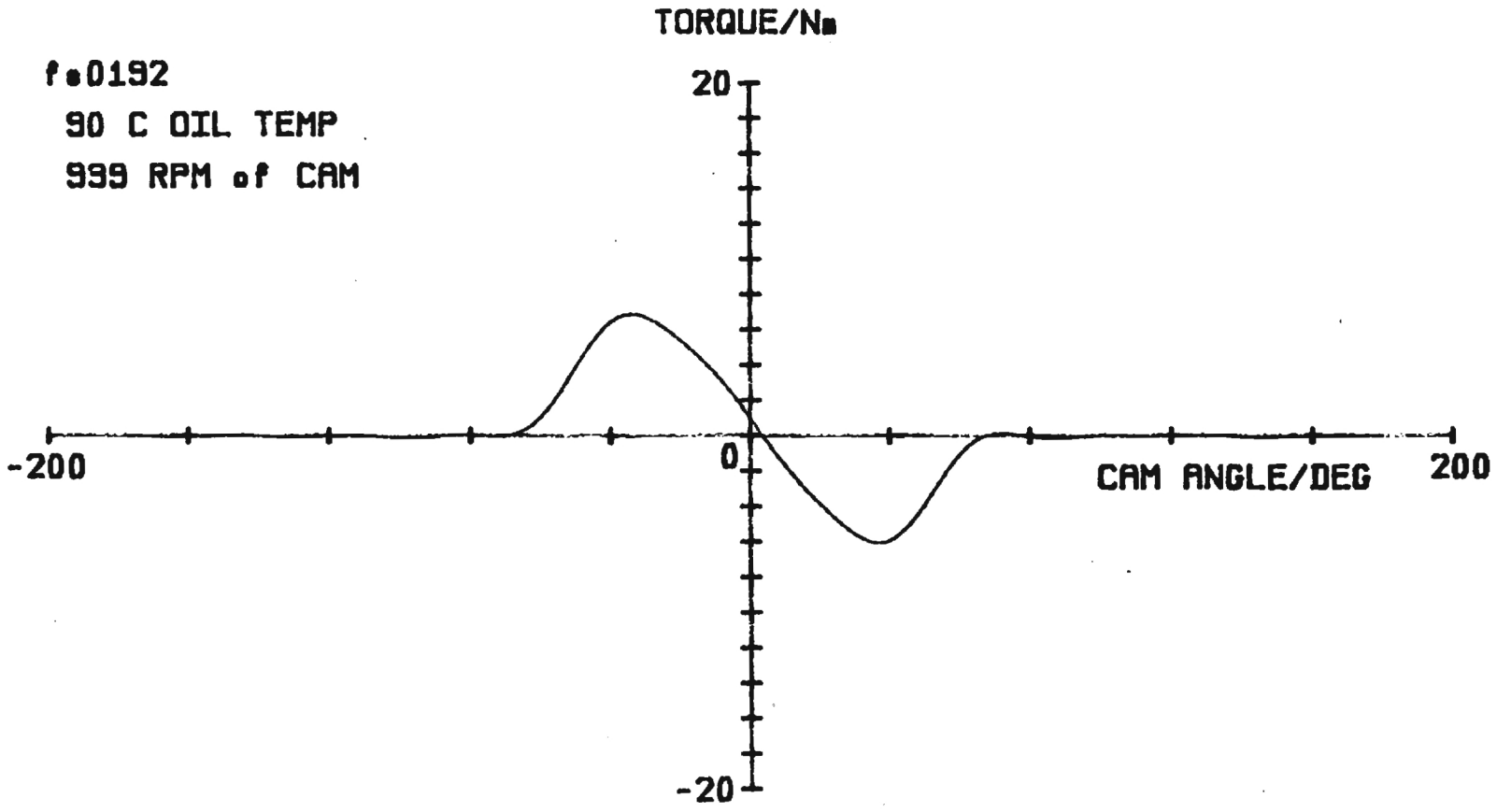


FIGURE 10a: Cam Torque

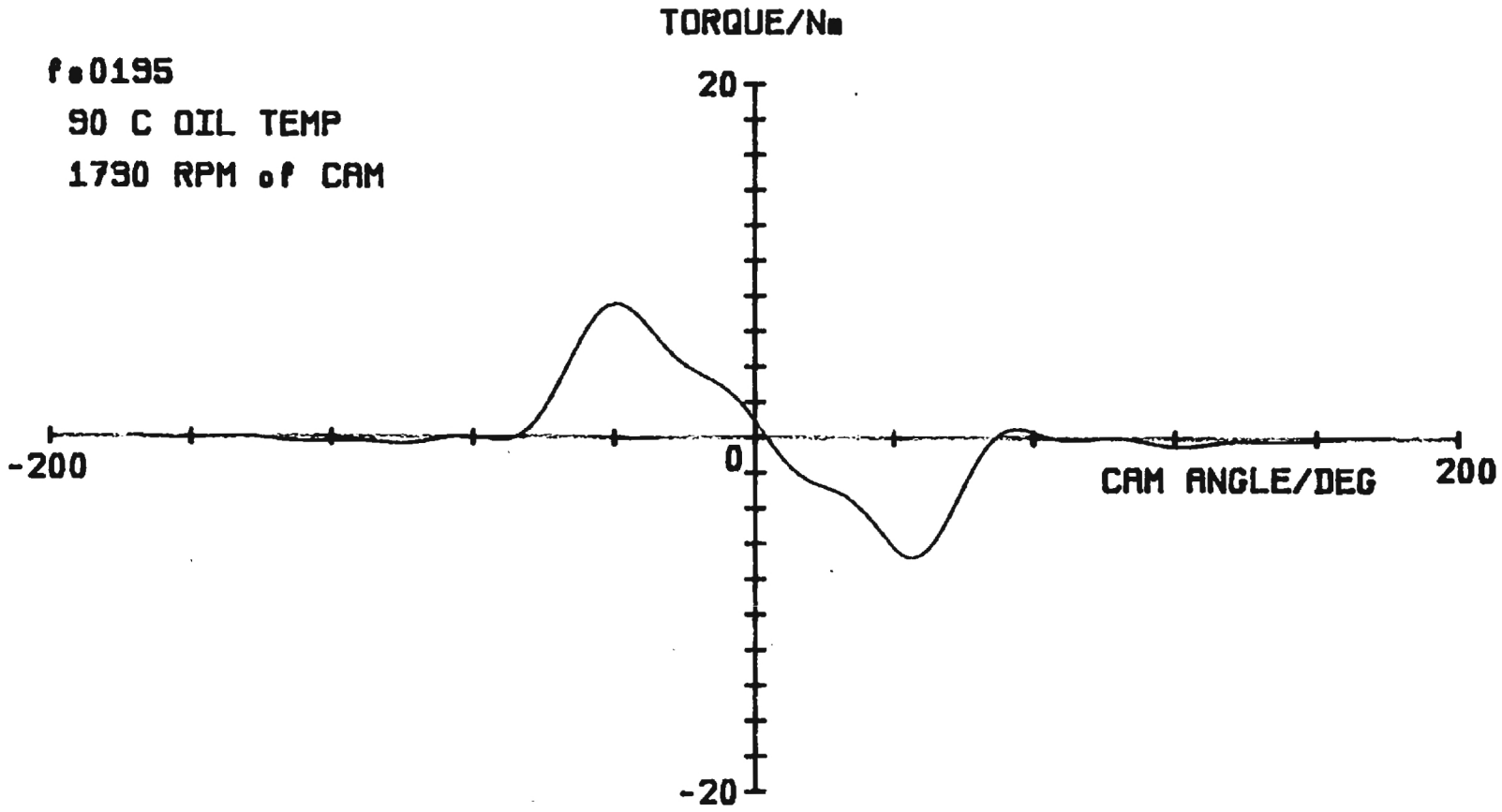


FIGURE 10b: Cam Torque

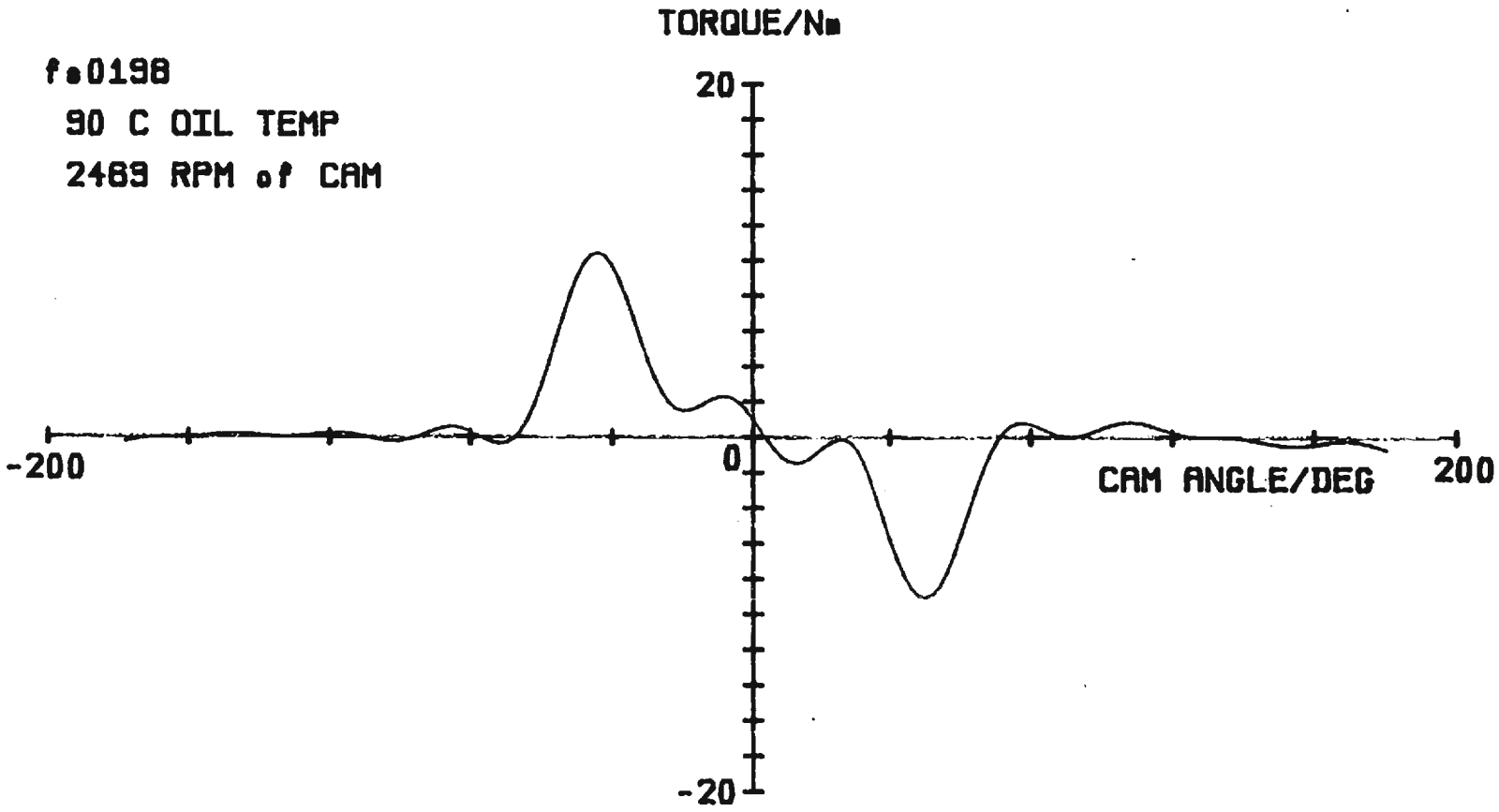


FIGURE 10c: Cam Torque

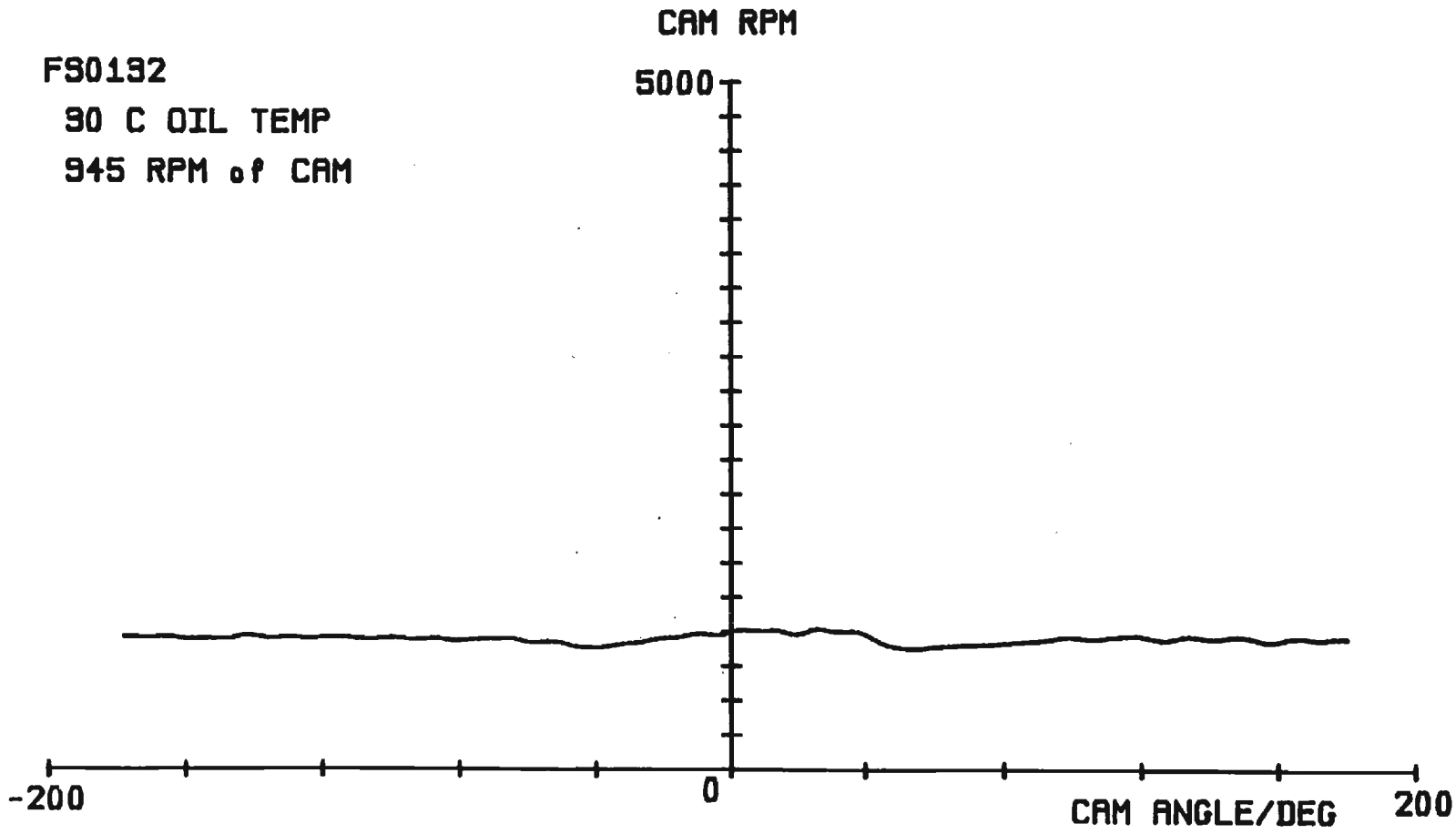


FIGURE 11a: Cam RPM

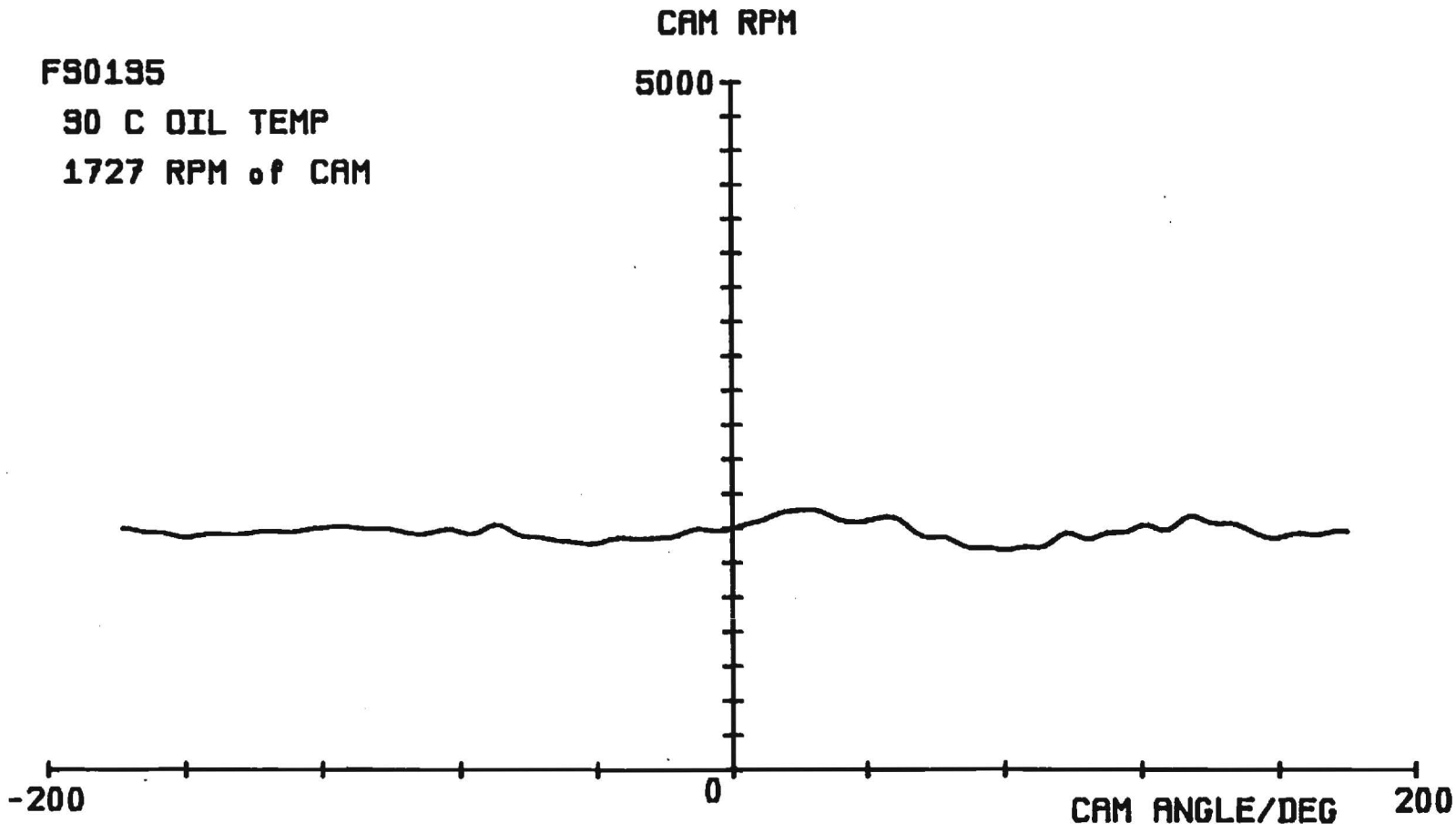


FIGURE 11 b : Cam RPM

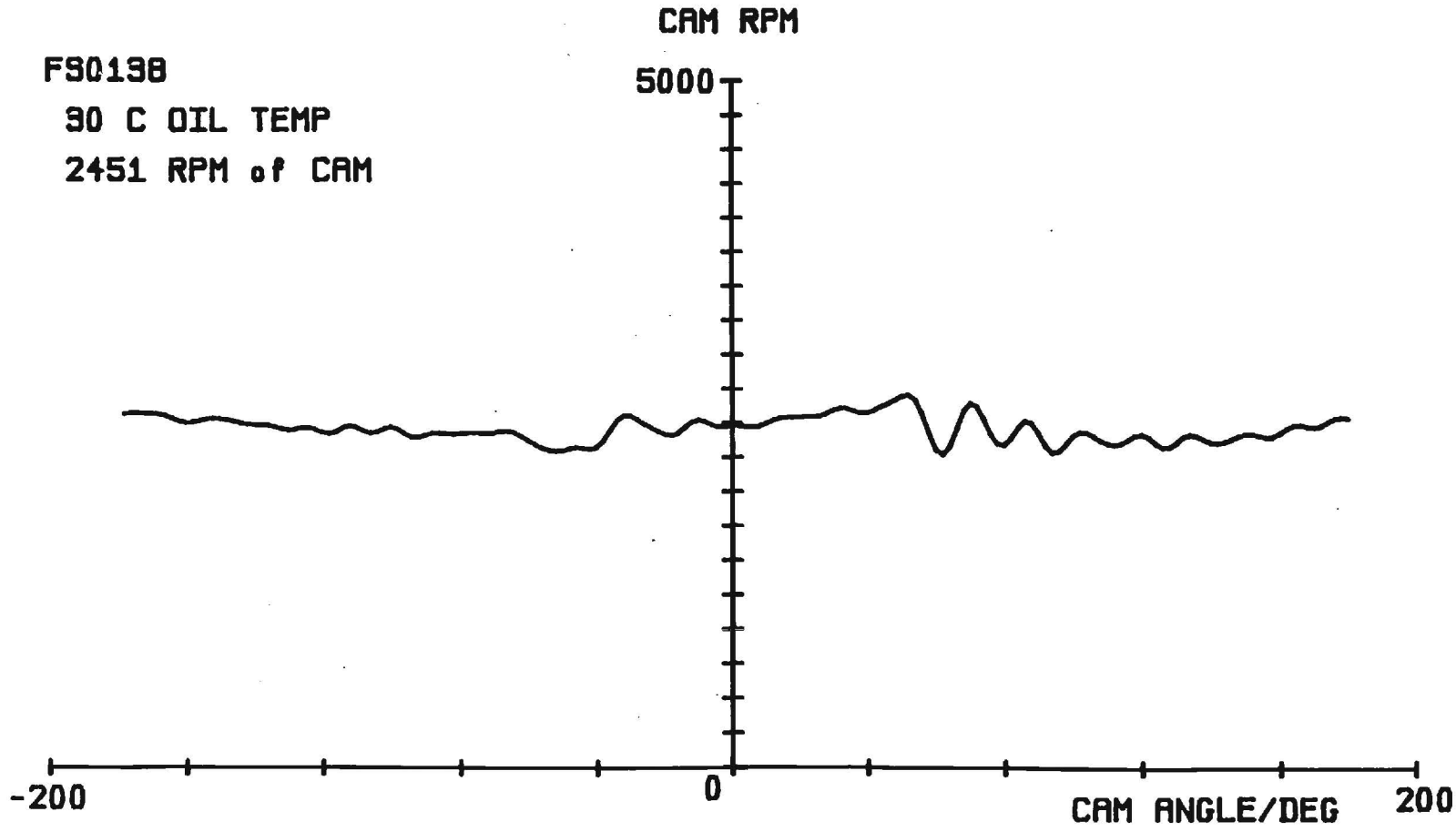


FIGURE 11c: Cam RPM

# APPENDIX A

## Surface Velocity Plots

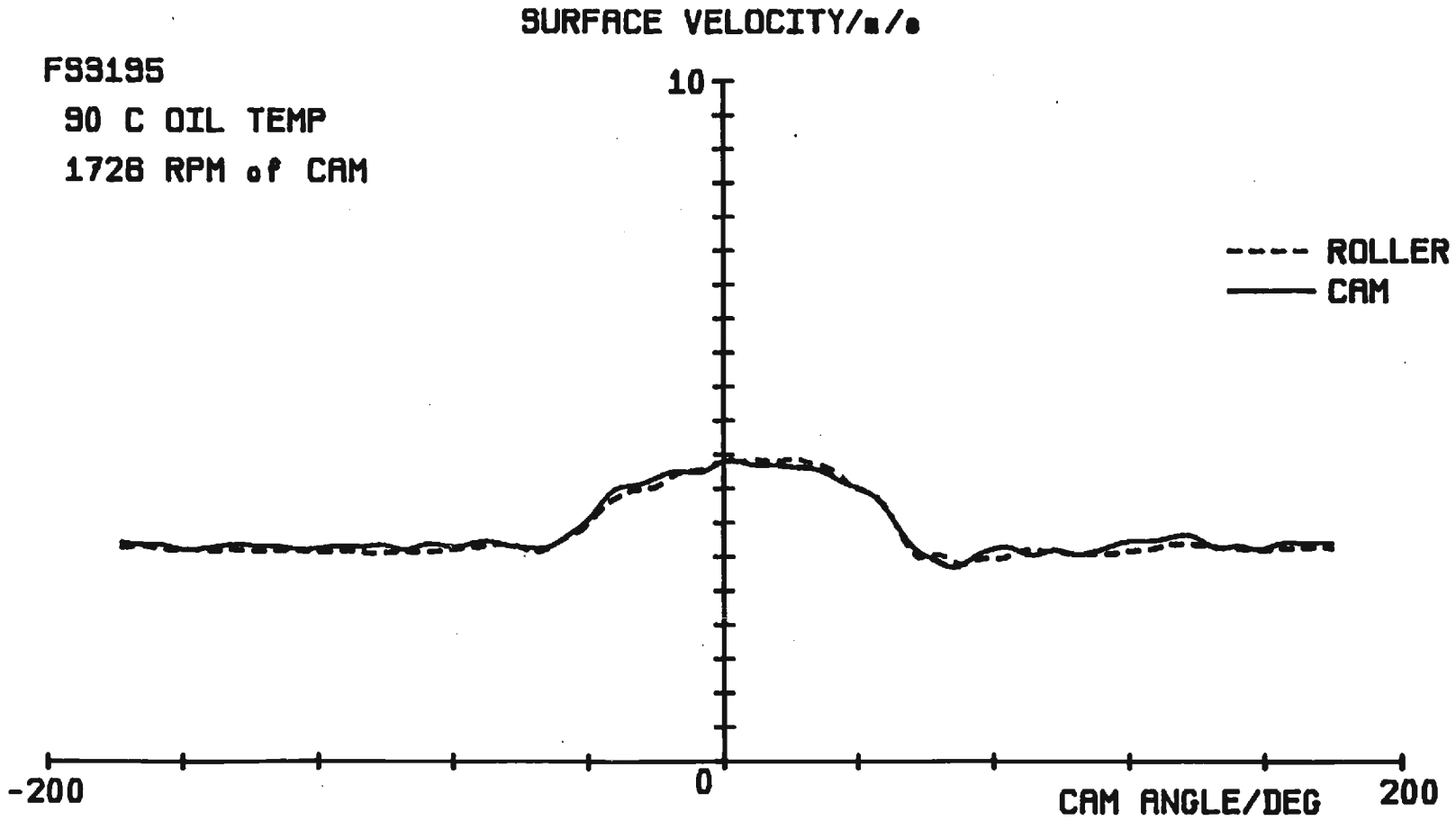
SURFACE VELOCITY/m/s
FS3195
90 C OIL TEMP
1726 RPM of CAM
10
ROLLER
CAM
-200
0
200
CAM ANGLE/DEG

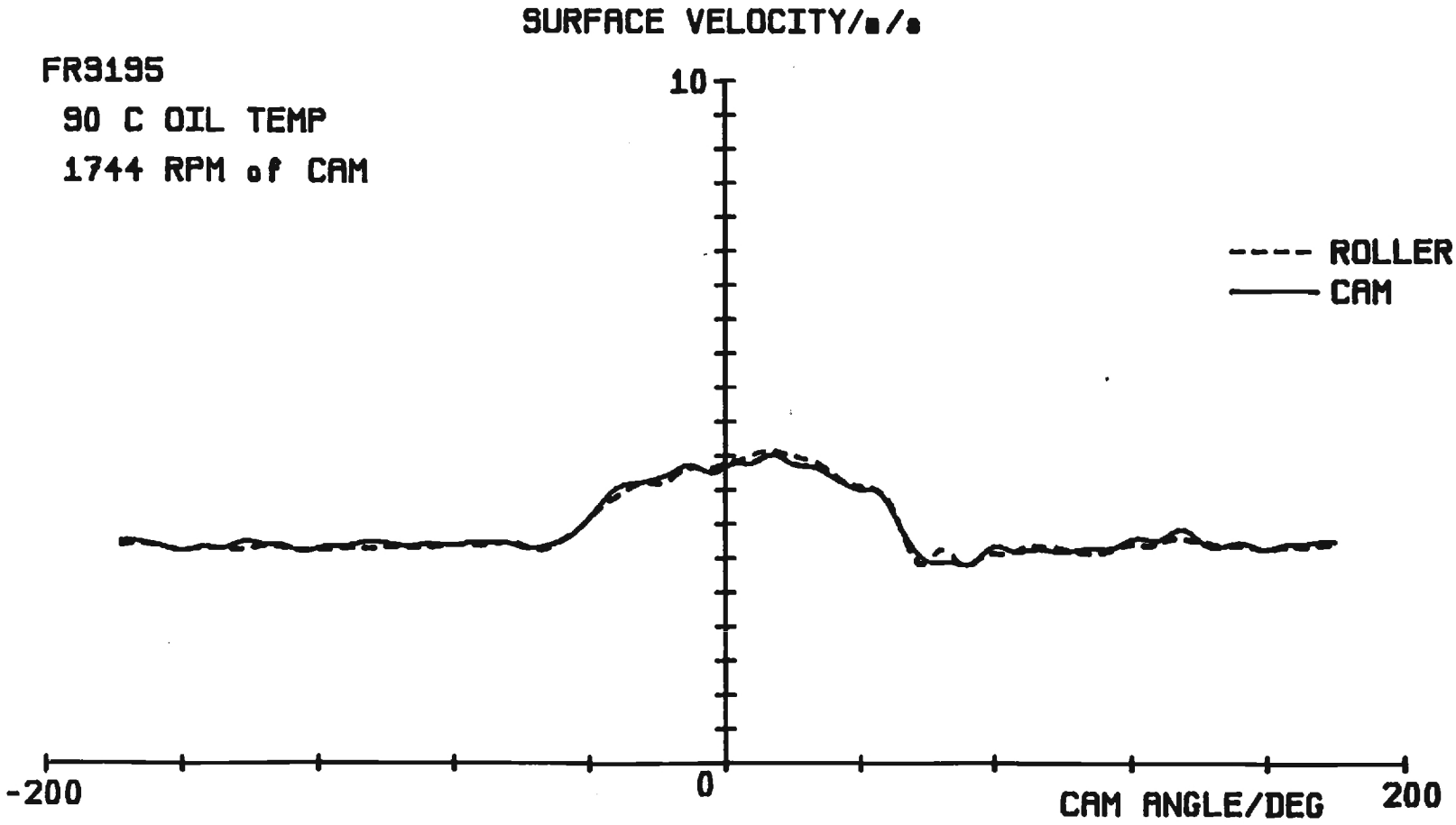
SURFACE VELOCITY/m/s
FR9195
90 C OIL TEMP
1744 RPM of CAM
10
ROLLER
CAM
-200
0
200
CAM ANGLE/DEG

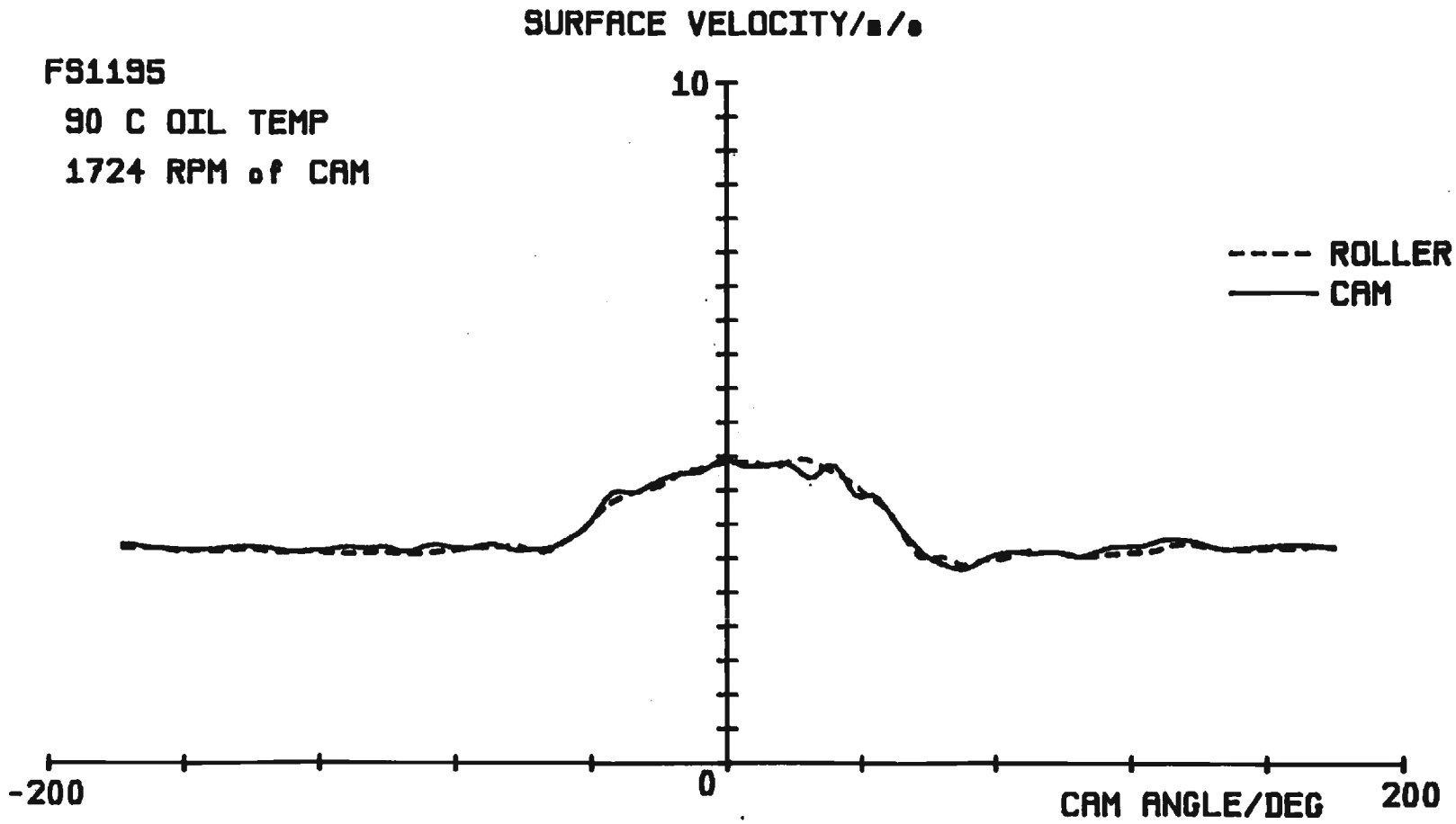
SURFACE VELOCITY/m/s
FS1195
90 C OIL TEMP
1724 RPM of CAM
10
ROLLER
CAM
-200
0
200
CAM ANGLE/DEG

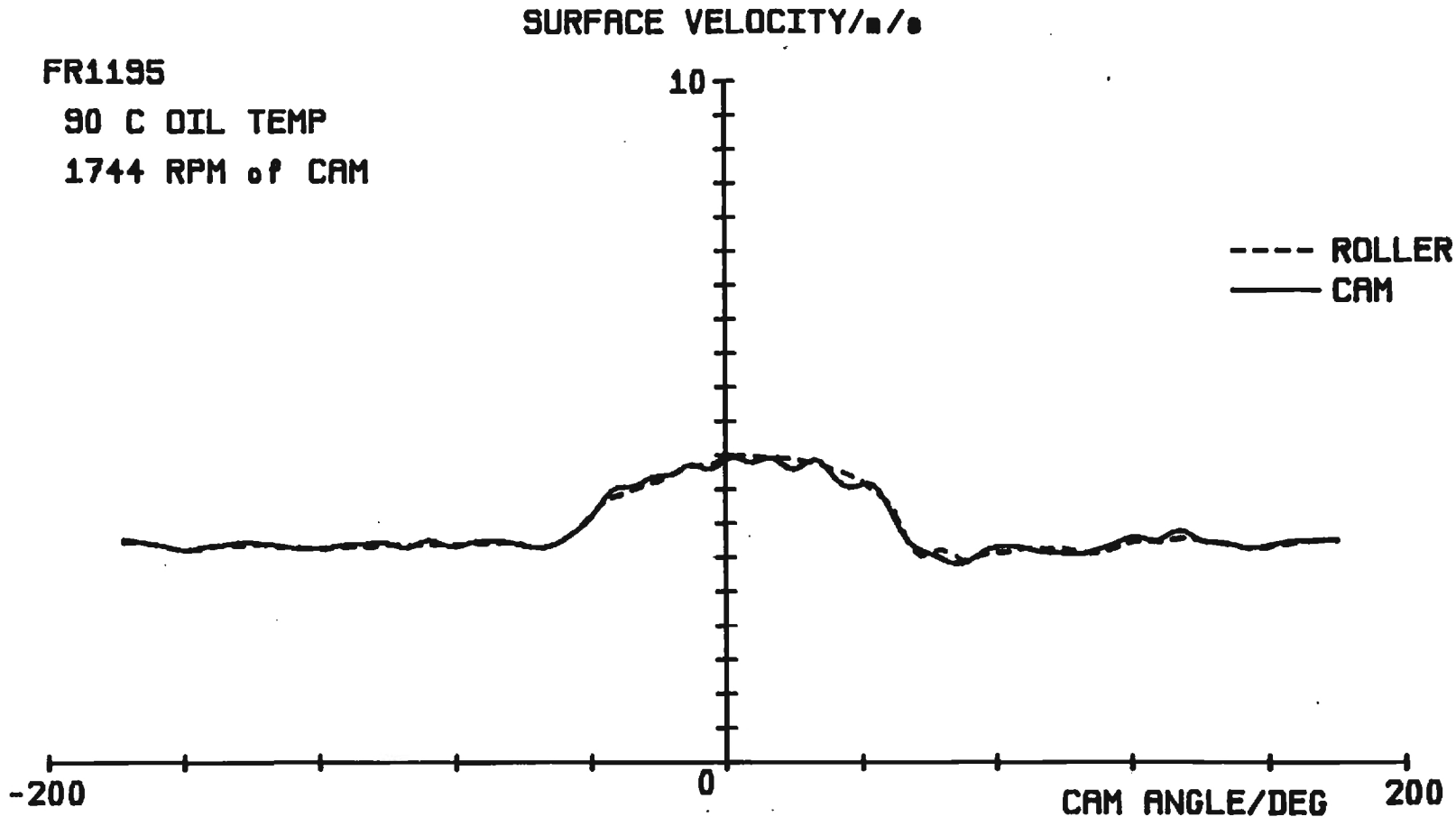
SURFACE VELOCITY/■/●
FR1195
90 C OIL TEMP
1744 RPM of CAM
10
---- ROLLER
—— CAM
-200
0
200
CAM ANGLE/DEG

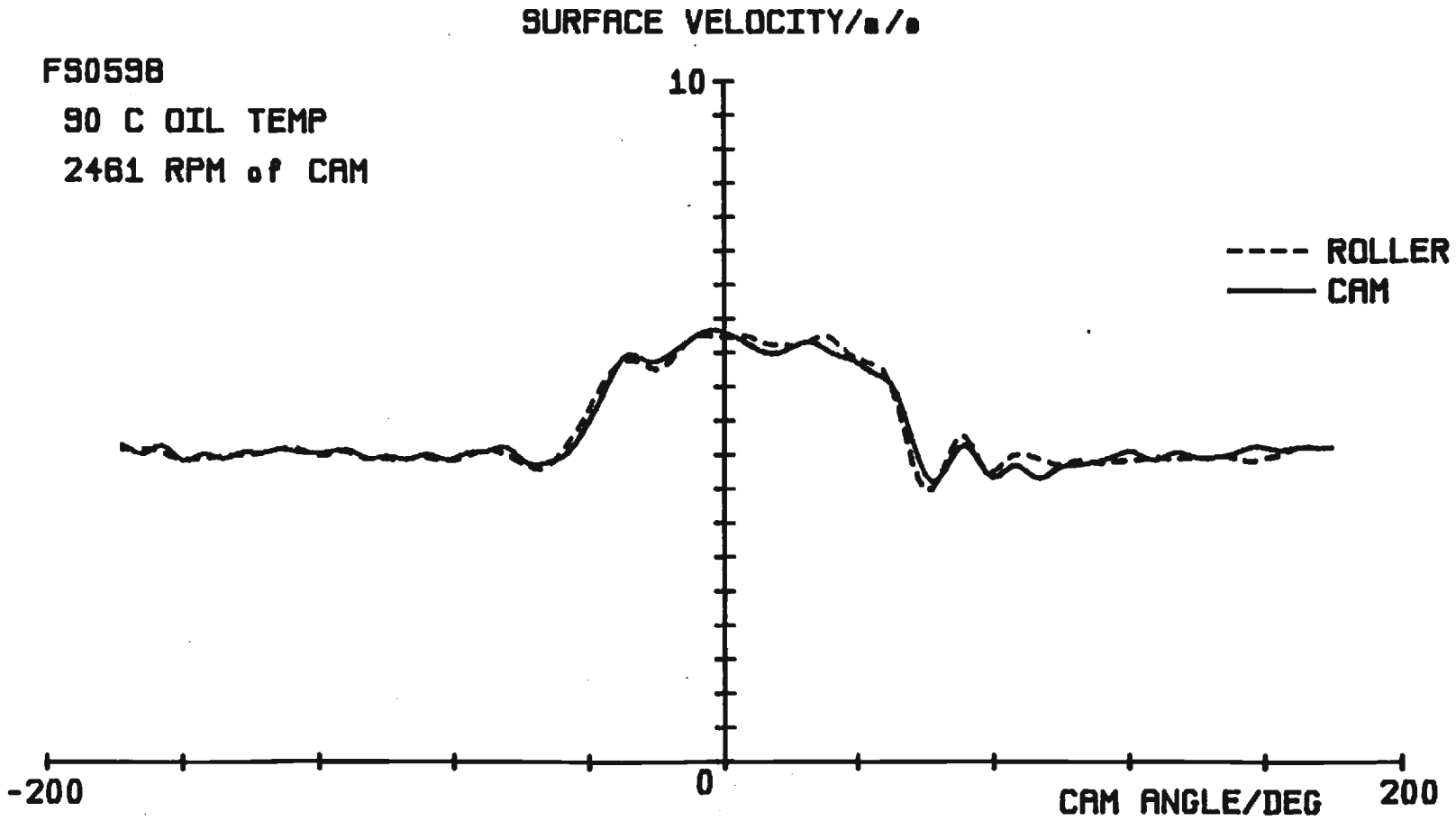
SURFACE VELOCITY/m/s
FS0598
90 C OIL TEMP
2461 RPM of CAM
10
ROLLER
CAM
-200
0
CAM ANGLE/DEG
200

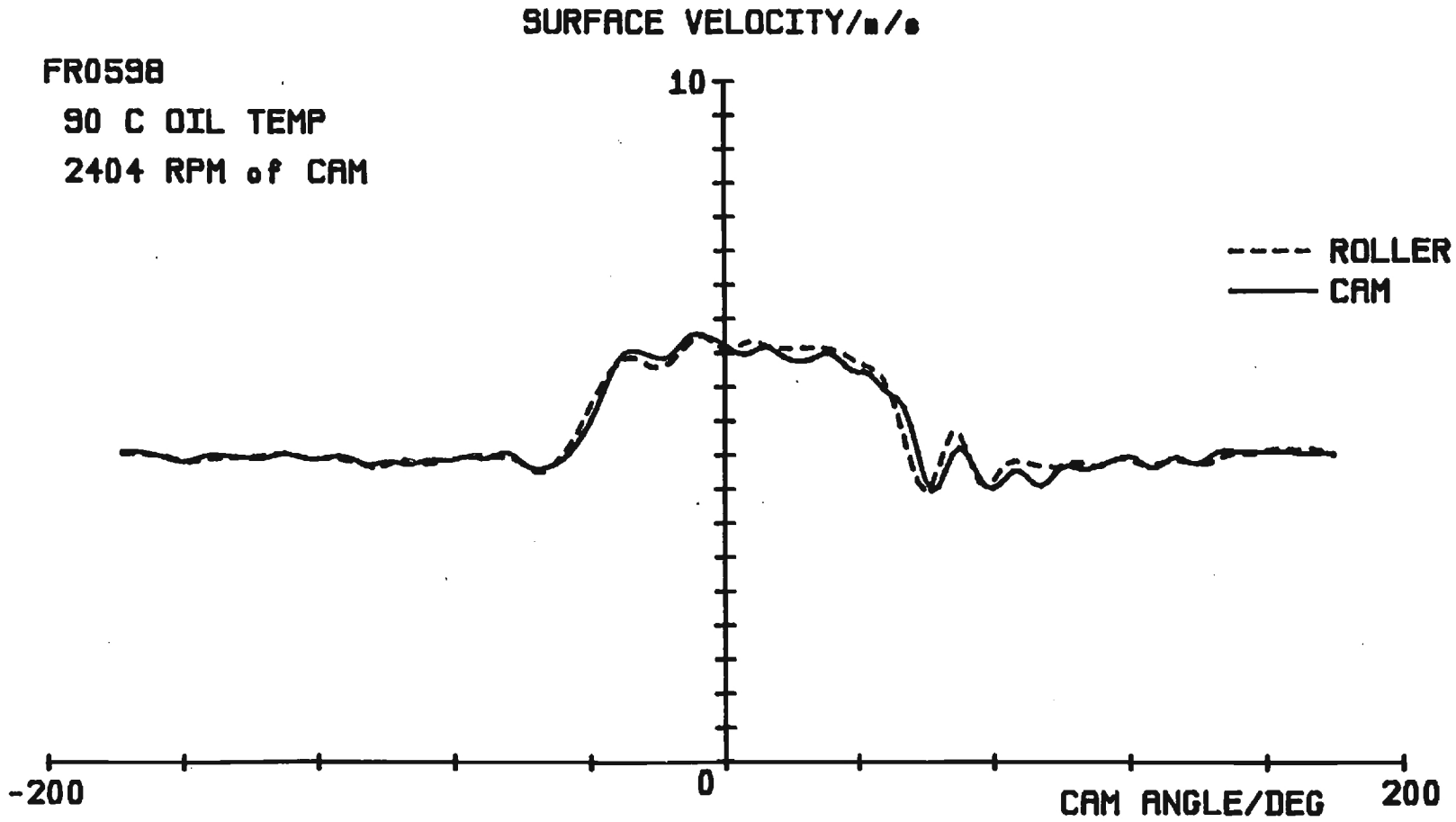
SURFACE VELOCITY/m/s
FR0598
90 C OIL TEMP
2404 RPM of CAM
10
ROLLER
CAM
-200
0
200
CAM ANGLE/DEG

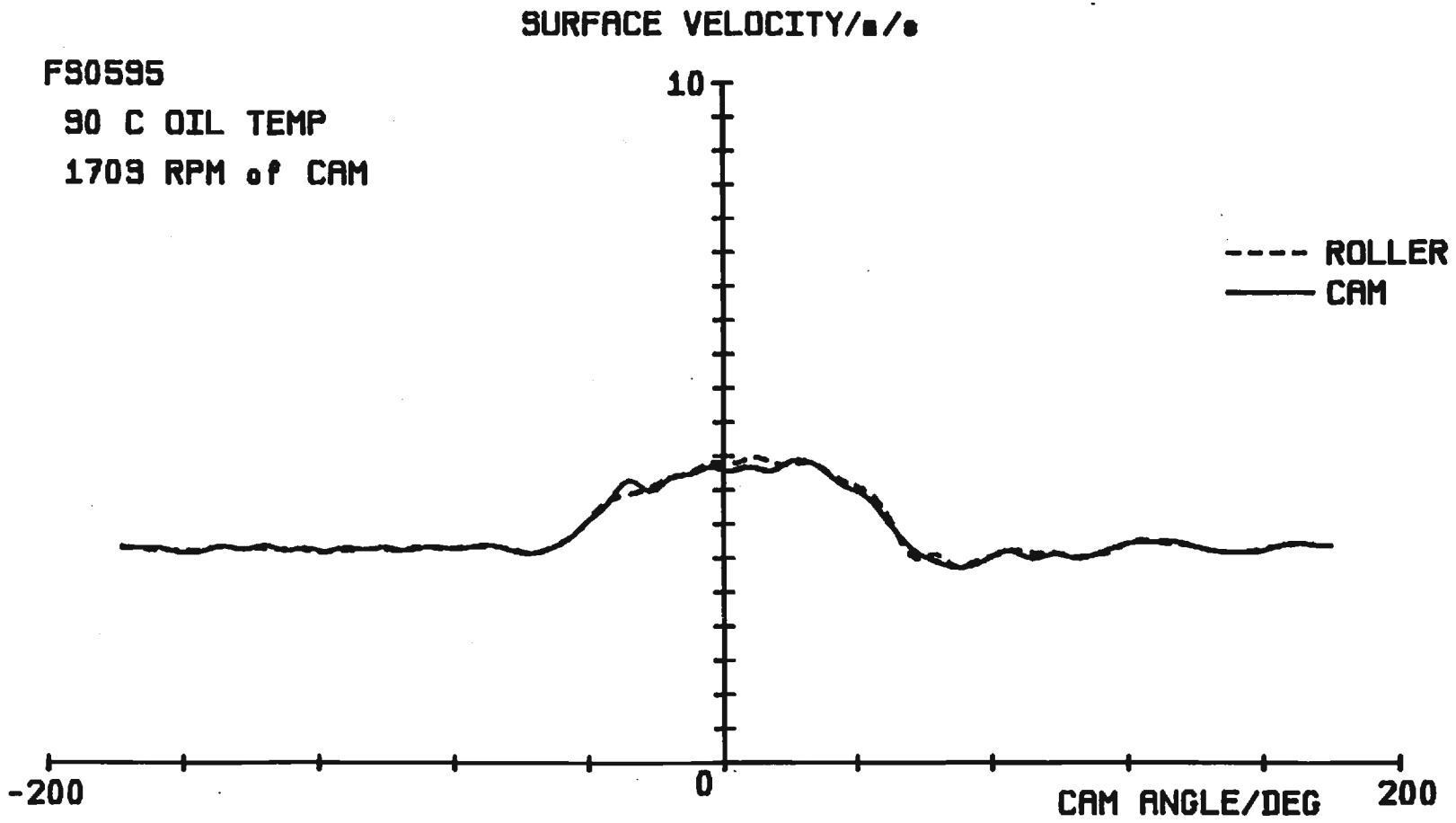
SURFACE VELOCITY/m/s
FS0595
90 C OIL TEMP
1709 RPM of CAM
10
ROLLER
CAM
-200
0
200
CAM ANGLE/DEG

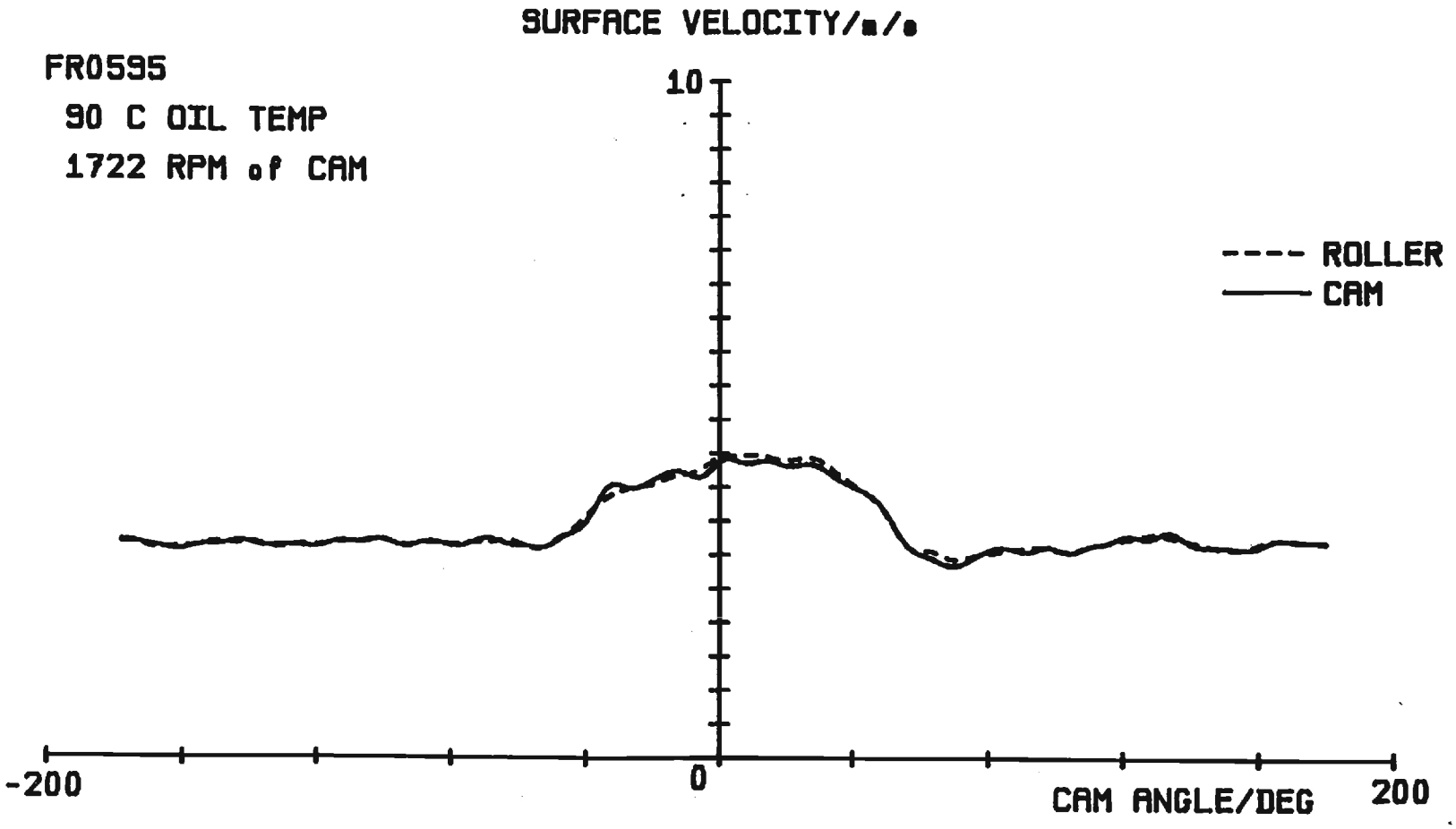
SURFACE VELOCITY/m/s
FR0595
90 C OIL TEMP
1722 RPM of CAM
10
ROLLER
CAM
-200
0
200
CAM ANGLE/DEG

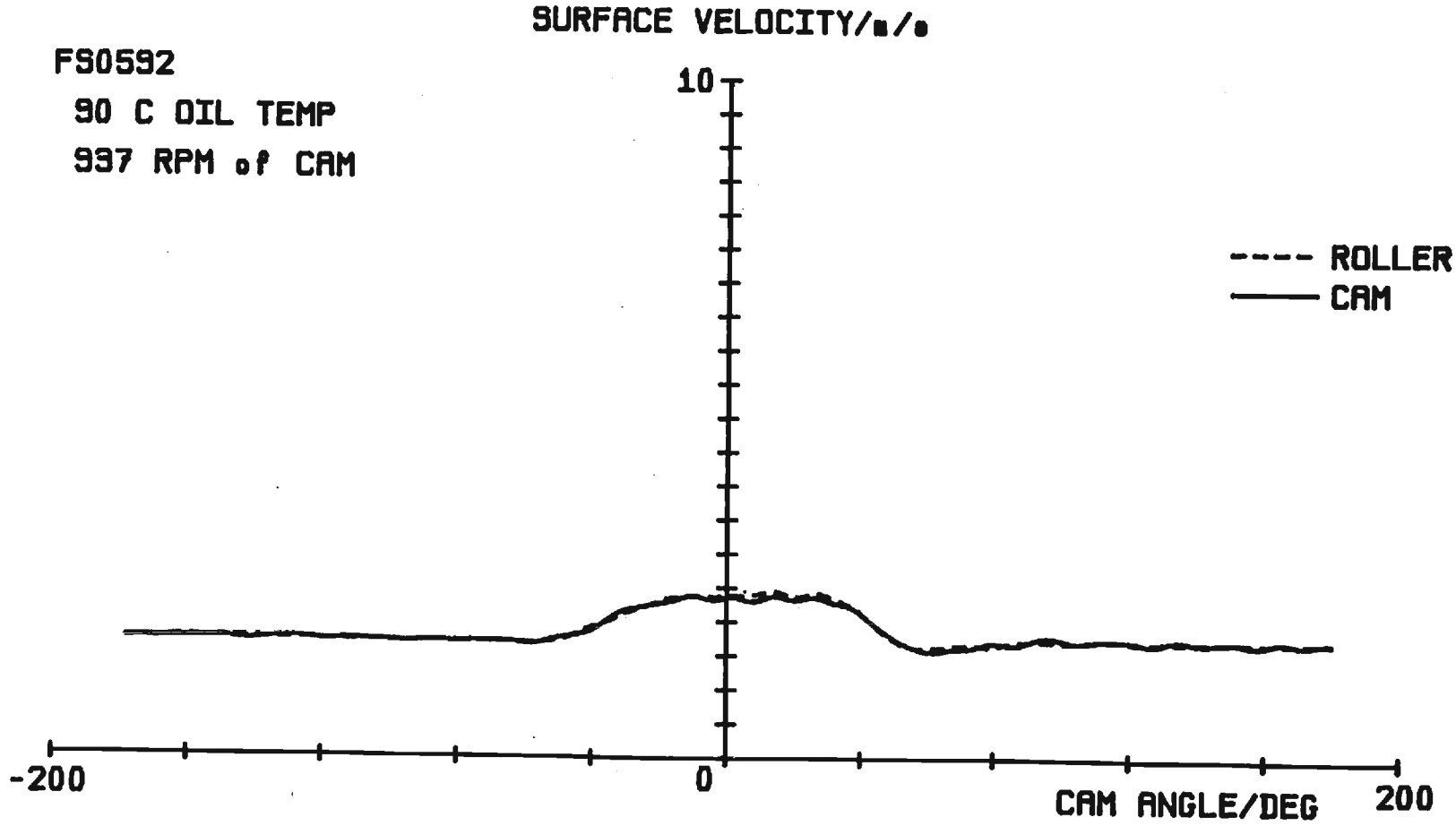
SURFACE VELOCITY/m/s
FS0592
90 C OIL TEMP
937 RPM of CAM
10
---- ROLLER
—— CAM
-200
0
CAM ANGLE/DEG
200

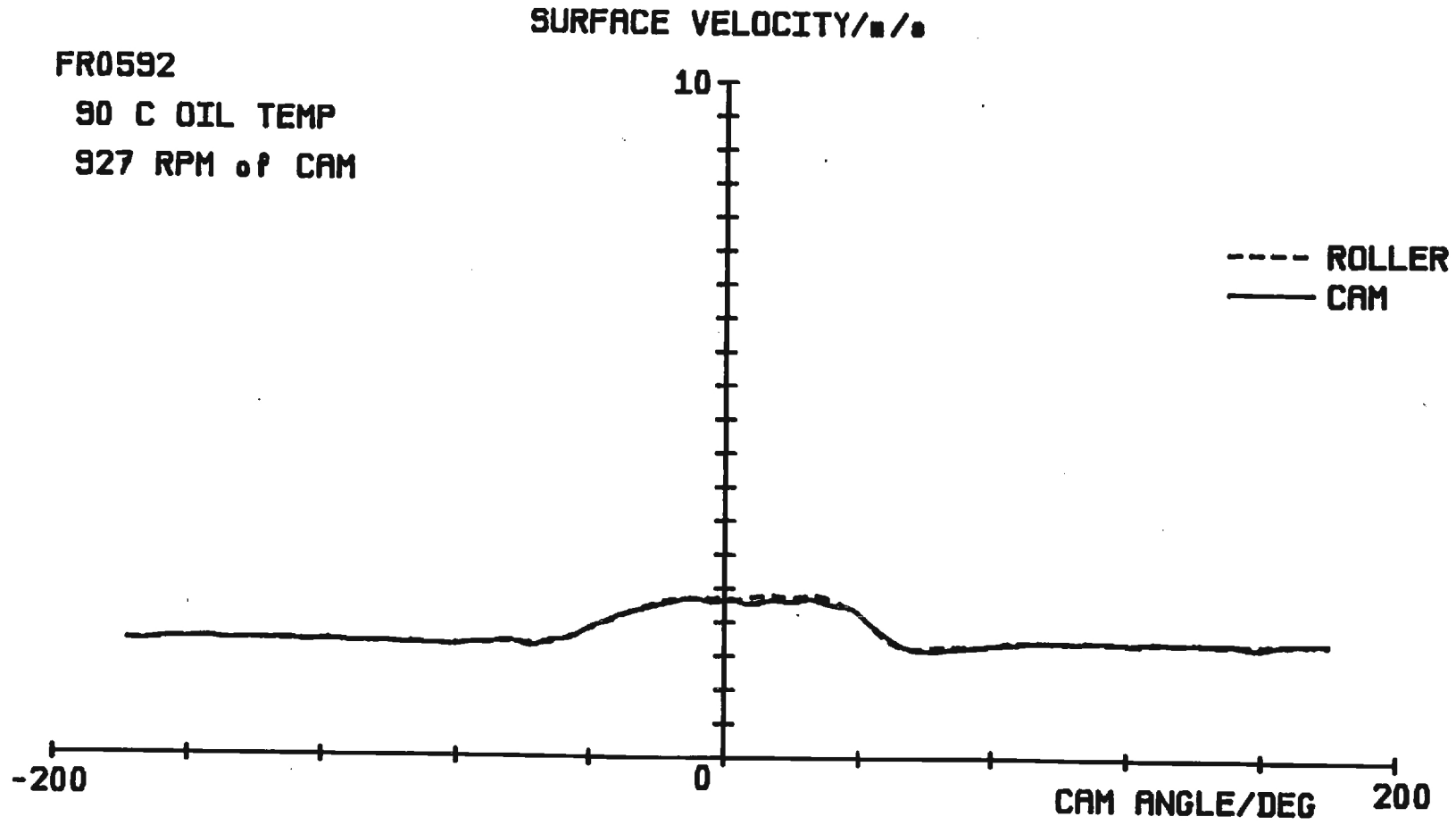
SURFACE VELOCITY/m/s
FR0592
90 C OIL TEMP
927 RPM of CAM
10
ROLLER
CAM
-200
0
200
CAM ANGLE/DEG

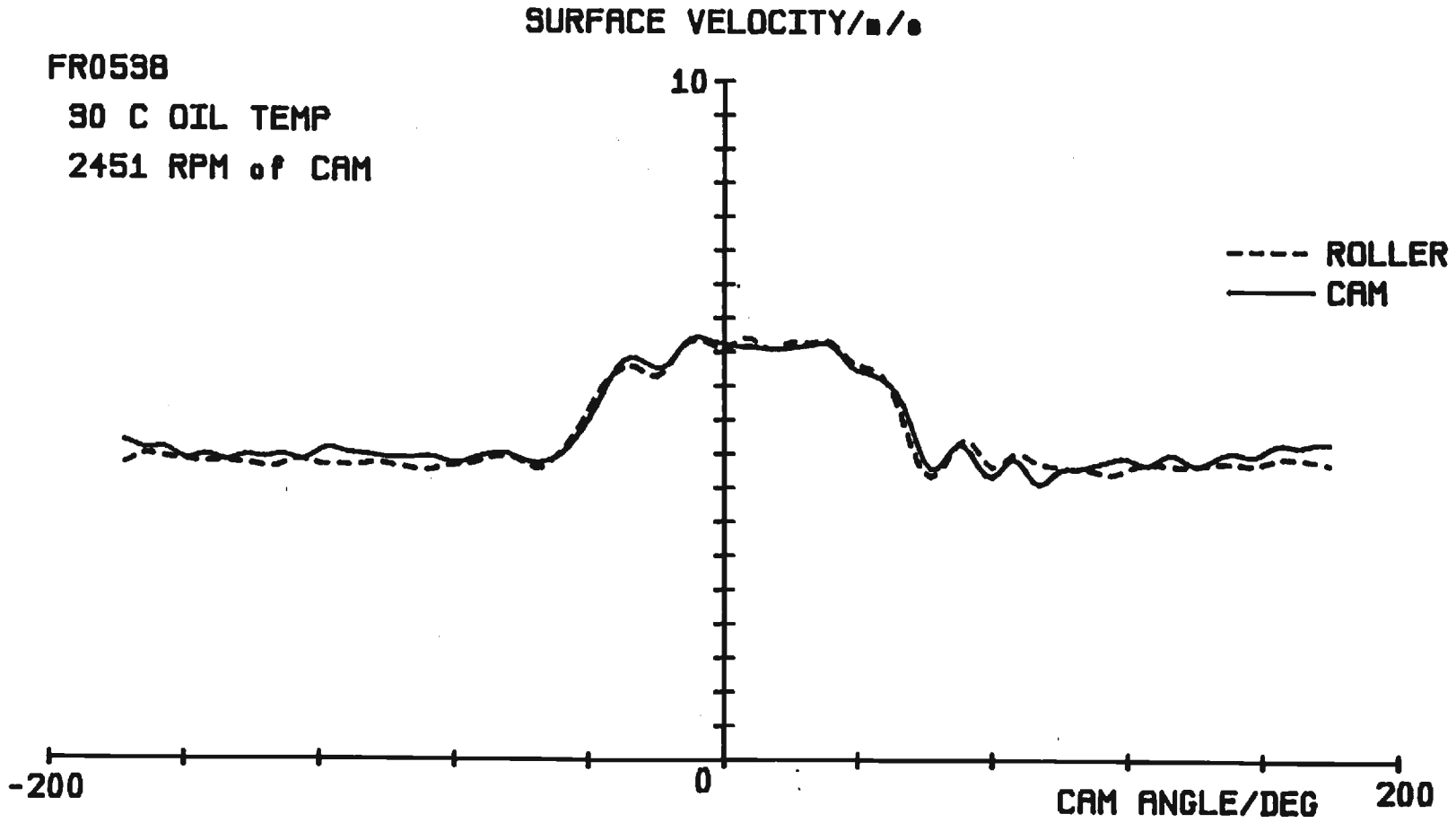
SURFACE VELOCITY/m/s
FR0538
30 C OIL TEMP
2451 RPM of CAM
10
ROLLER
CAM
-200
0
200
CAM ANGLE/DEG

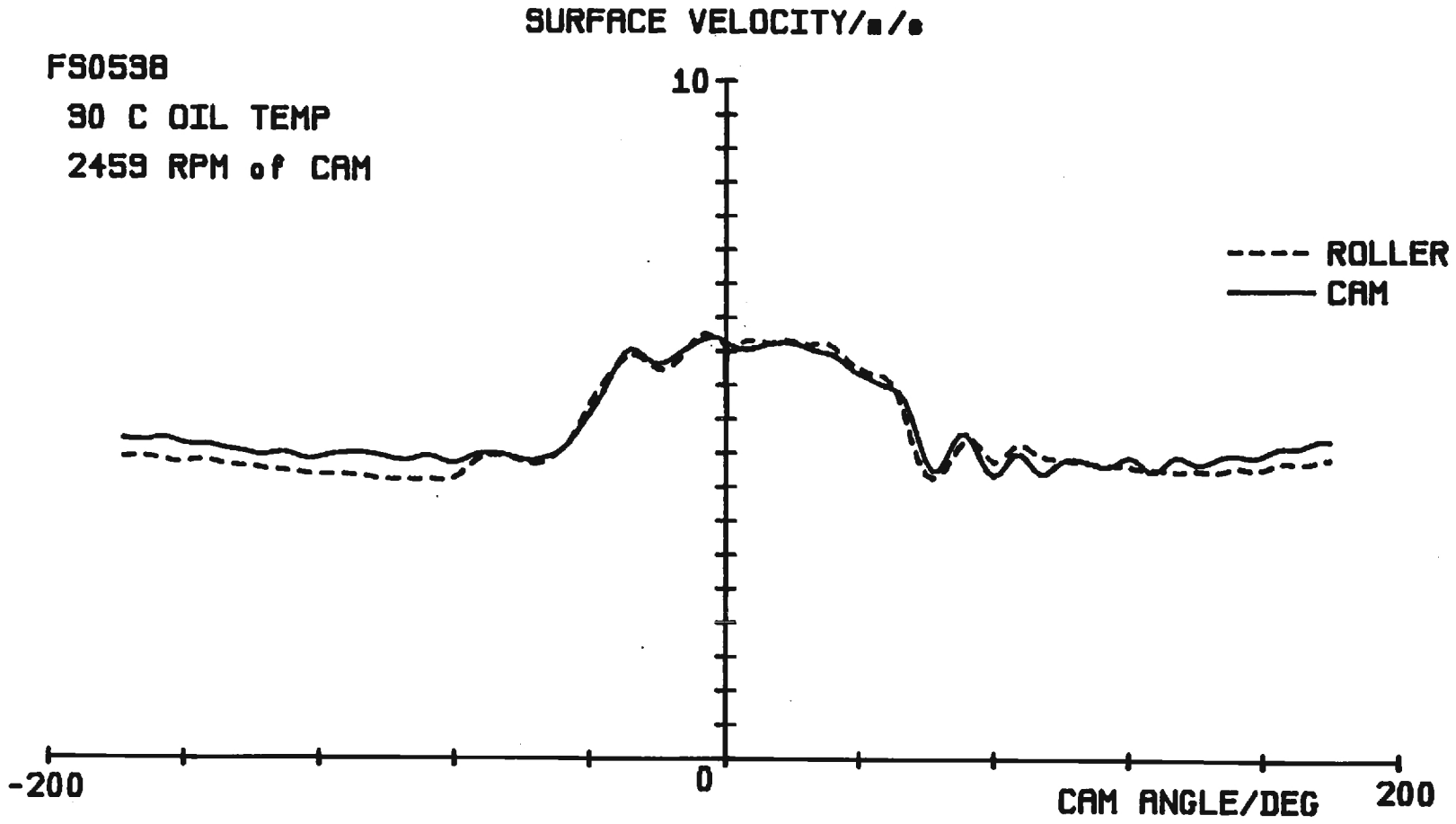
SURFACE VELOCITY/m/s
FS0538
30 C OIL TEMP
2459 RPM of CAM
10
ROLLER
CAM
-200
0
200
CAM ANGLE/DEG

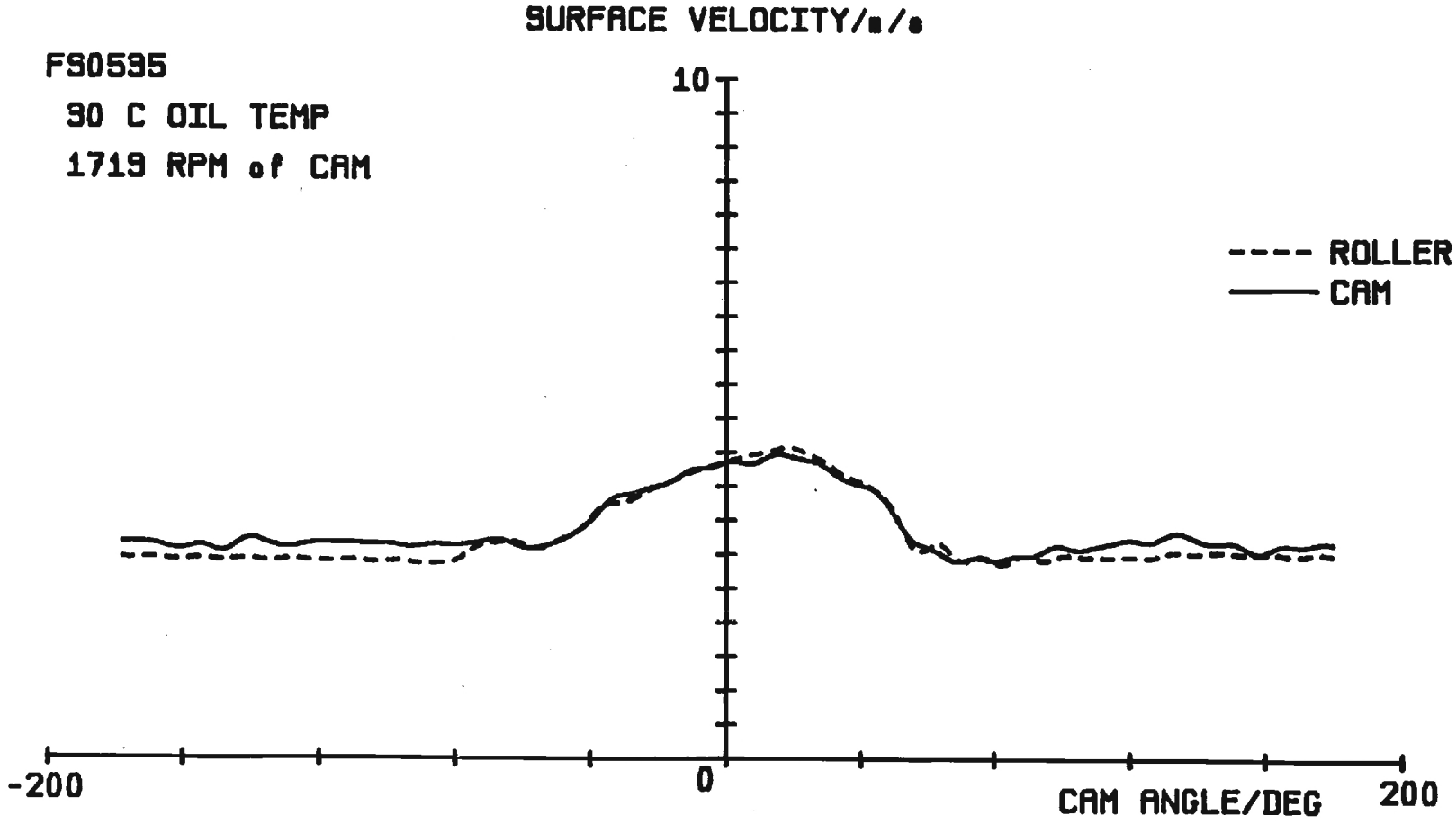
SURFACE VELOCITY/m/s
FS0595
30 C OIL TEMP
1719 RPM of CAM
10
ROLLER
CAM
-200
0
200
CAM ANGLE/DEG

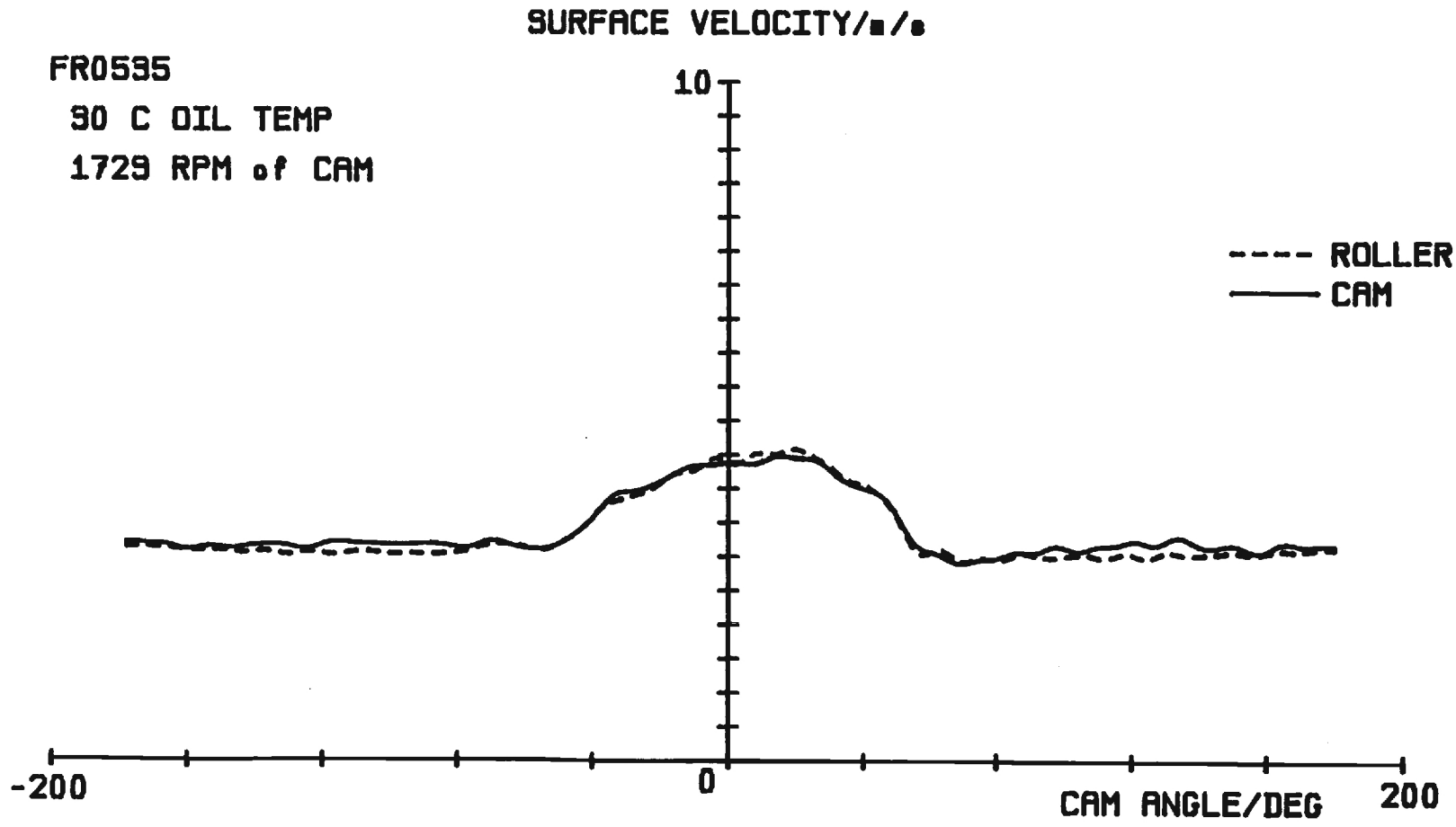
SURFACE VELOCITY/m/s
FR0535
90 C OIL TEMP
1729 RPM of CAM
10
ROLLER
CAM
-200
0
200
CAM ANGLE/DEG

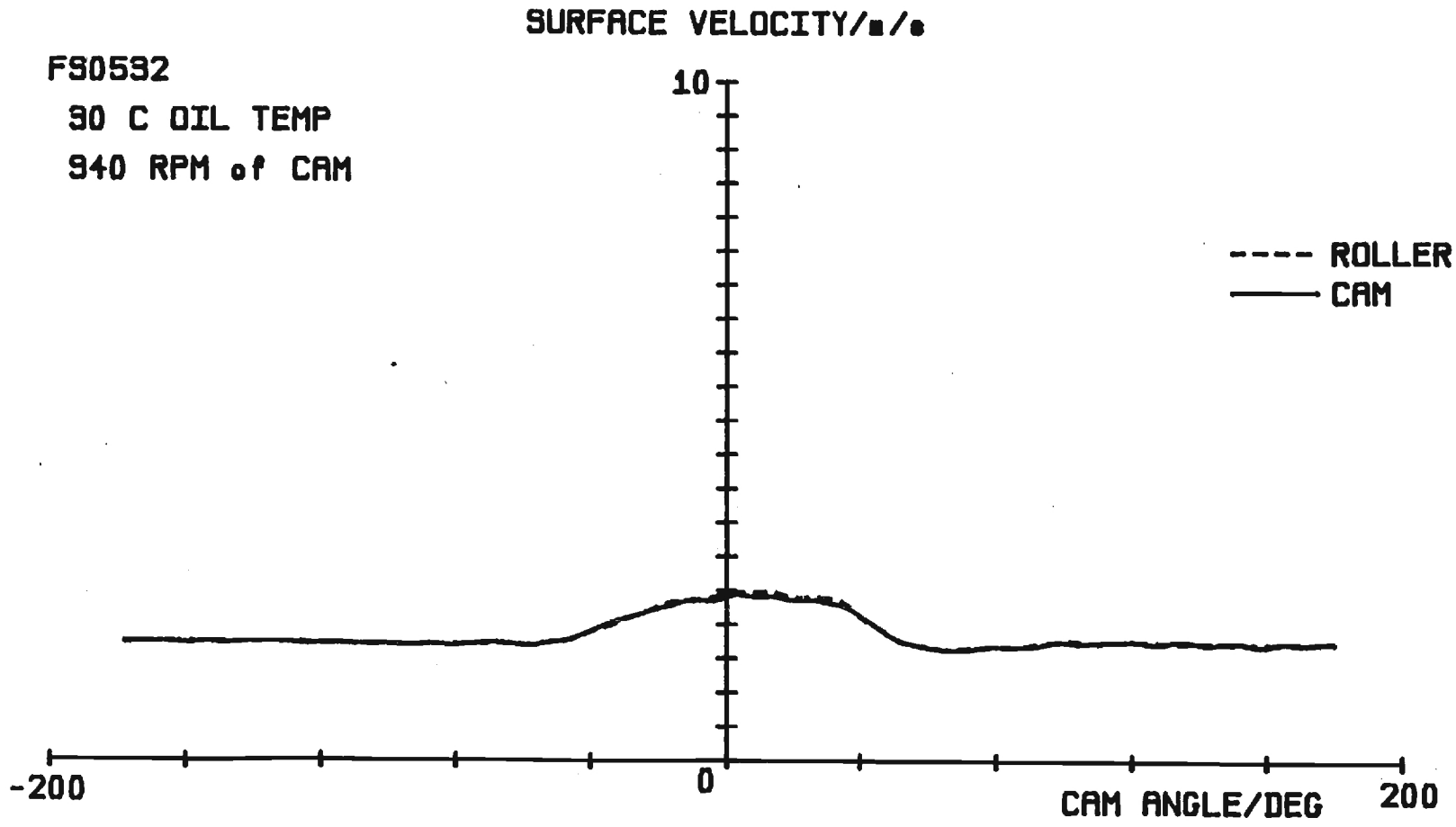
SURFACE VELOCITY/m/s
FS0532
30 C OIL TEMP
940 RPM of CAM
10
ROLLER
CAM
-200
0
200
CAM ANGLE/DEG

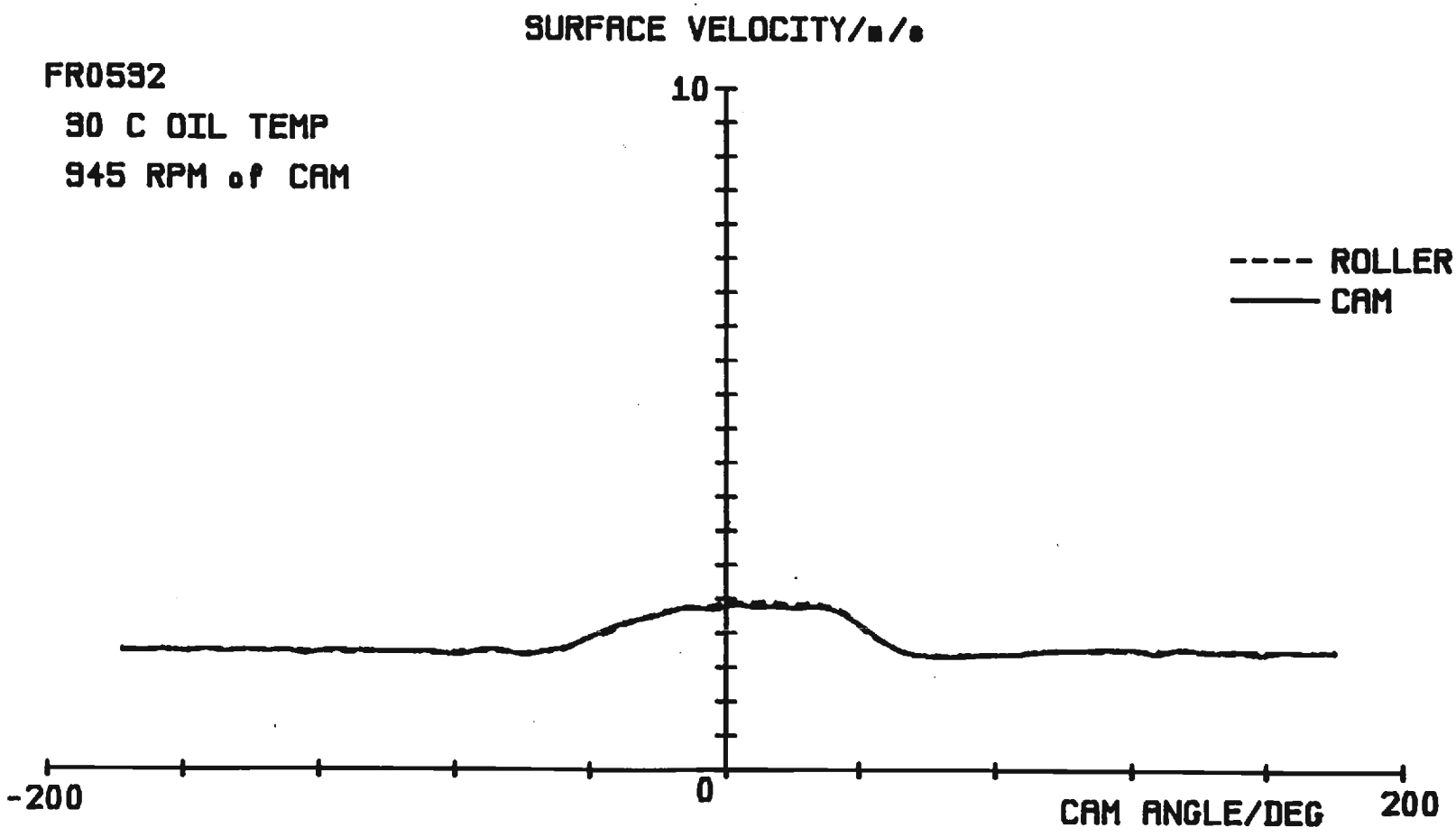
SURFACE VELOCITY/m/s
FR0532
90 C OIL TEMP
945 RPM of CAM
10
---- ROLLER
—— CAM
-200
0
CAM ANGLE/DEG
200

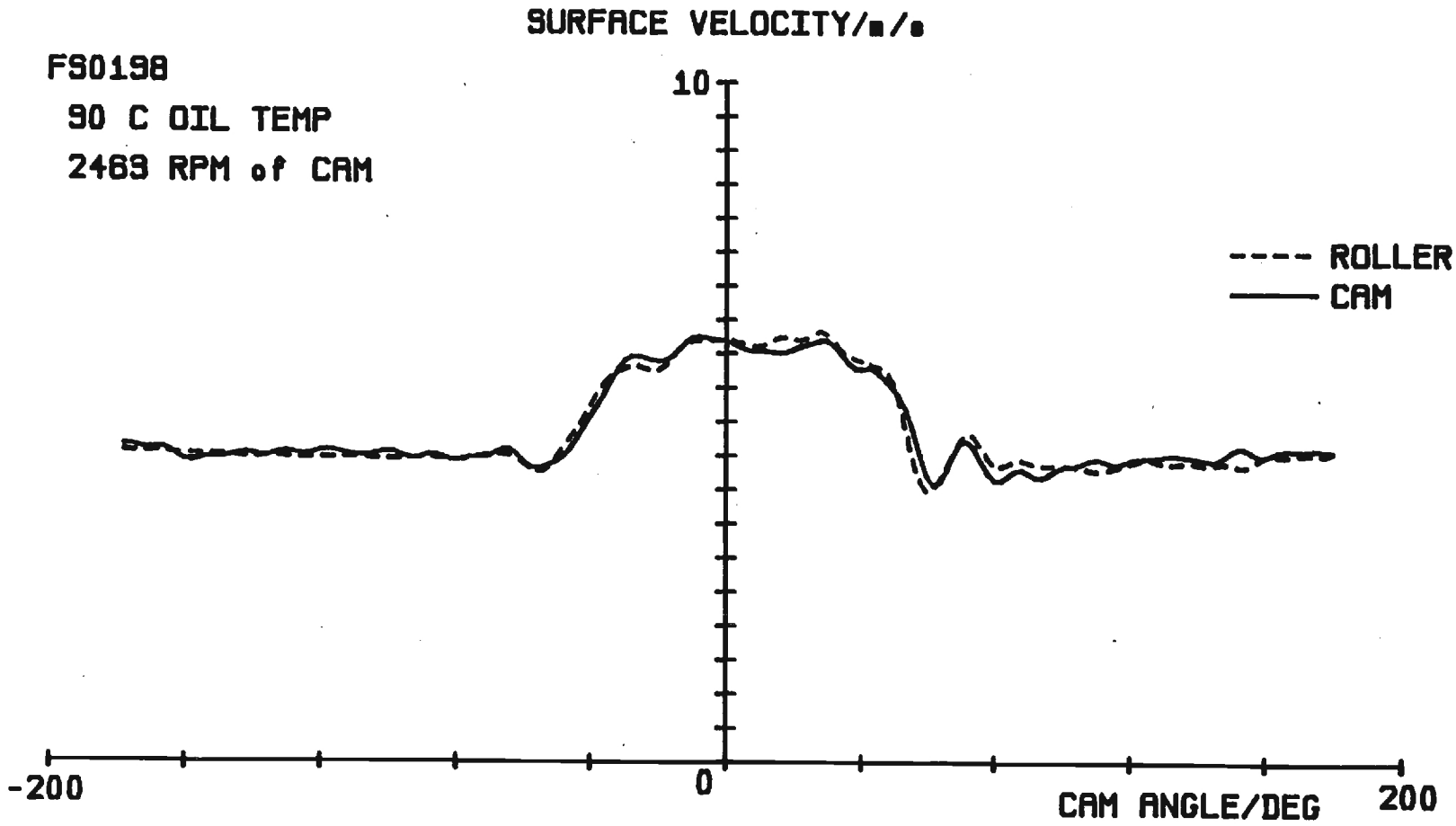
SURFACE VELOCITY/m/s
FS0198
90 C OIL TEMP
2469 RPM of CAM
10
ROLLER
CAM
-200
0
CAM ANGLE/DEG
200

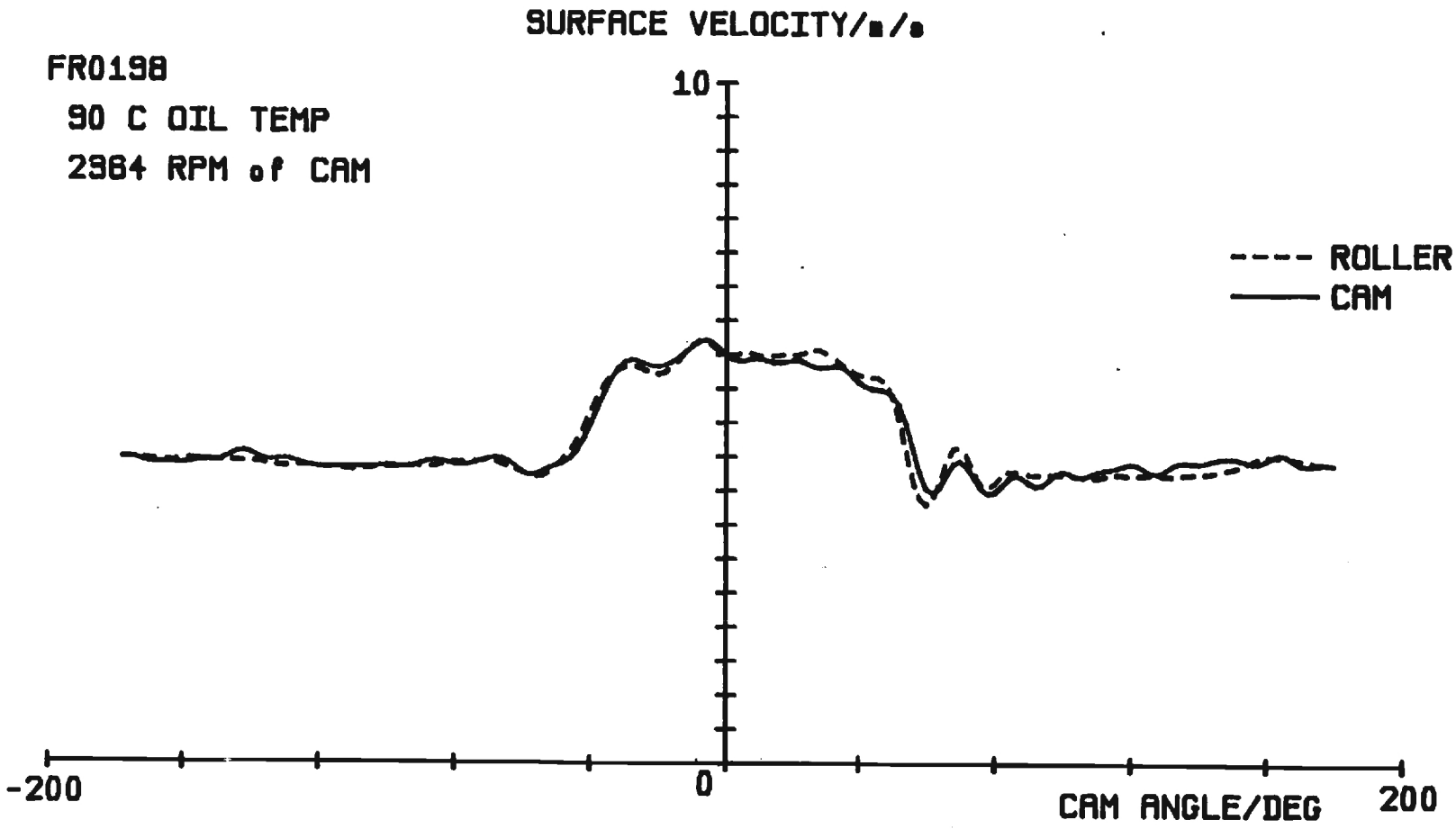
SURFACE VELOCITY/m/s
FR0198
90 C OIL TEMP
2384 RPM of CAM
10
ROLLER
CAM
-200
0
CAM ANGLE/DEG
200

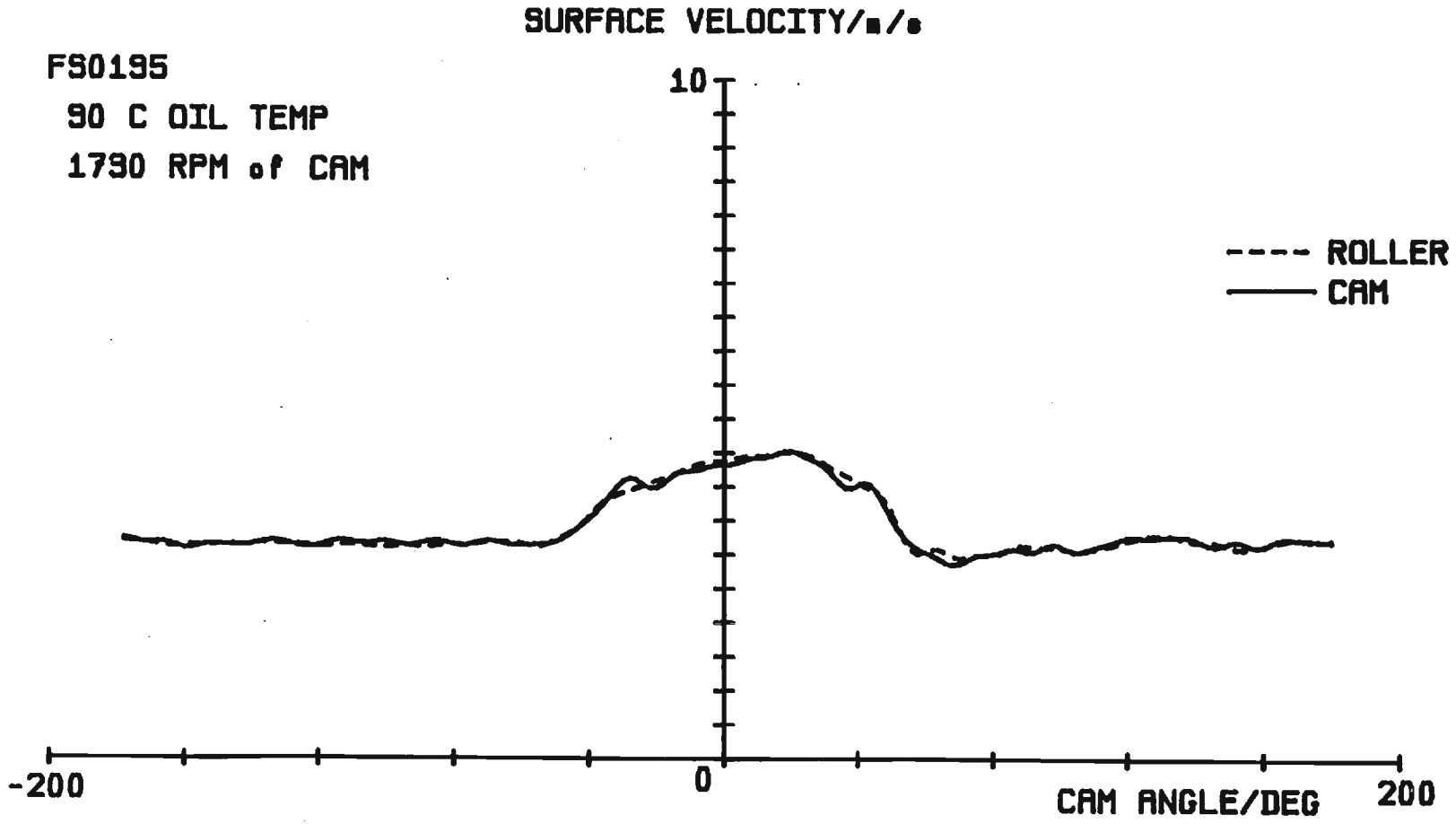
SURFACE VELOCITY/m/s
FS0195
90 C OIL TEMP
1730 RPM of CAM
10
ROLLER
CAM
-200
0
CAM ANGLE/DEG
200

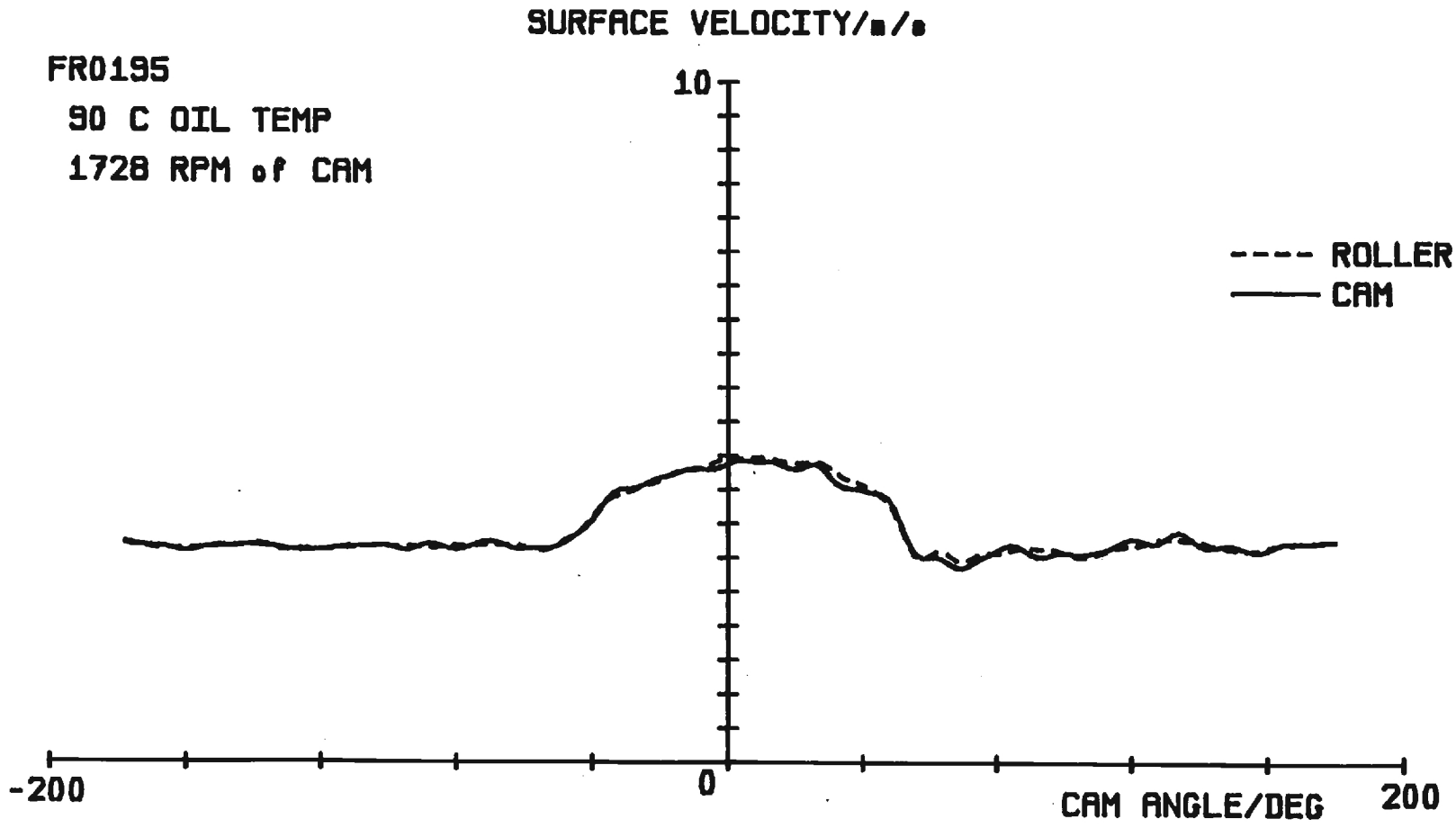
SURFACE VELOCITY/m/s
FR0195
90 C OIL TEMP
1728 RPM of CAM
10
ROLLER
CAM
-200
0
200
CAM ANGLE/DEG

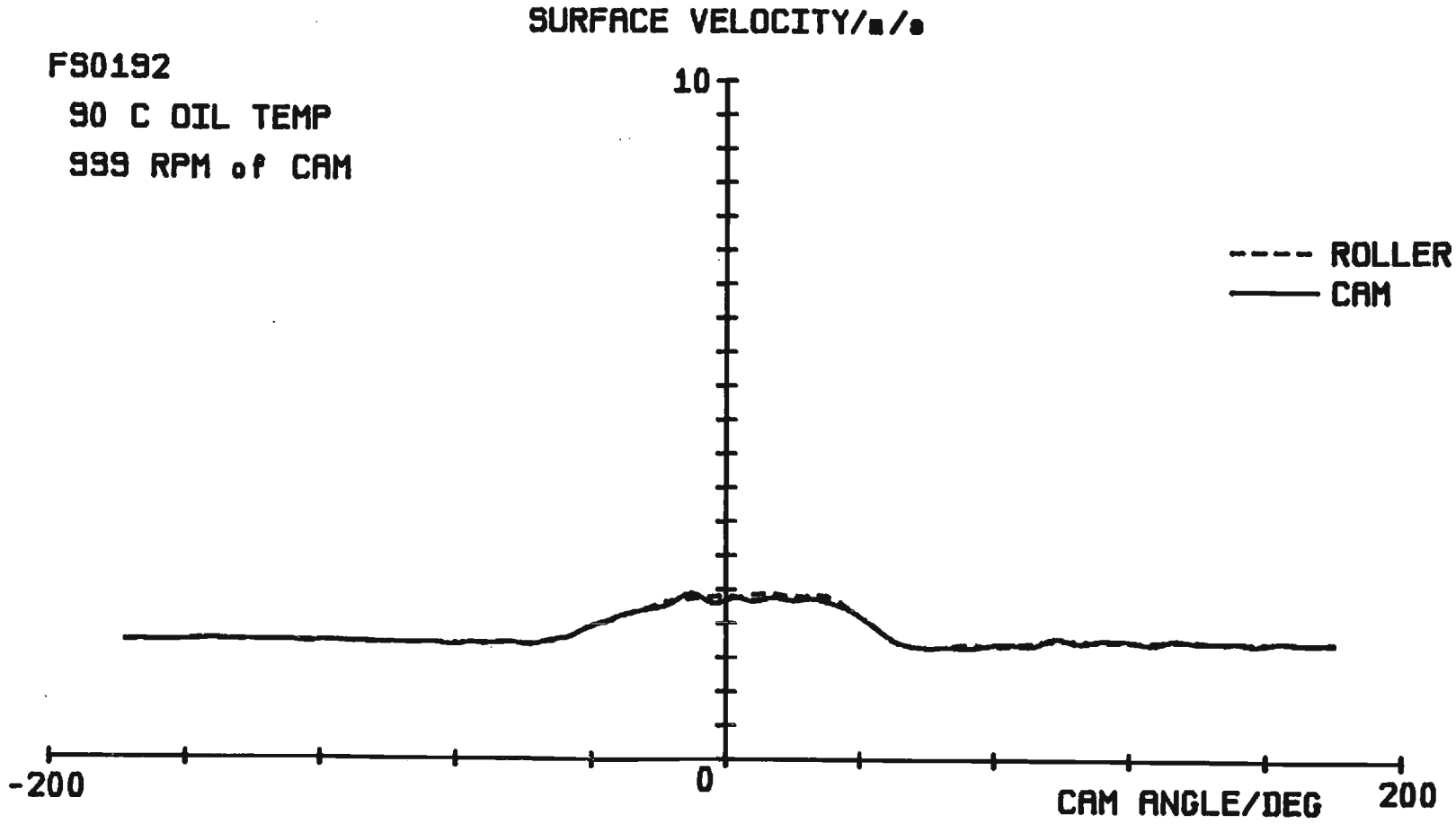
SURFACE VELOCITY/m/s
FS0192
90 C OIL TEMP
999 RPM of CAM
10
ROLLER
CAM
-200
0
200
CAM ANGLE/DEG

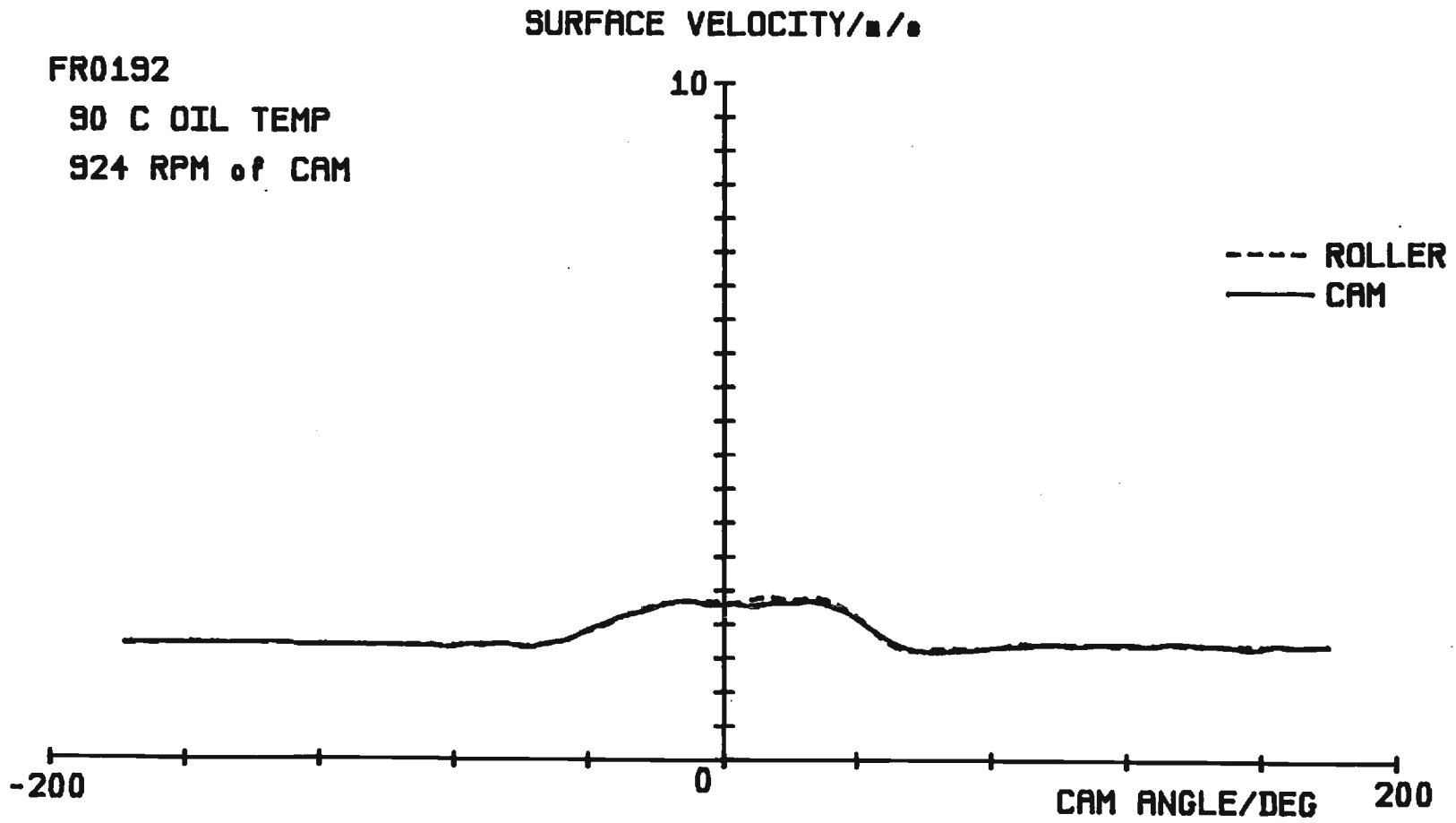
SURFACE VELOCITY/m/s
FR0192
90 C OIL TEMP
924 RPM of CAM
10
ROLLER
CAM
-200
0
200
CAM ANGLE/DEG

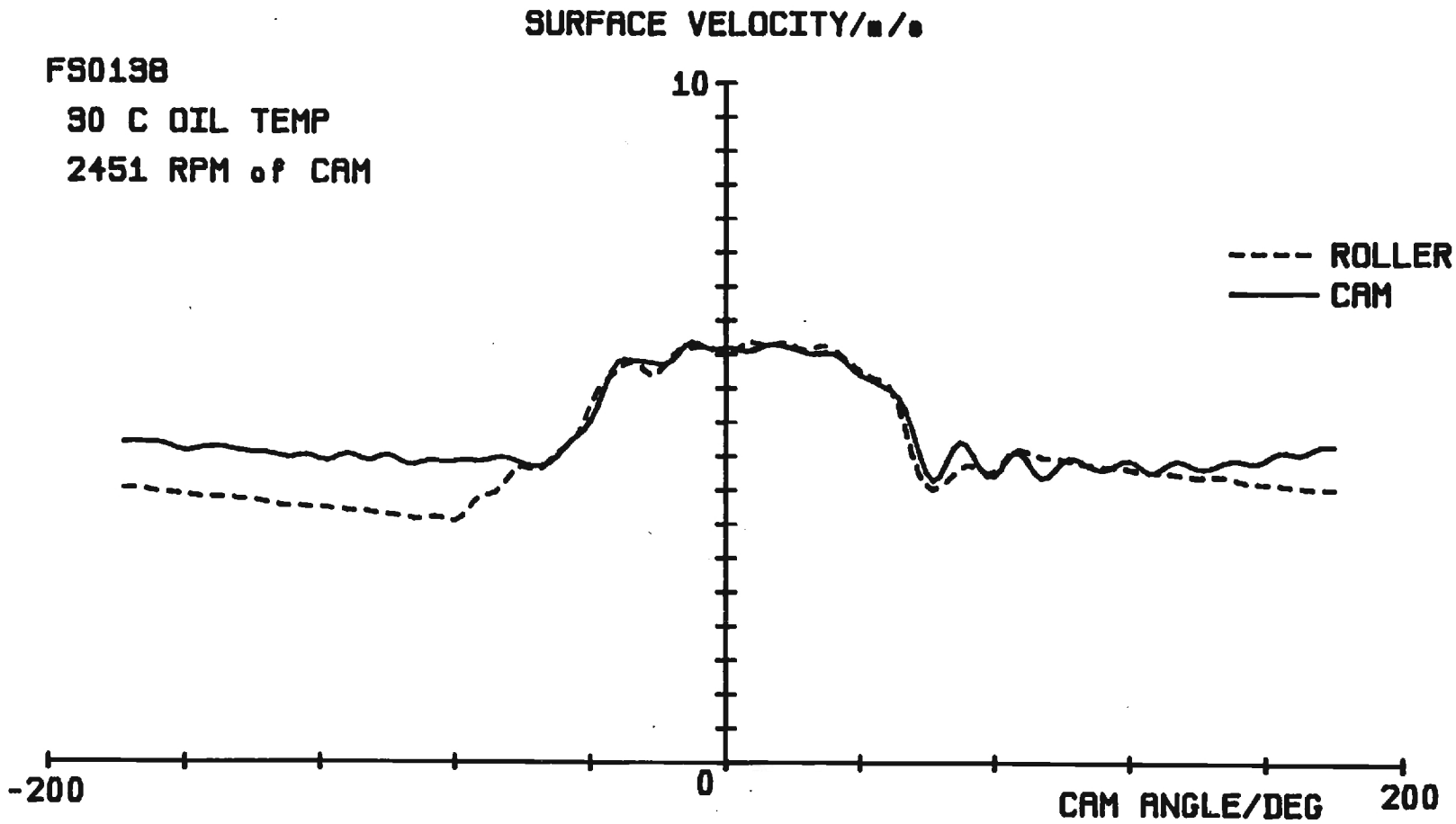
SURFACE VELOCITY/m/s
FS0138
30 C OIL TEMP
2451 RPM of CAM
10
ROLLER
CAM
-200
0
200
CAM ANGLE/DEG

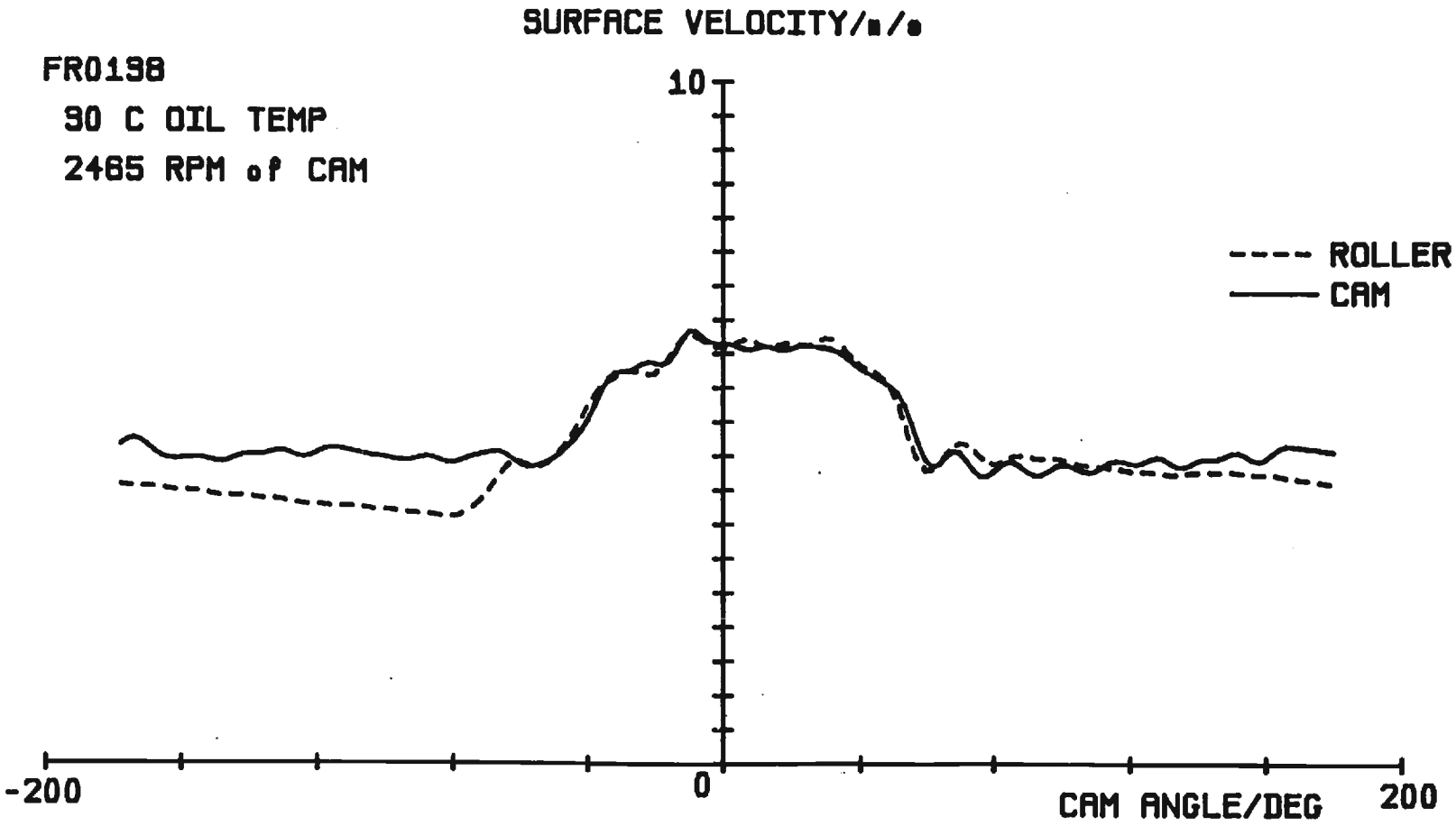
SURFACE VELOCITY/m/s
FR0198
90 C OIL TEMP
2465 RPM of CAM
10
ROLLER
CAM
-200
0
200
CAM ANGLE/DEG

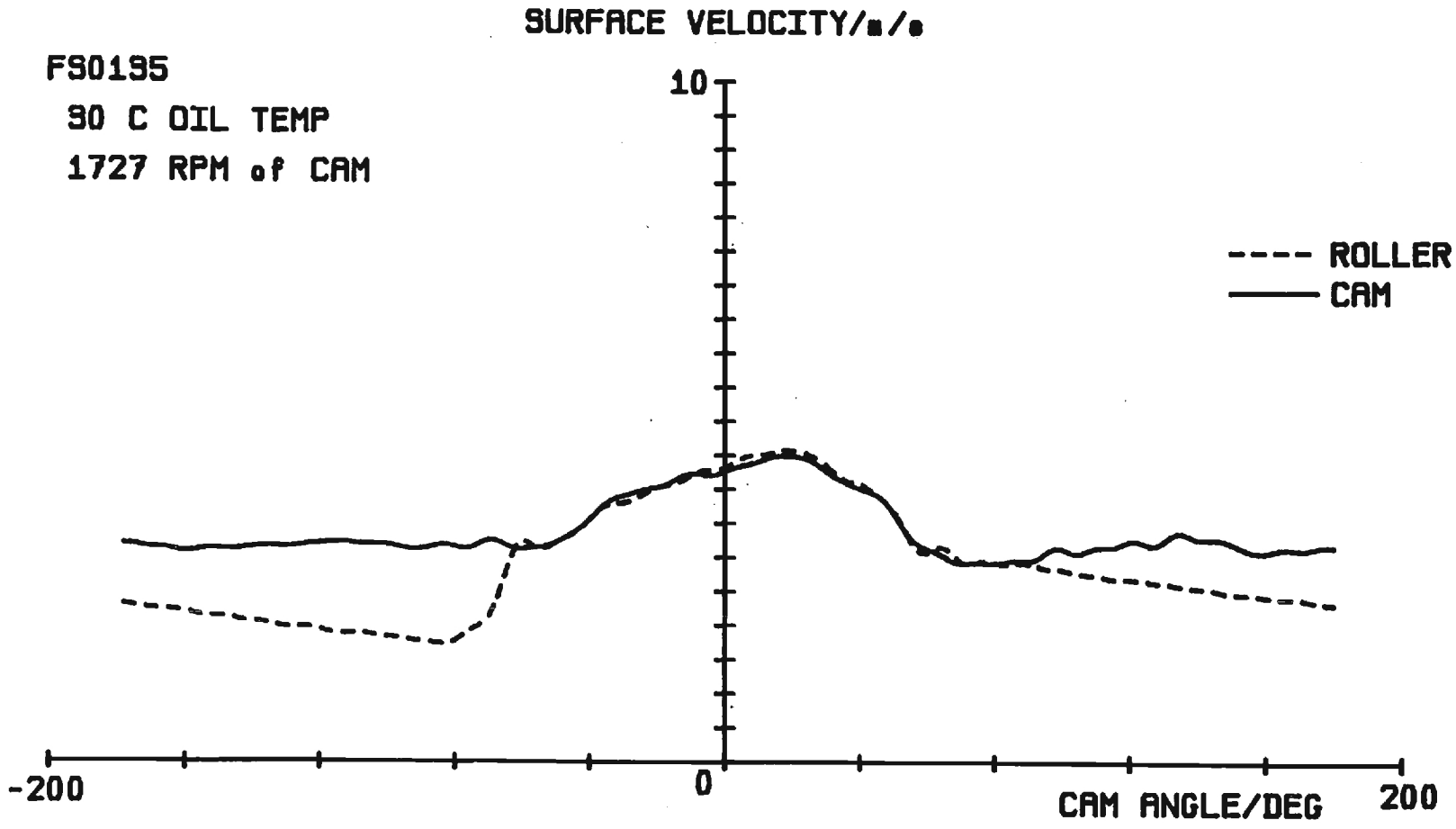
SURFACE VELOCITY/m/s
FS0195
90 C OIL TEMP
1727 RPM of CAM
10
ROLLER
CAM
-200
0
200
CAM ANGLE/DEG

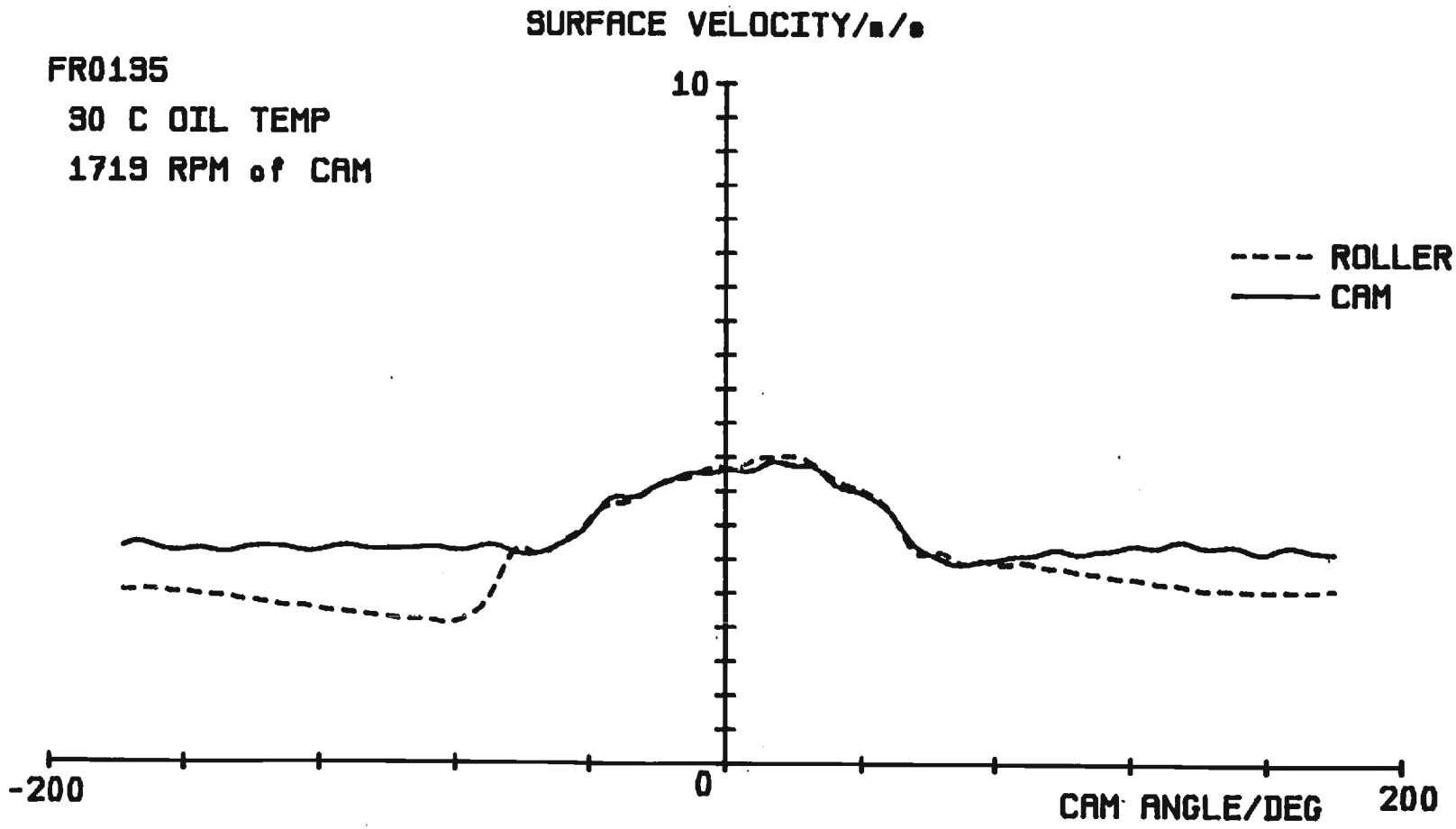
SURFACE VELOCITY/m/s
FR0195
30 C OIL TEMP
1719 RPM of CAM
10
ROLLER
CAM
-200
0
CAM ANGLE/DEG
200

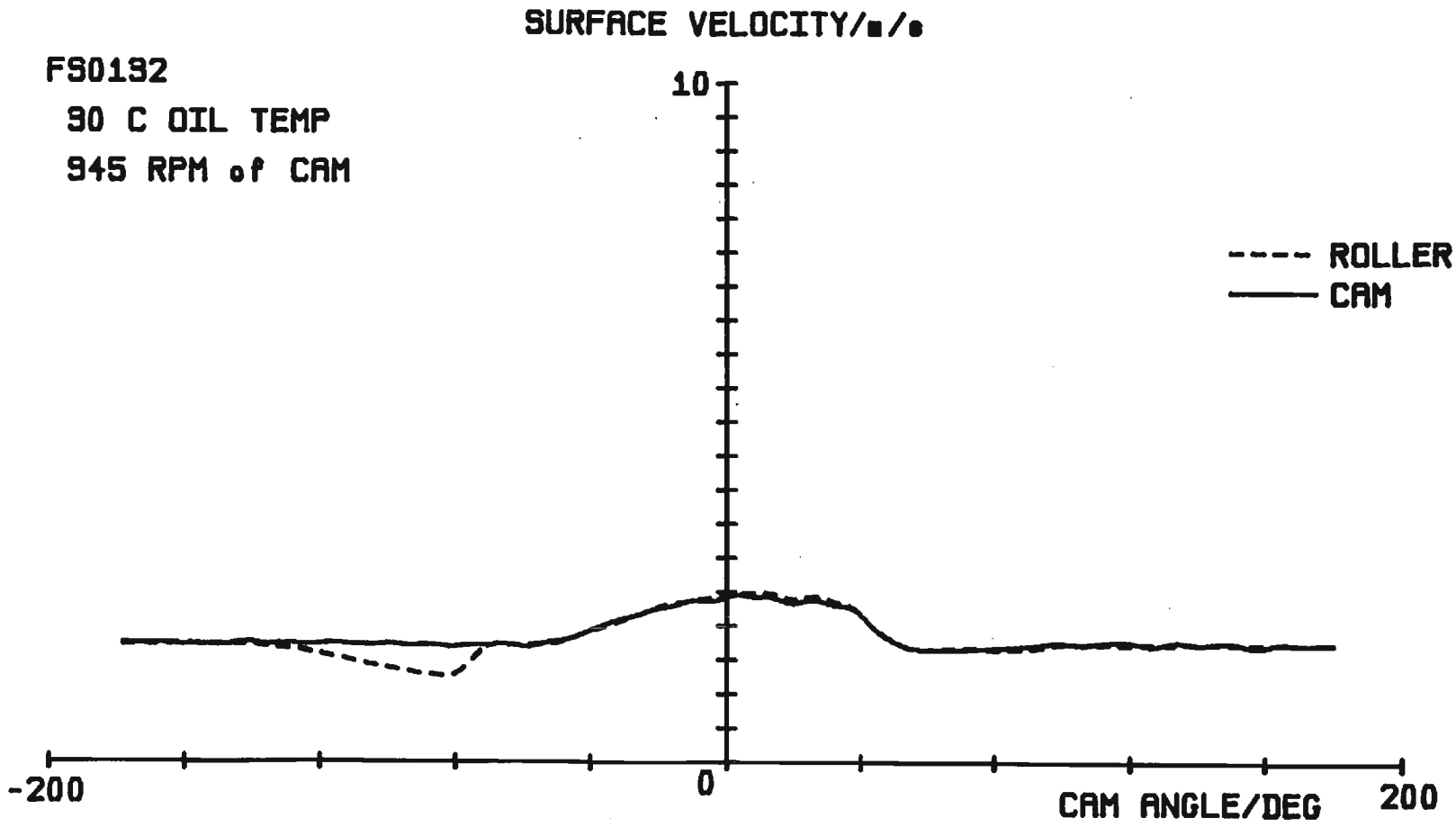
SURFACE VELOCITY/■/●
FS0132
30 C OIL TEMP
945 RPM of CAM
10
ROLLER
CAM
-200
0
200
CAM ANGLE/DEG

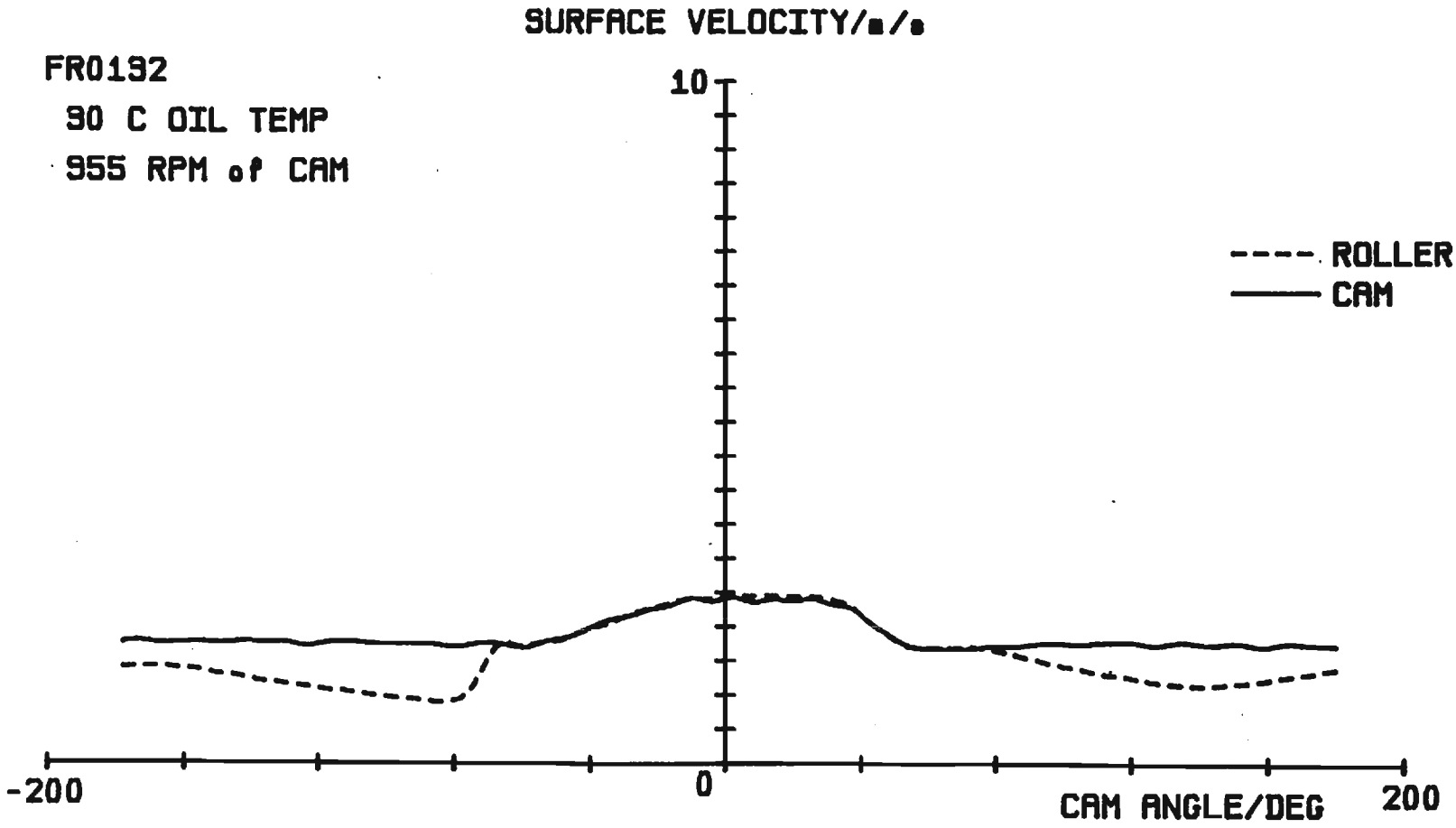
SURFACE VELOCITY/m/s
FR0192
90 C OIL TEMP
955 RPM of CAM
10
ROLLER
CAM
-200
0
200
CAM ANGLE/DEG

# APPENDIX B

## Sliding Velocity Plots

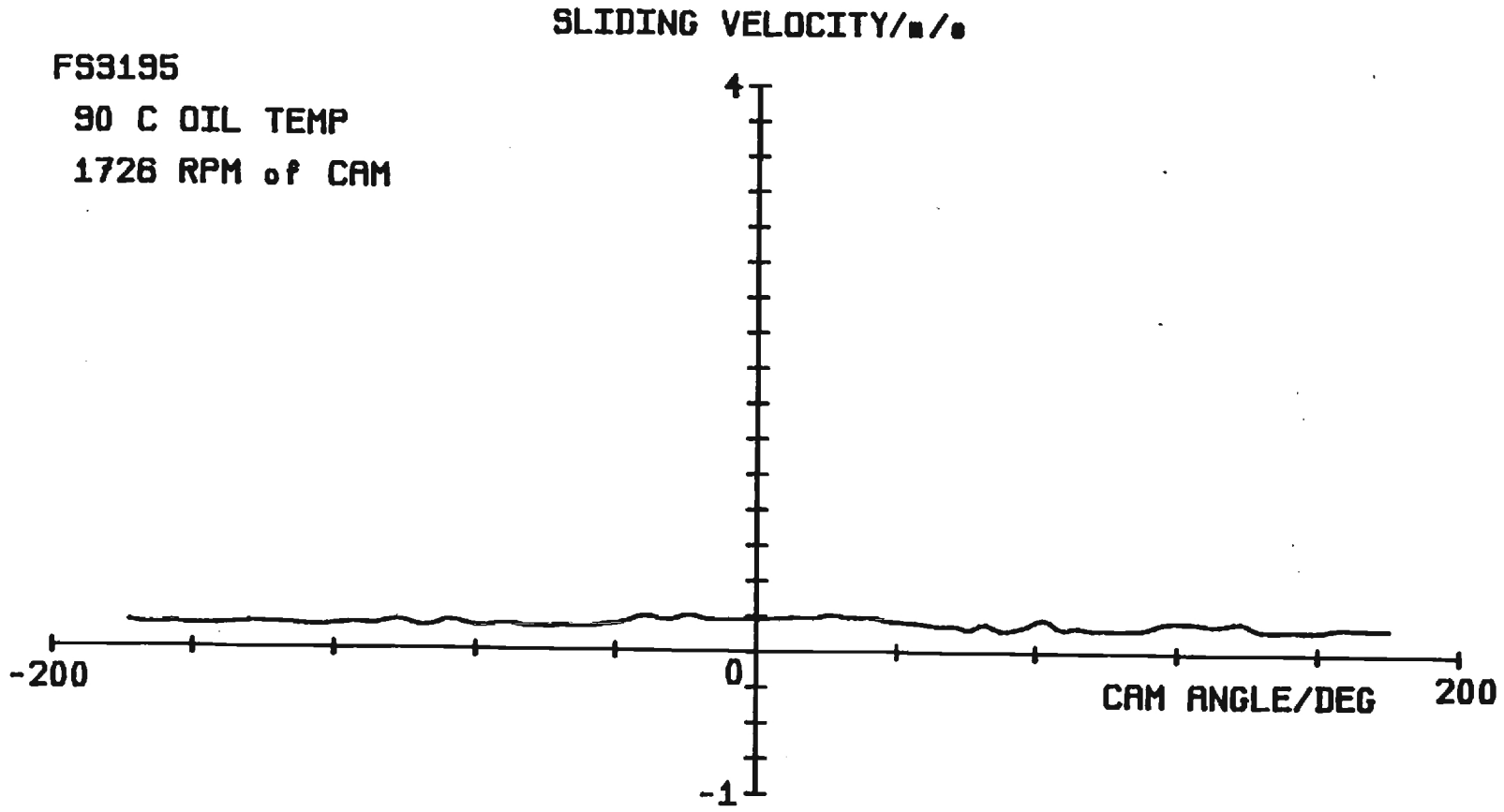
SLIDING VELOCITY/m/s
FS3195
90 C OIL TEMP
1726 RPM of CAM
4
-200
0
200
CAM ANGLE/DEG
-1

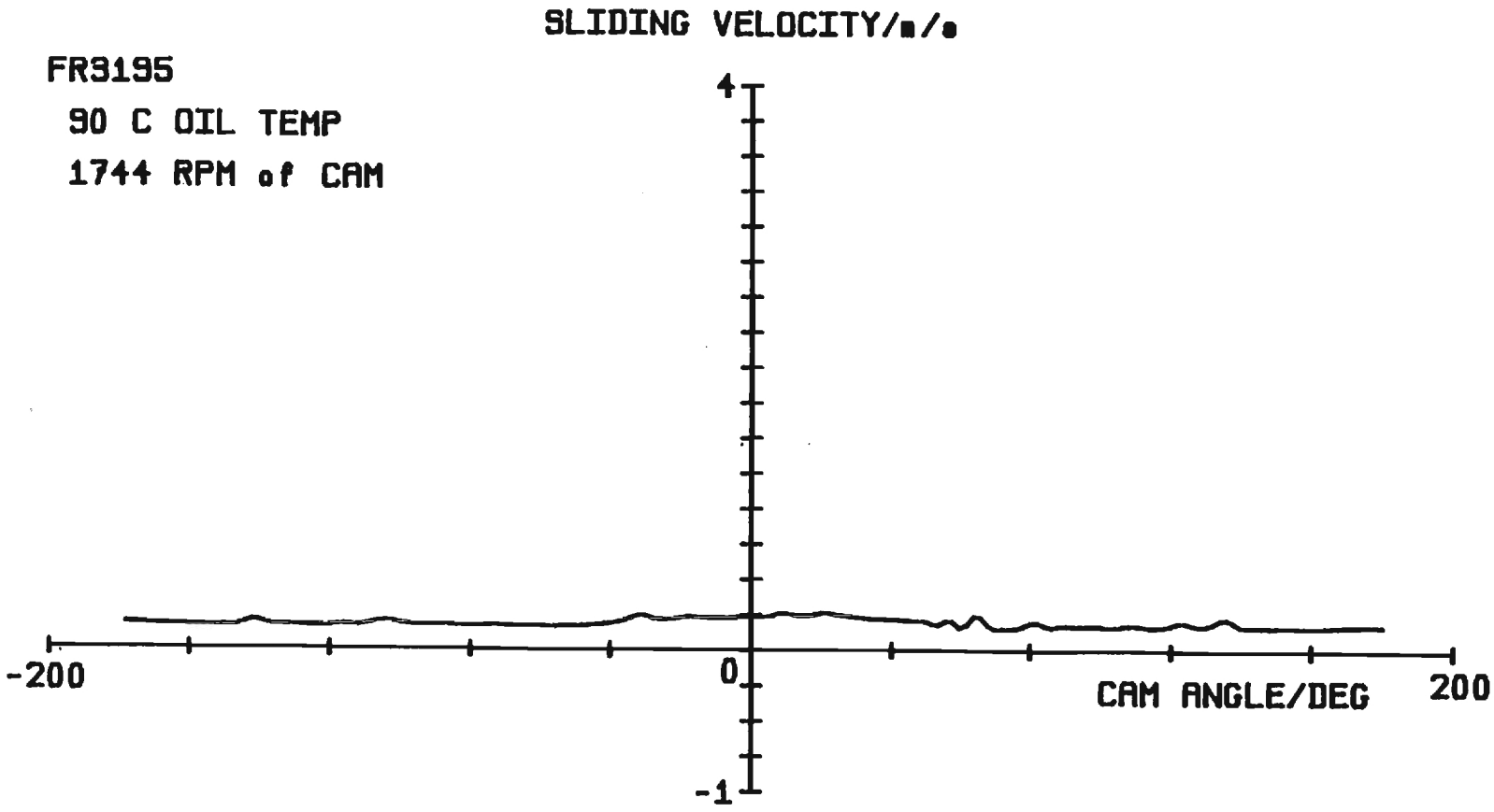
SLIDING VELOCITY/m/s
FR3195
90 C OIL TEMP
1744 RPM of CAM
4
-1
-200
0
200
CAM ANGLE/DEG

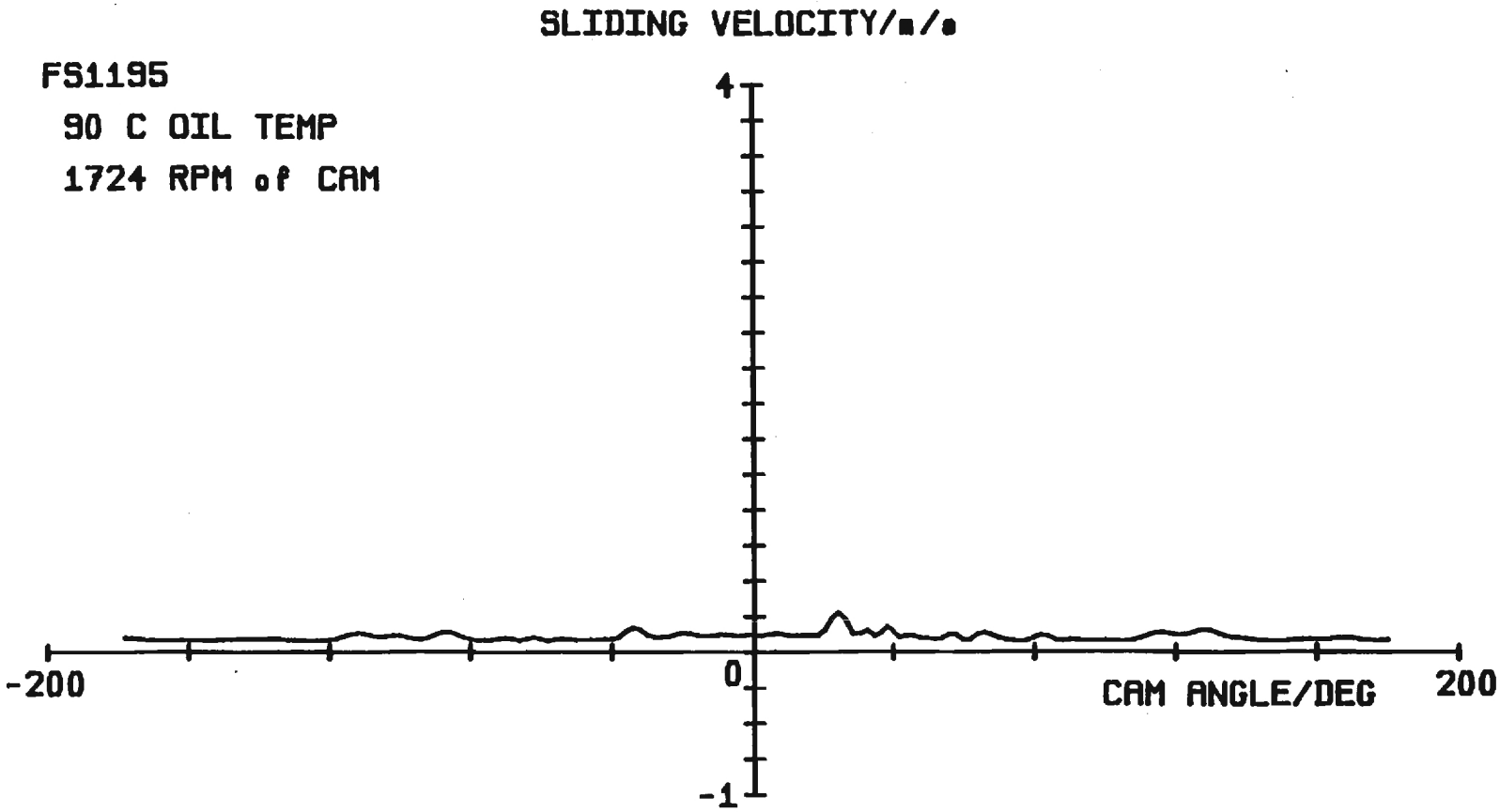
SLIDING VELOCITY/m/s
FS1195
90 C OIL TEMP
1724 RPM of CAM
4
0
-1
-200
200
CAM ANGLE/DEG

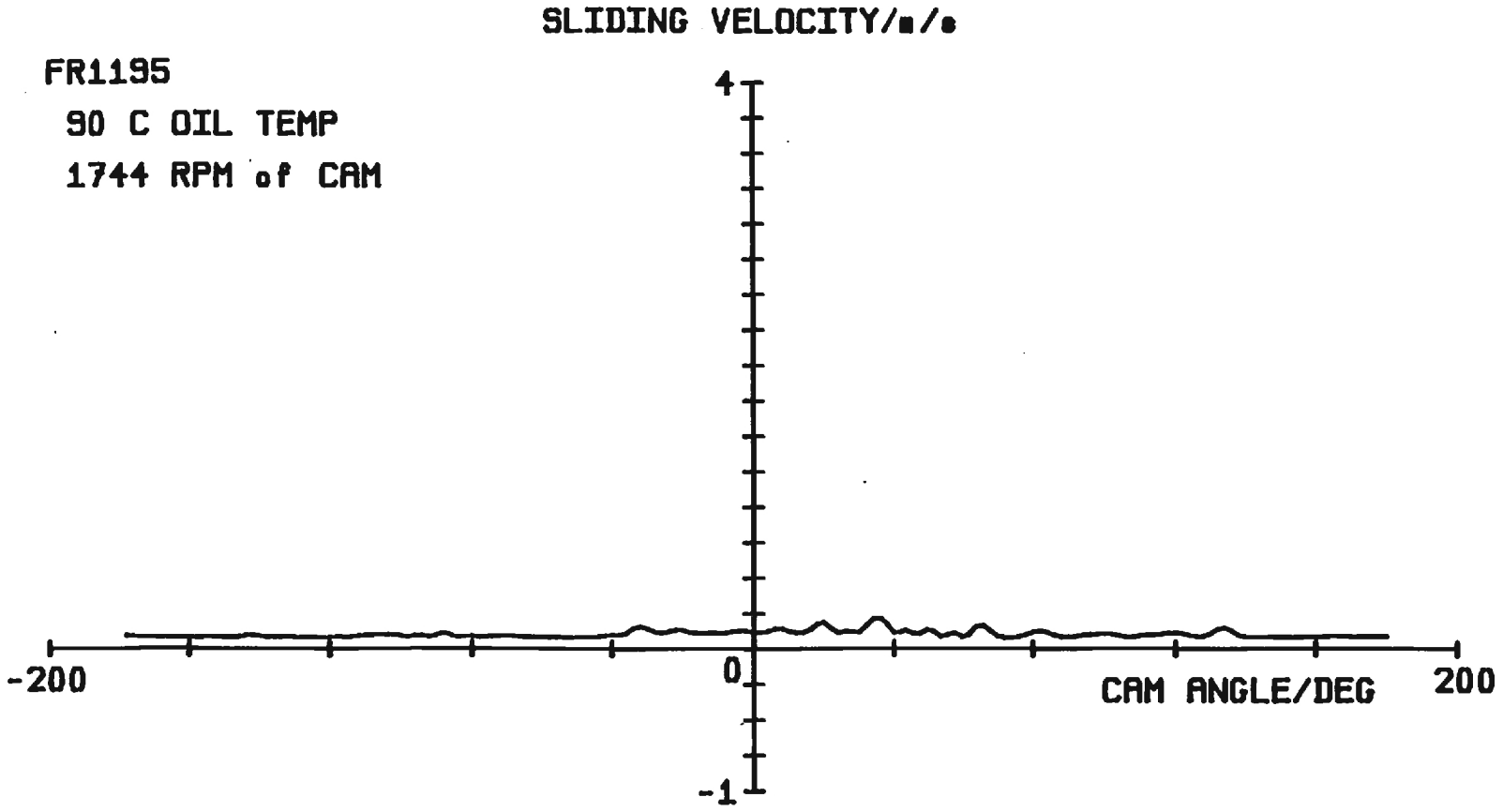
SLIDING VELOCITY/m/s
FR1195
90 C OIL TEMP
1744 RPM of CAM
4
0
-1
-200
200
CAM ANGLE/DEG

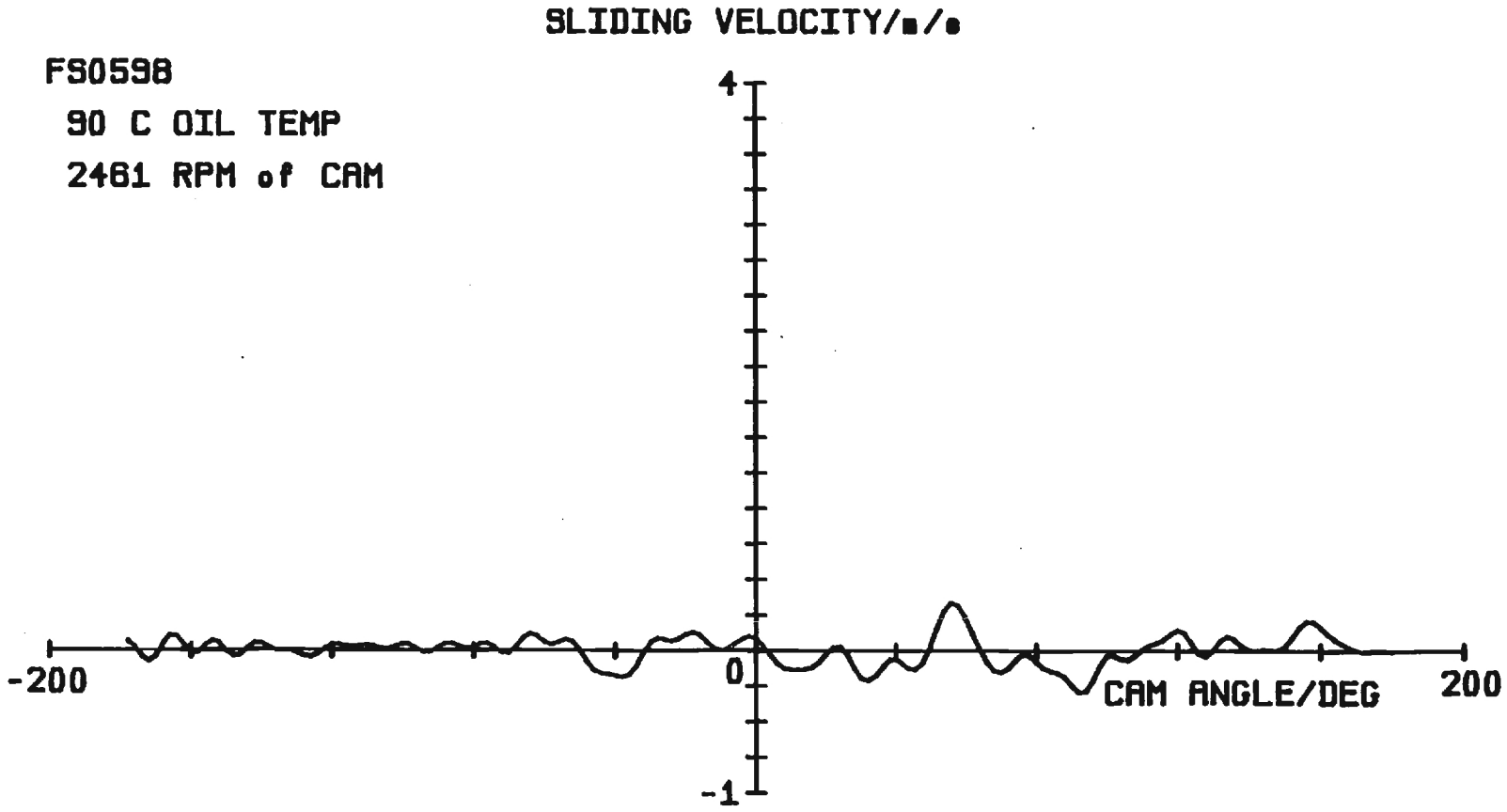
SLIDING VELOCITY/m/s
FS0598
90 C OIL TEMP
2461 RPM of CAM
4
-1
-200
0
200
CAM ANGLE/DEG

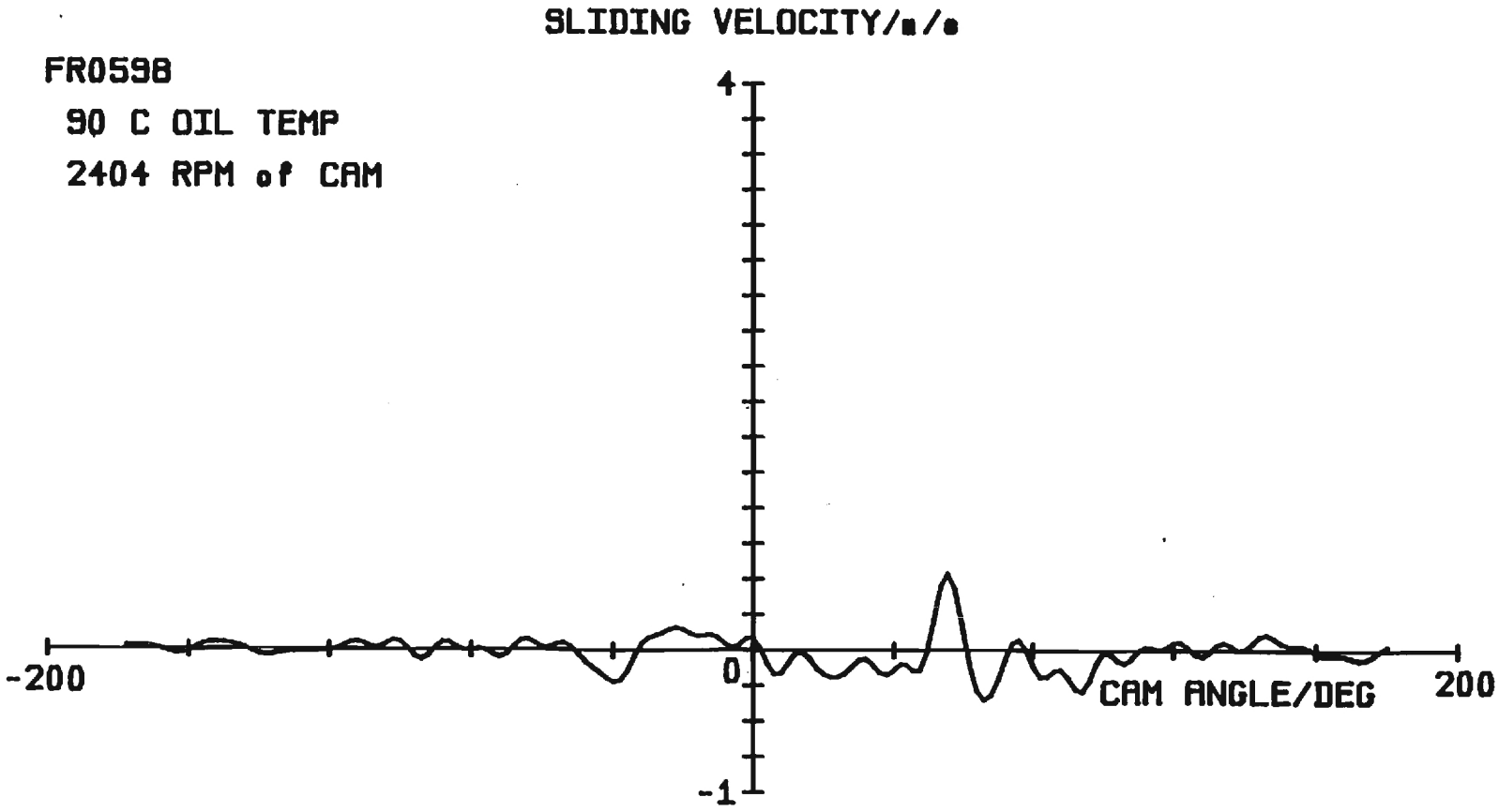
SLIDING VELOCITY/m/s
FR0598
90 C OIL TEMP
2404 RPM of CAM
4
-1
0
-200
200
CAM ANGLE/DEG

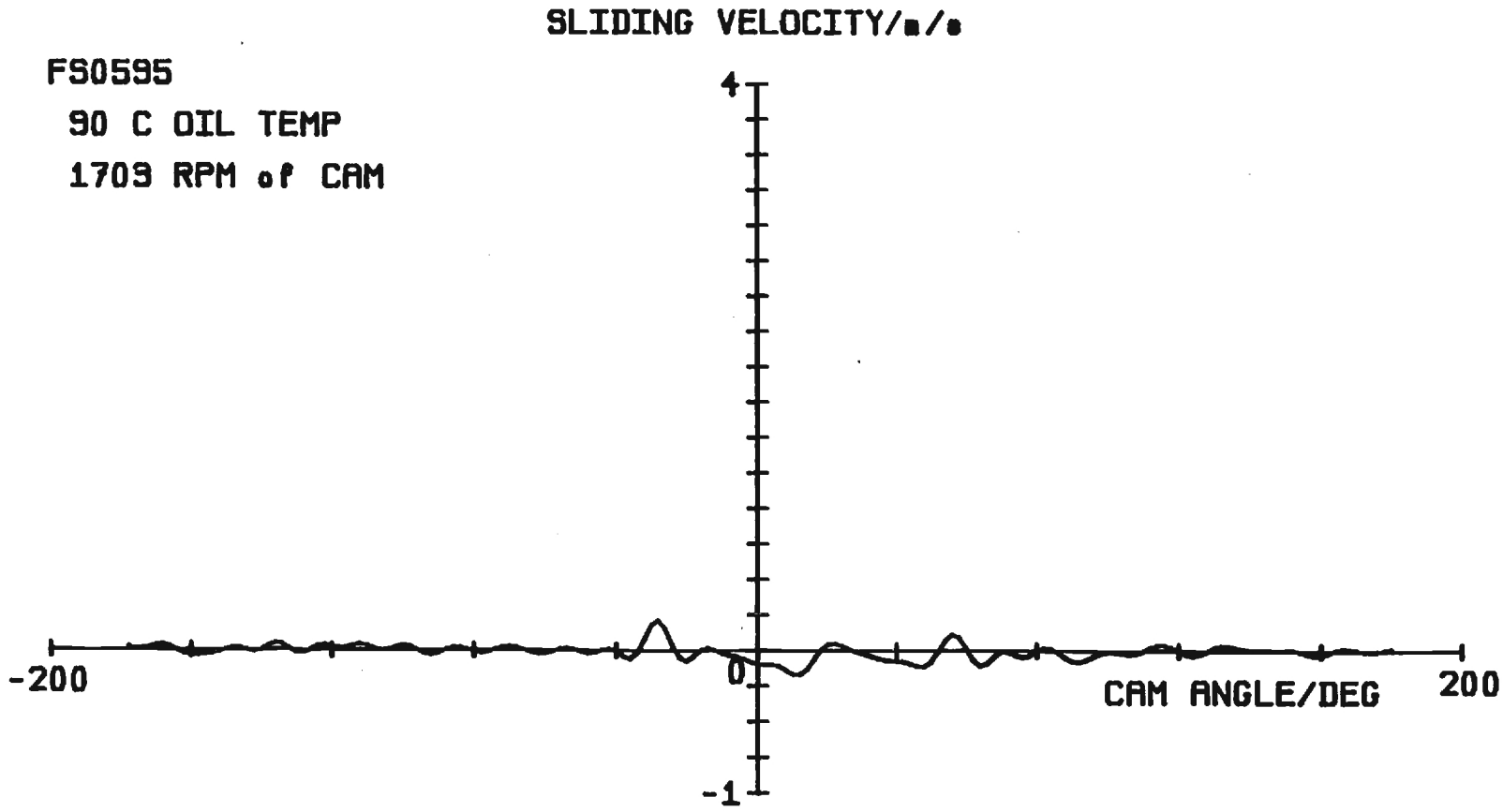
SLIDING VELOCITY/a/a
FS0595
90 C OIL TEMP
1709 RPM of CAM
4
0
-1
-200
200
CAM ANGLE/DEG

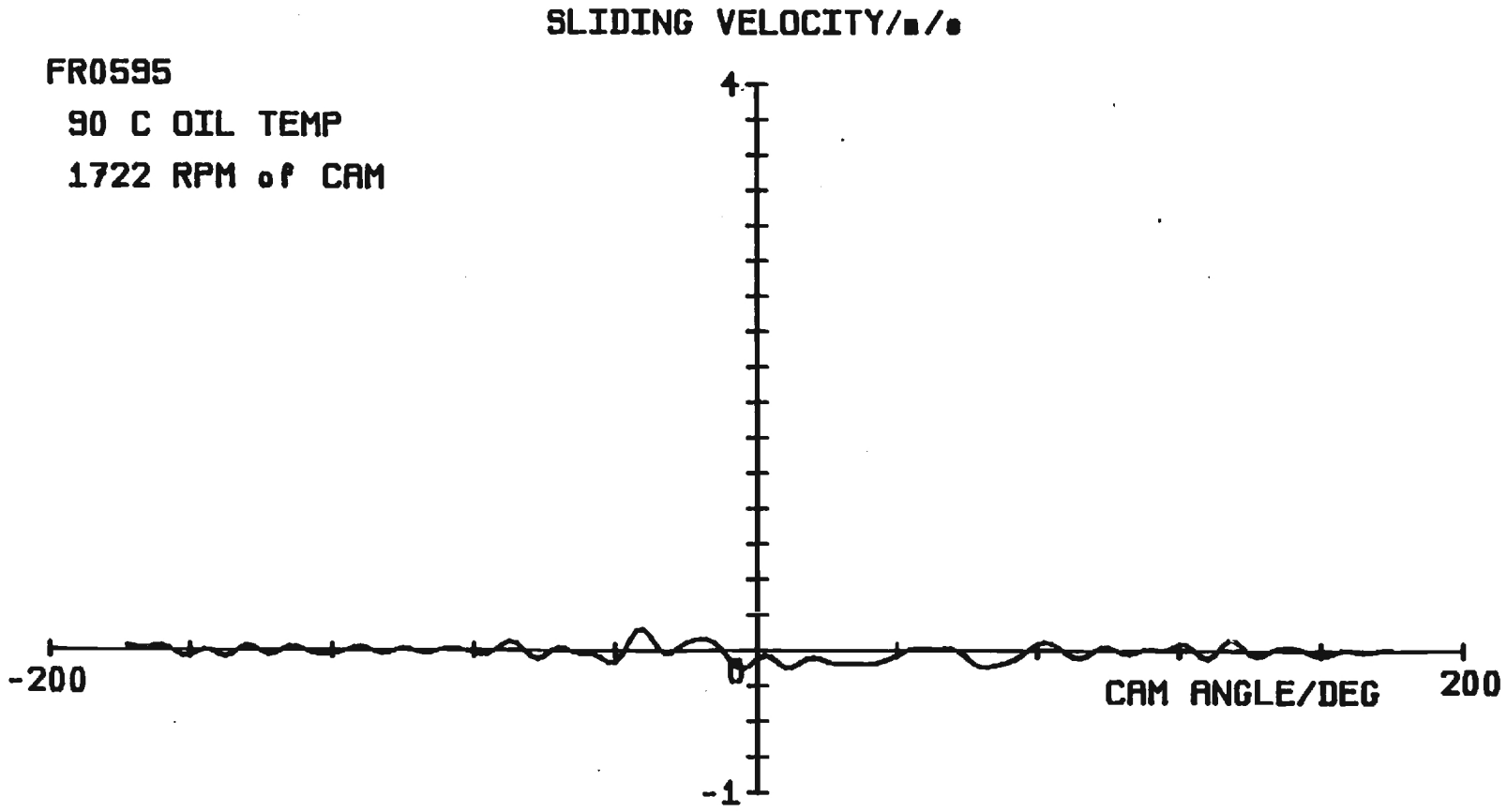
SLIDING VELOCITY/■/●
FR0595
90 C OIL TEMP
1722 RPM of CAM
4
-1
-200
0
200
CAM ANGLE/DEG

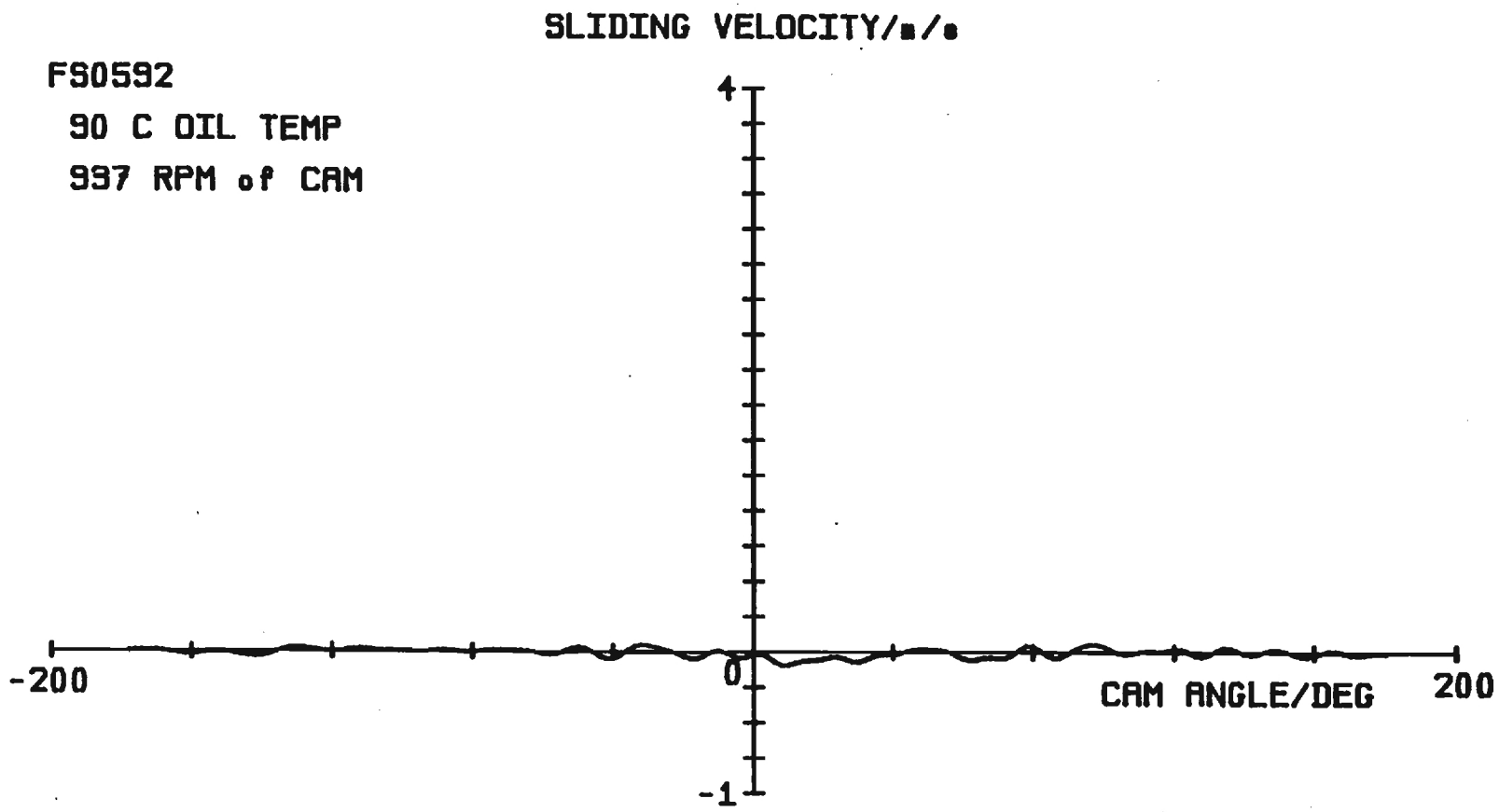
SLIDING VELOCITY/m/s
FS0592
90 C OIL TEMP
937 RPM of CAM
4
-200
0
CAM ANGLE/DEG
200
-1

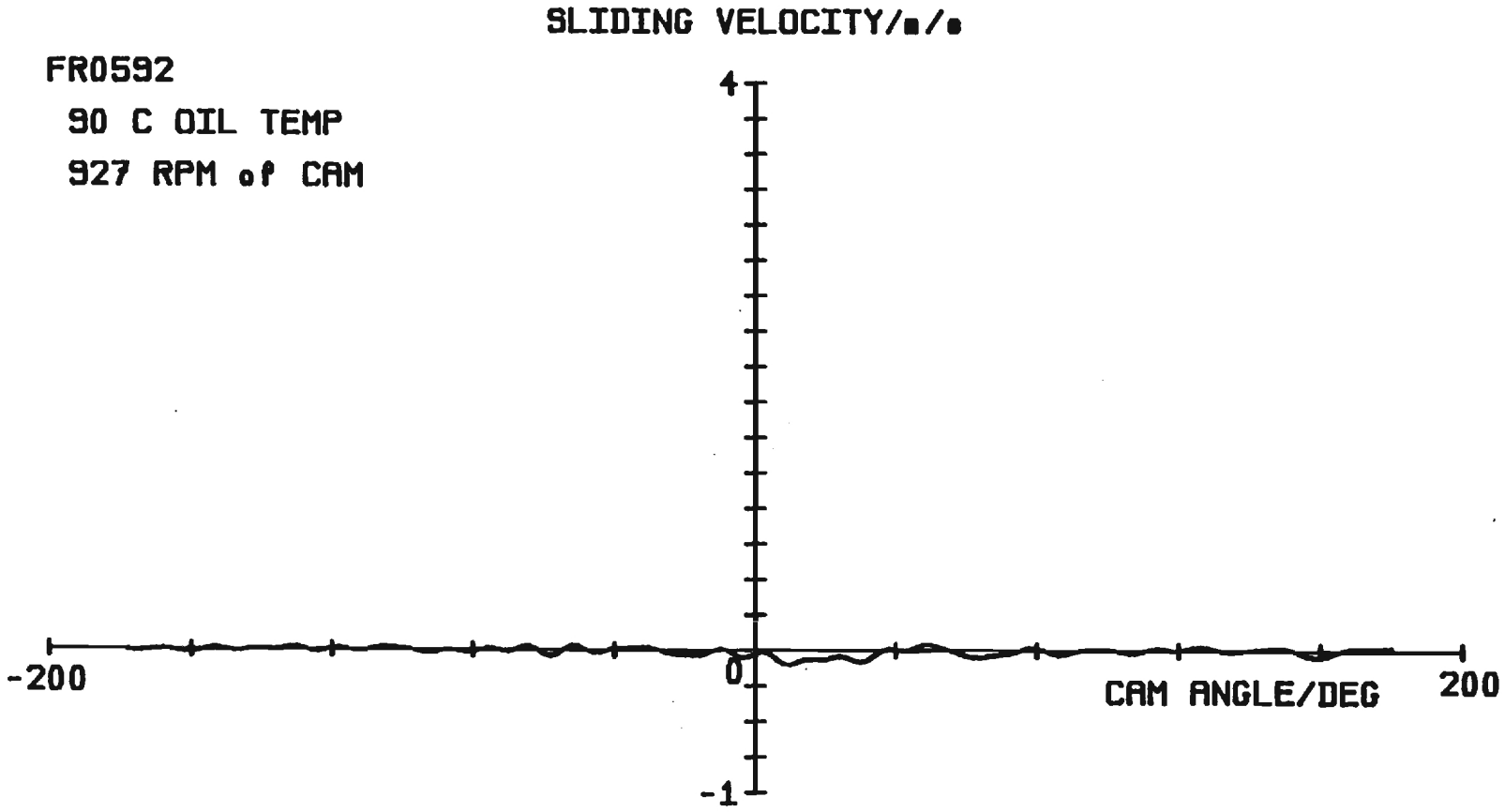
SLIDING VELOCITY/m/s
FR0592
90 C OIL TEMP
927 RPM of CAM
4
-1
0
-200
200
CAM ANGLE/DEG

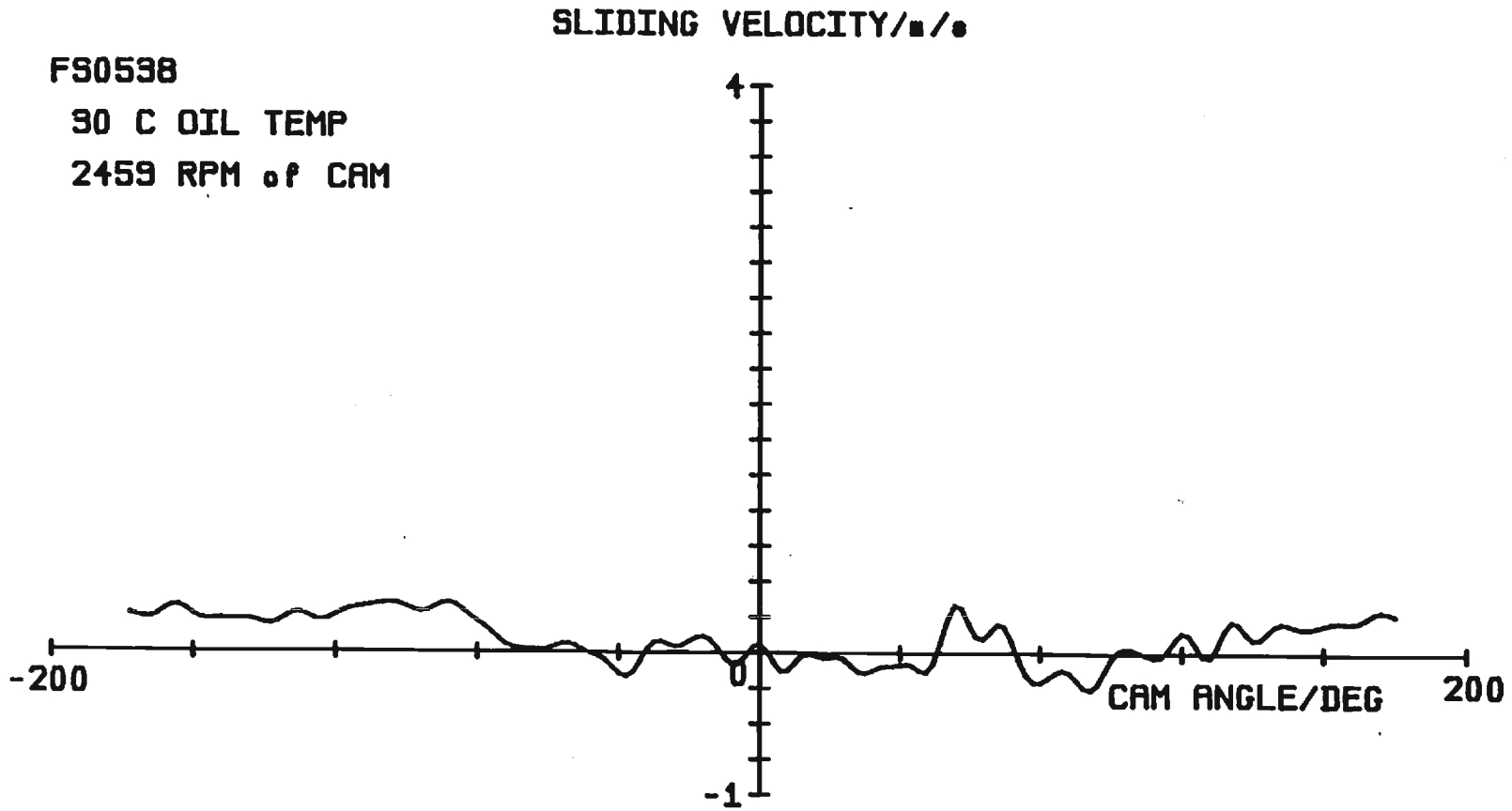
SLIDING VELOCITY/m/s
FS0538
90 C OIL TEMP
2459 RPM of CAM
4
-1
-200
0
200
CAM ANGLE/DEG

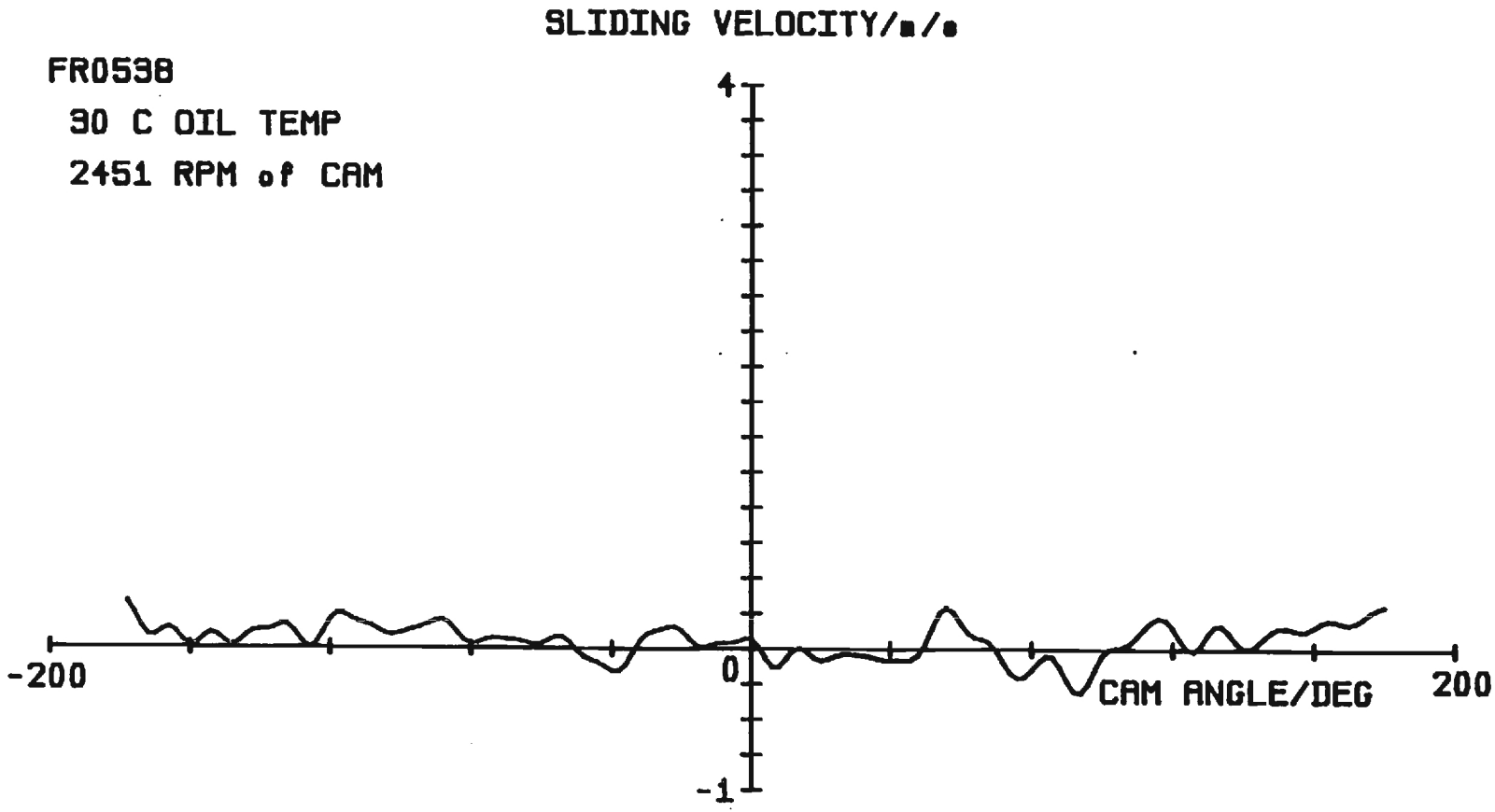
SLIDING VELOCITY/m/s
FR0538
30 C OIL TEMP
2451 RPM of CAM
4
-1
0
-200
200
CAM ANGLE/DEG

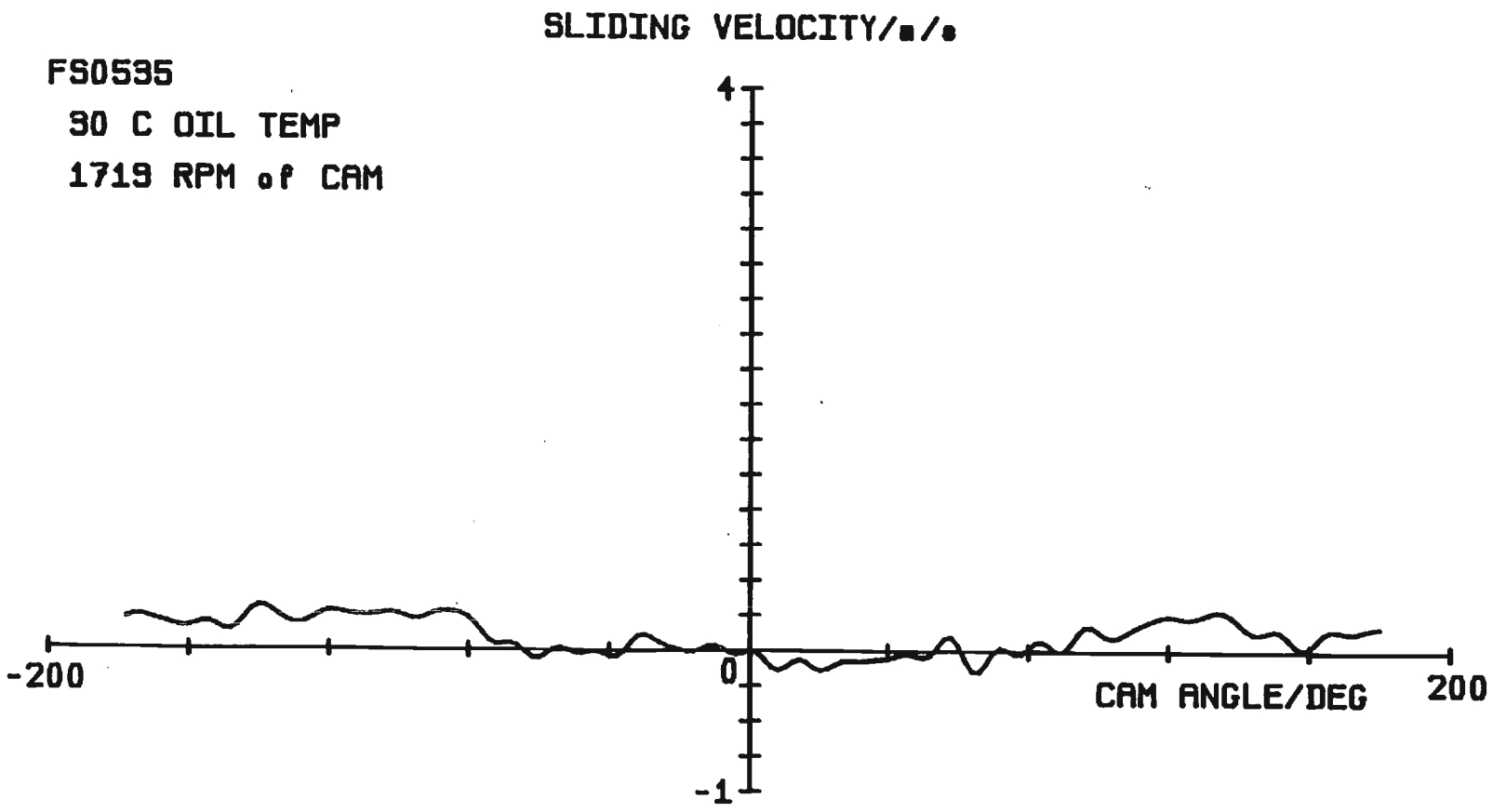
SLIDING VELOCITY/m/s
FS0535
30 C OIL TEMP
1719 RPM of CAM
4
-1
-200
0
200
CAM ANGLE/DEG

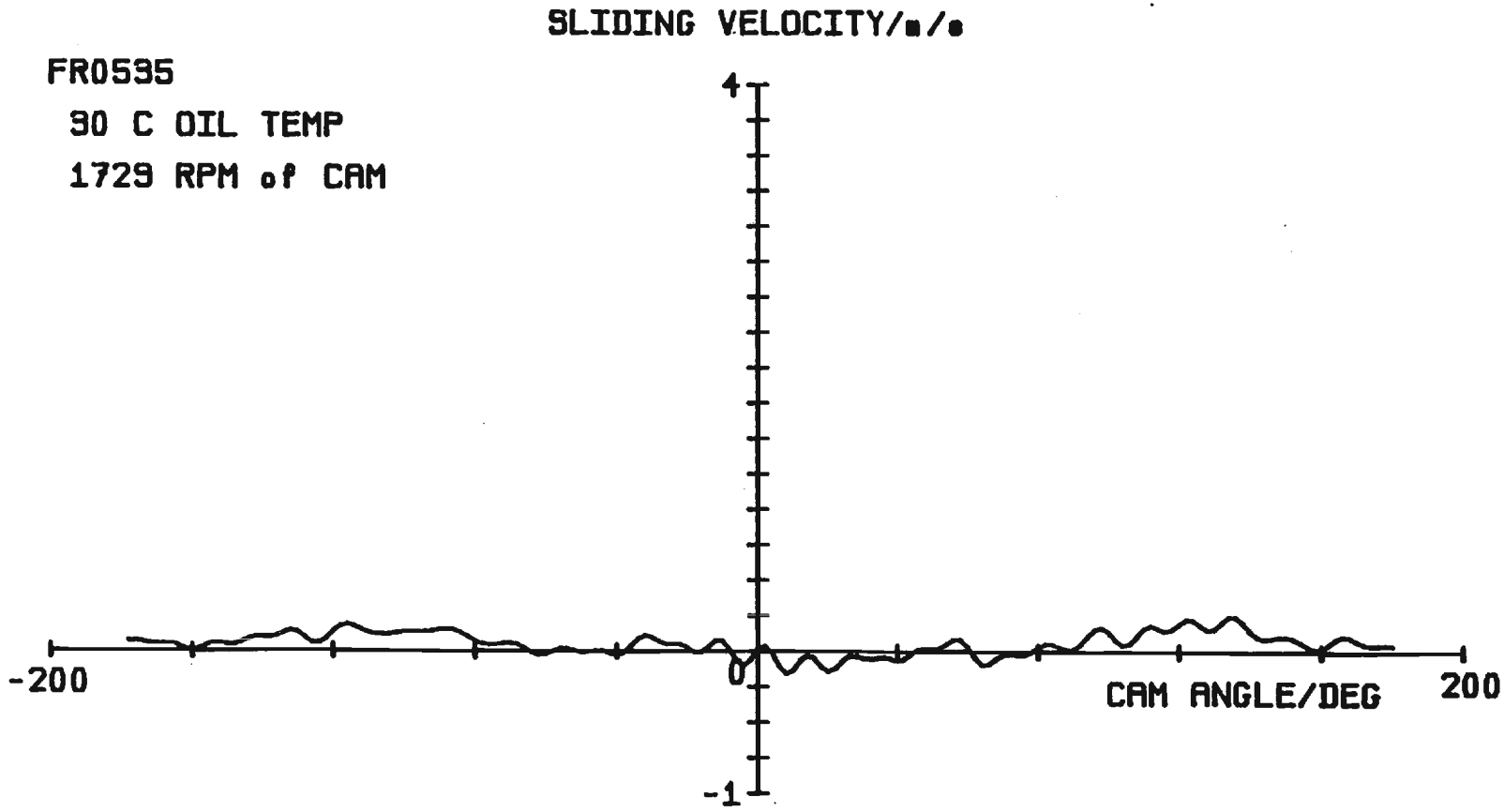
SLIDING VELOCITY/■/●
FR0535
30 C OIL TEMP
1729 RPM of CAM
4
-1
-200
0
200
CAM ANGLE/DEG

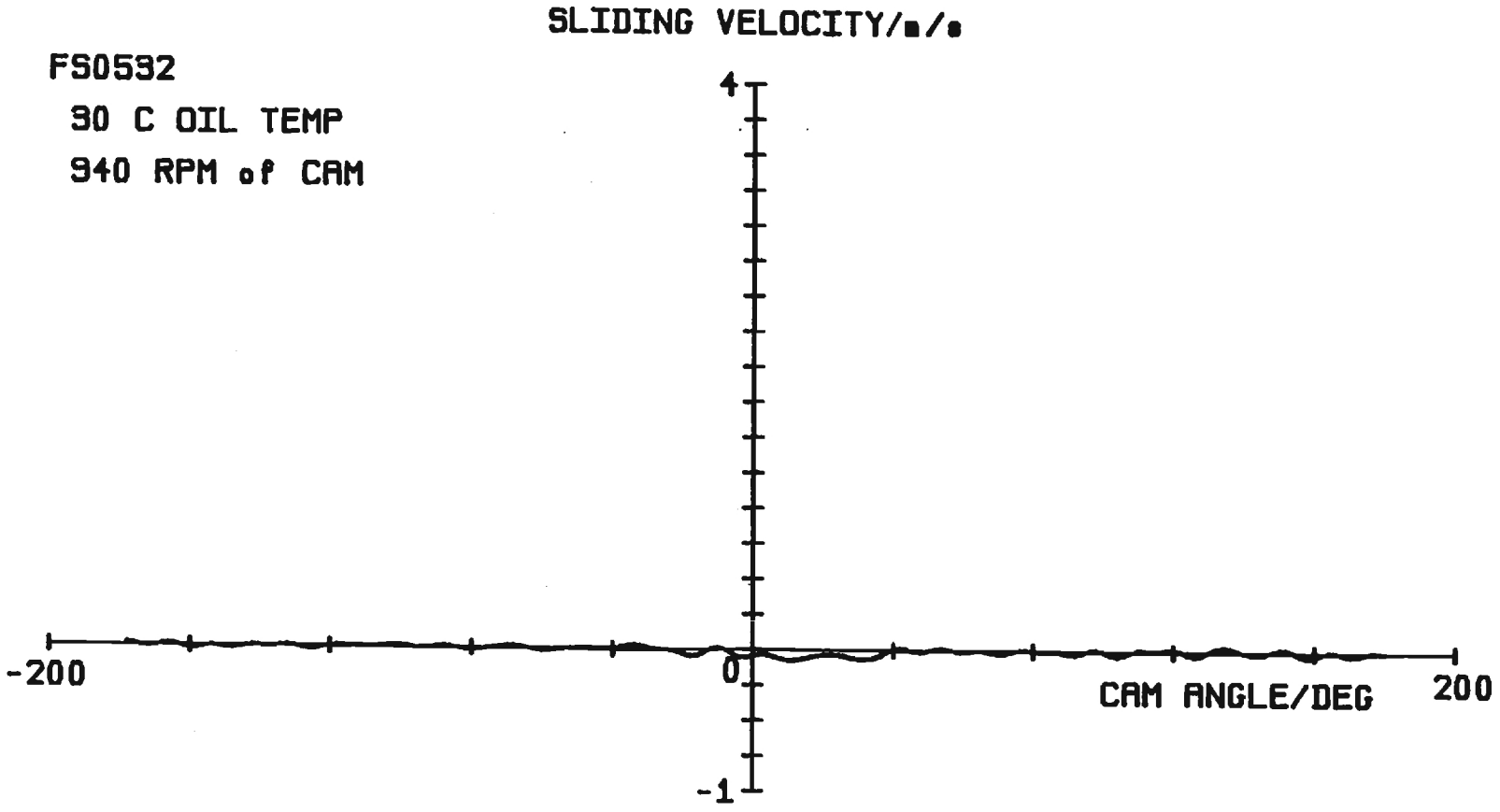
SLIDING VELOCITY/m/s
FS0532
30 C OIL TEMP
940 RPM of CAM
4
-200
0
200
CAM ANGLE/DEG
-1

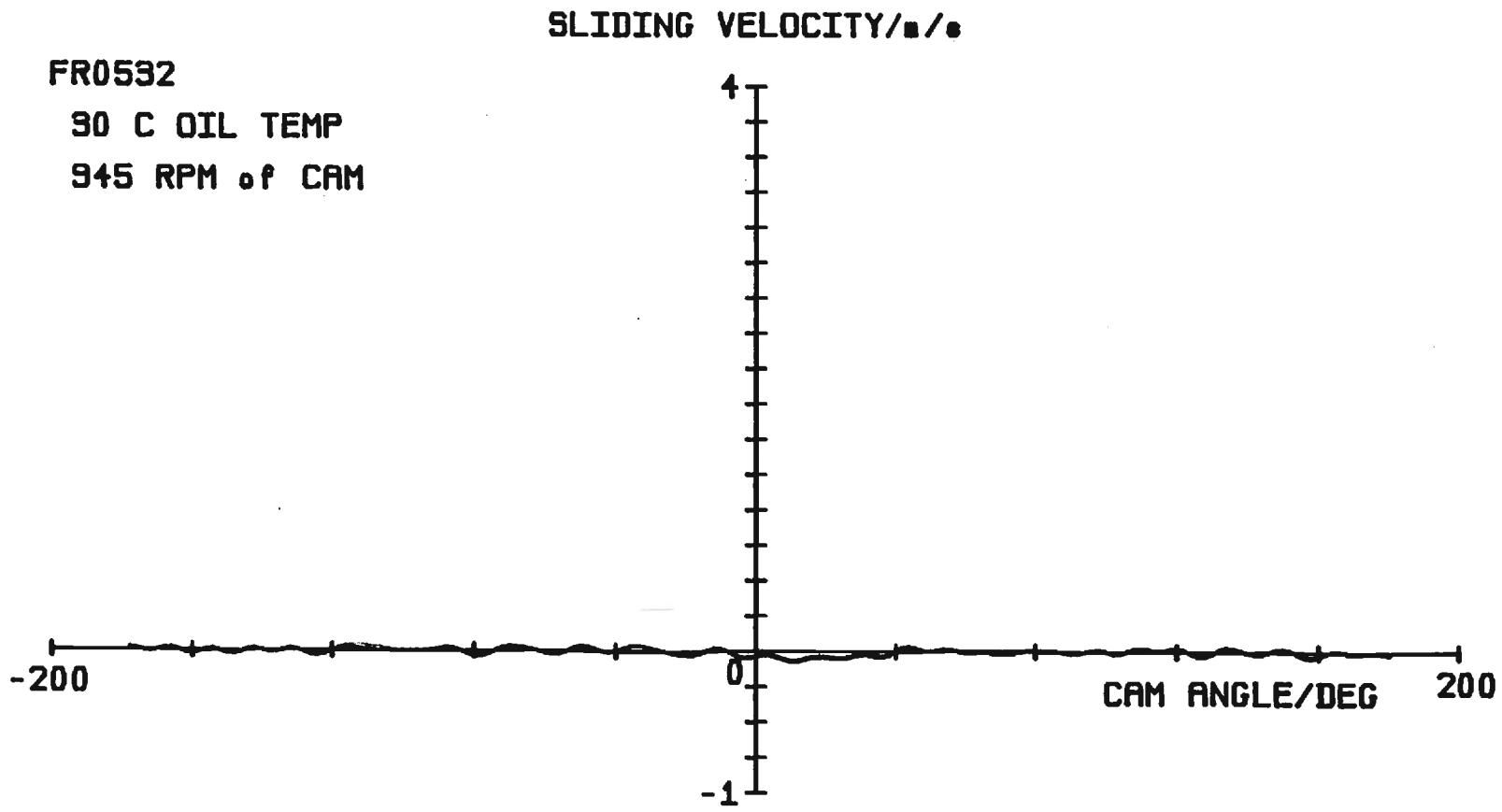
SLIDING VELOCITY/m/s
FR0532
90 C OIL TEMP
945 RPM of CAM
4
0
-1
-200
200
CAM ANGLE/DEG

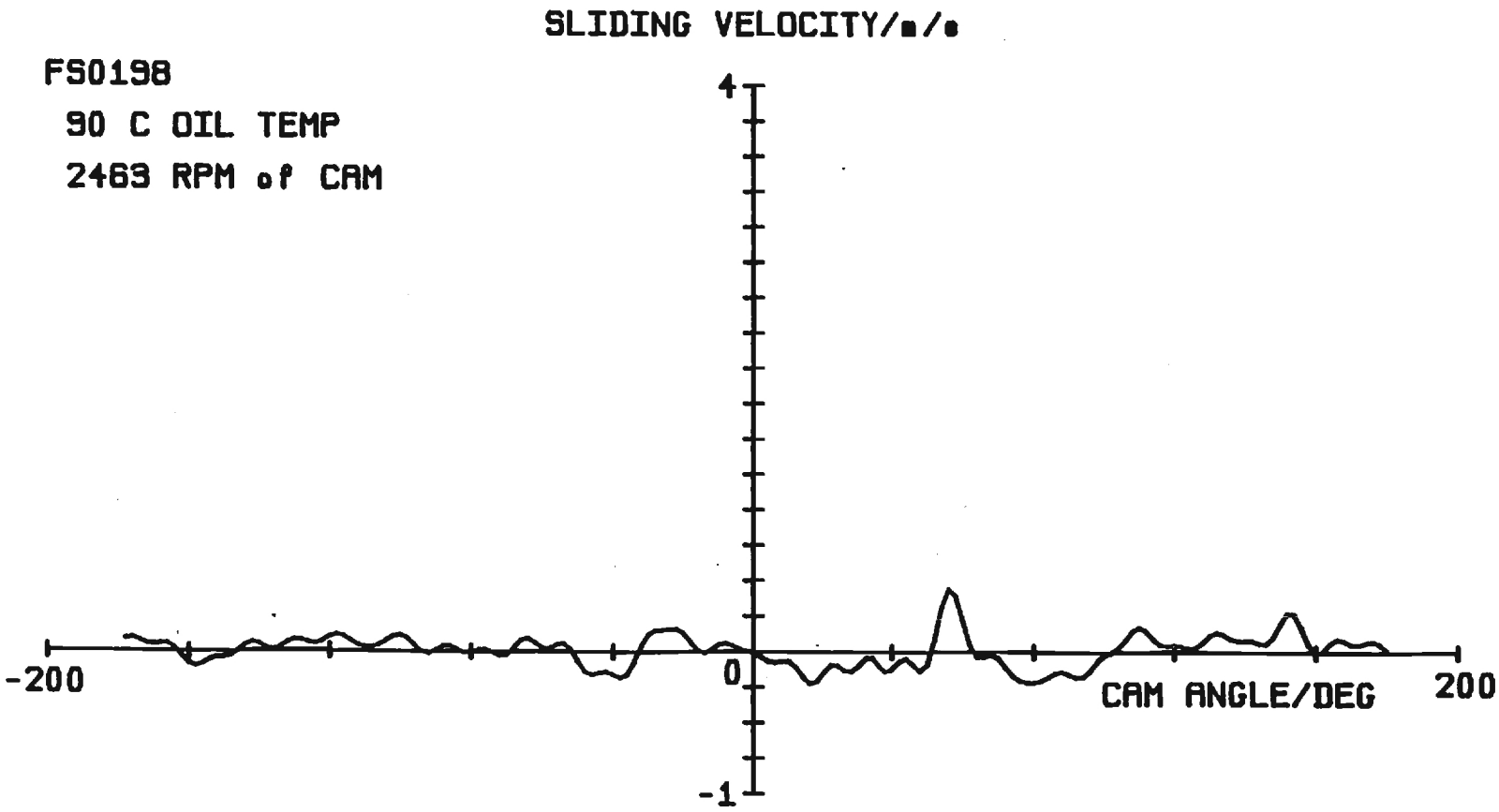
SLIDING VELOCITY/■/●
FS0198
90 C OIL TEMP
2463 RPM of CAM
4
0
-1
-200
200
CAM ANGLE/DEG

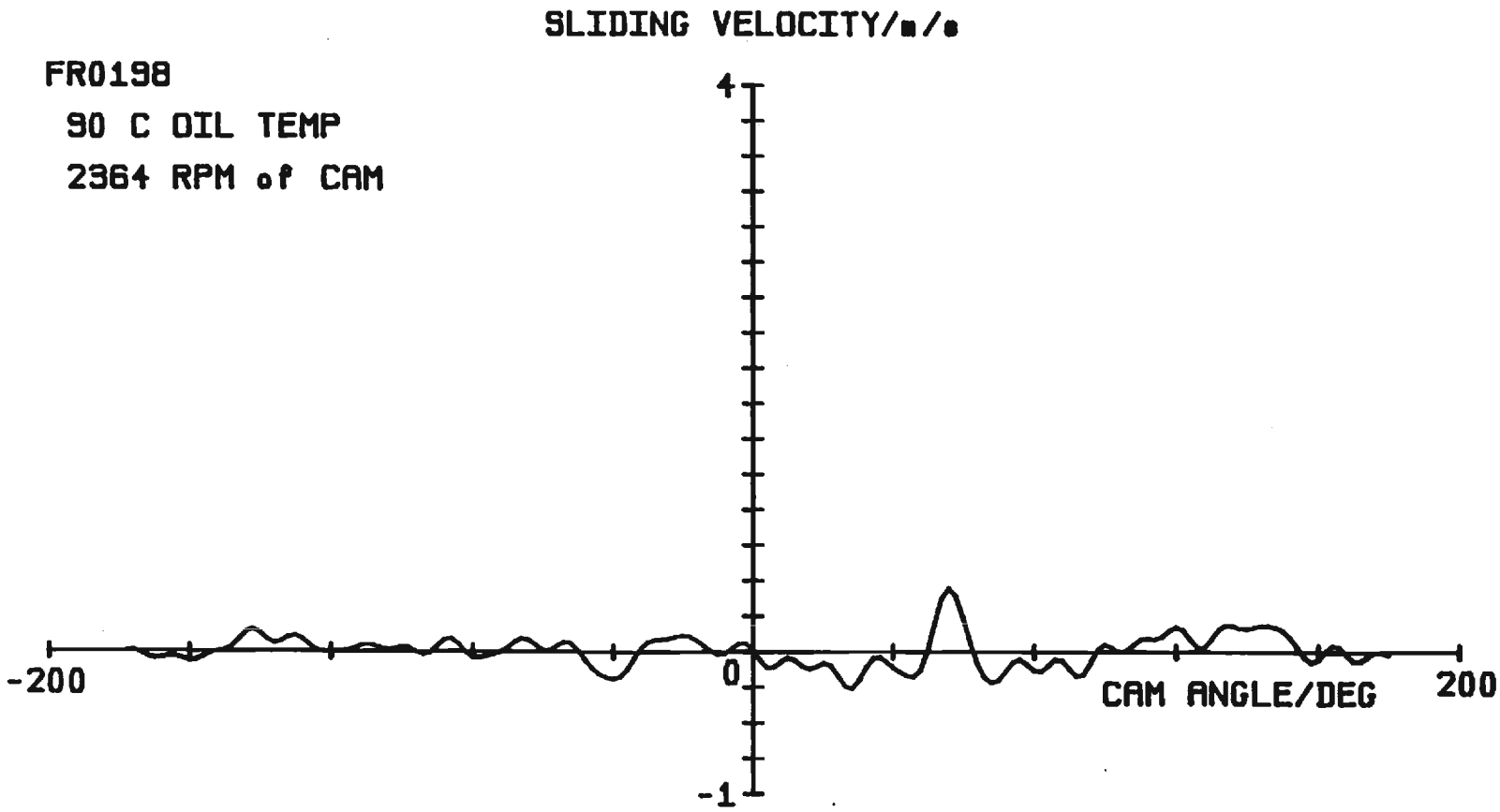
SLIDING VELOCITY/m/s
FR0198
90 C OIL TEMP
2364 RPM of CAM
4
0
-1
-200
200
CAM ANGLE/DEG

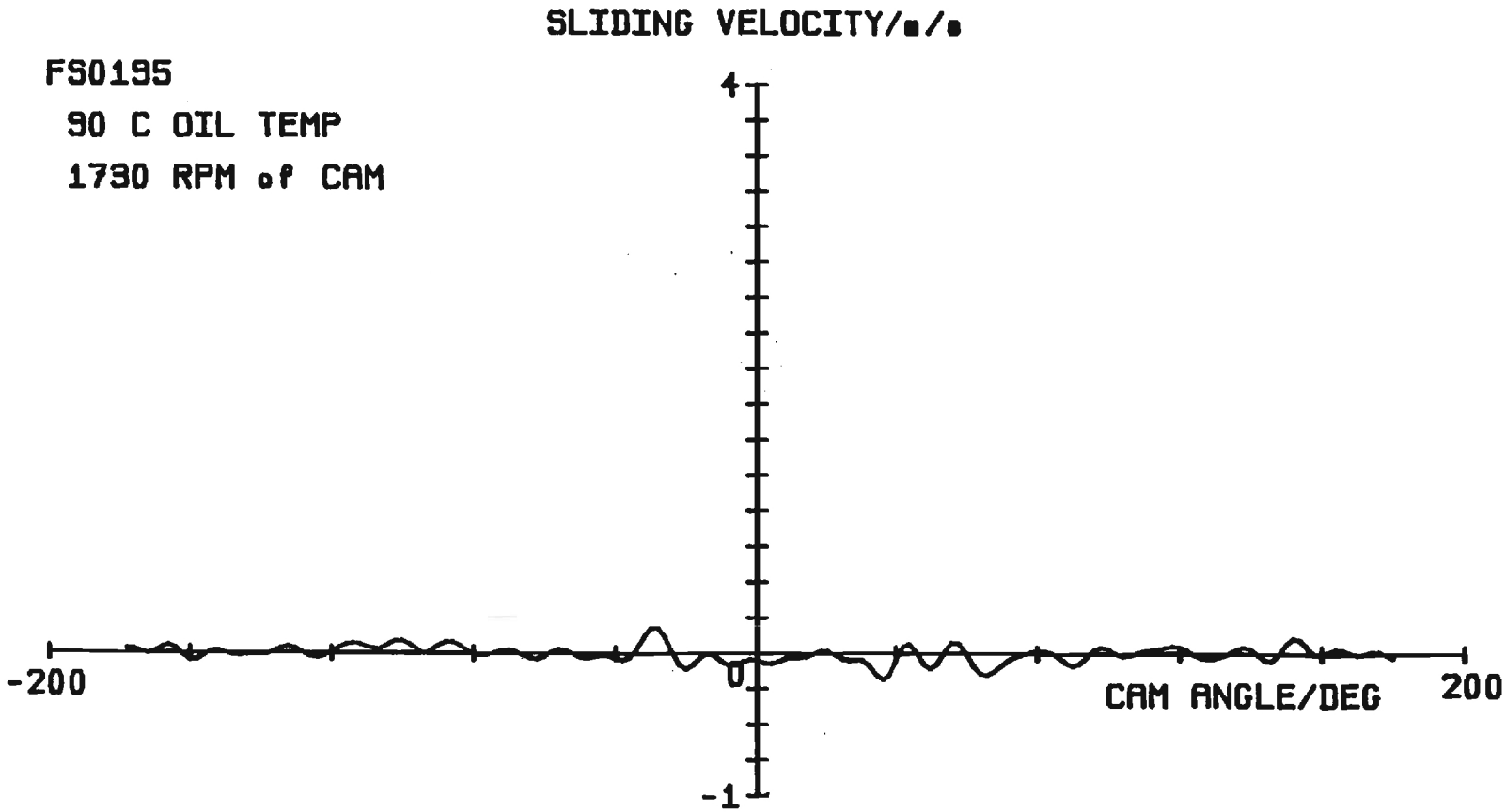
SLIDING VELOCITY/ø/ø
FS0195
90 C OIL TEMP
1730 RPM of CAM
4
-200
0
CAM ANGLE/DEG
200
-1

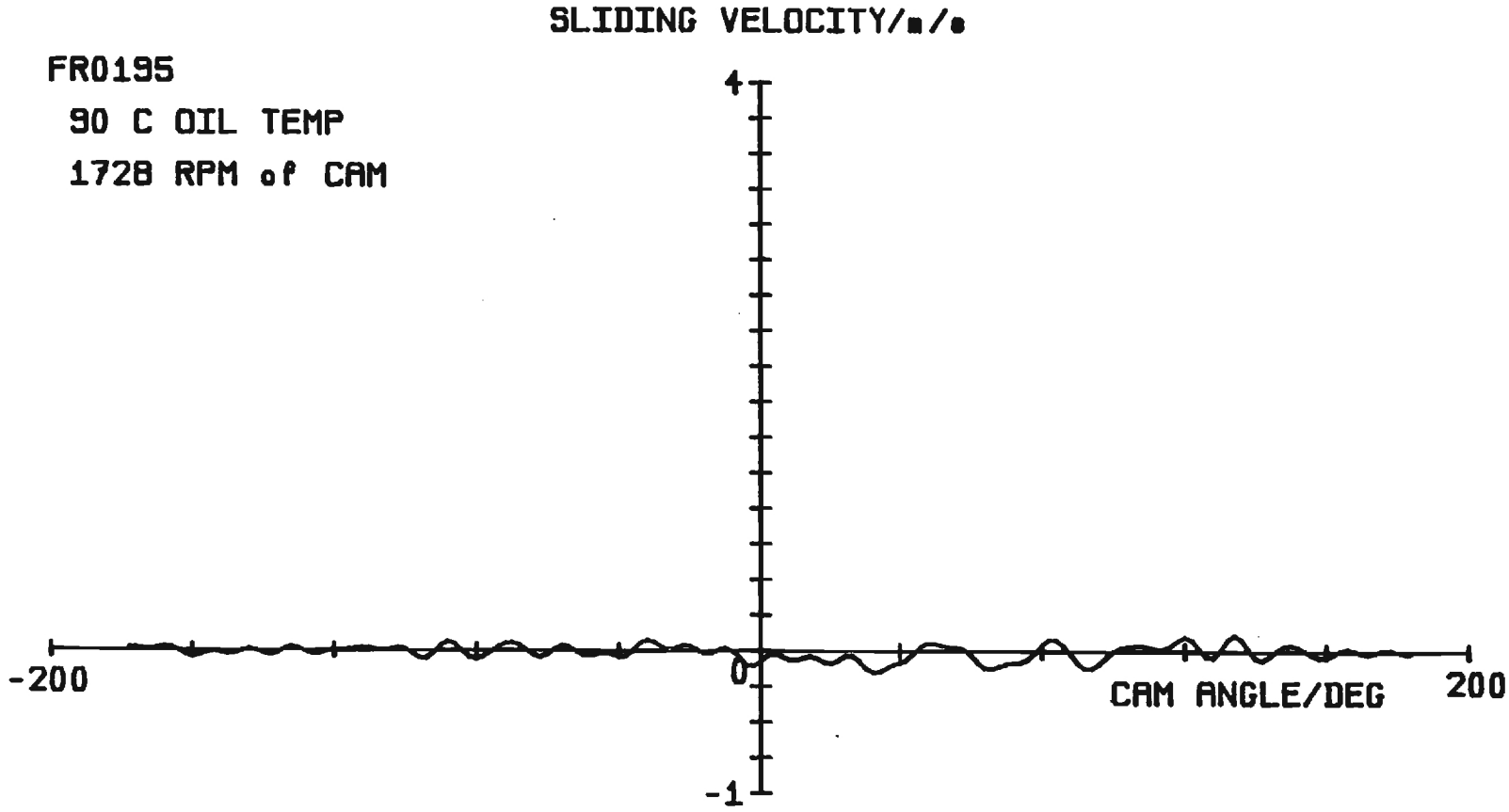
SLIDING VELOCITY/m/s
FR0195
90 C OIL TEMP
1728 RPM of CAM
4
-1
0
-200
200
CAM ANGLE/DEG

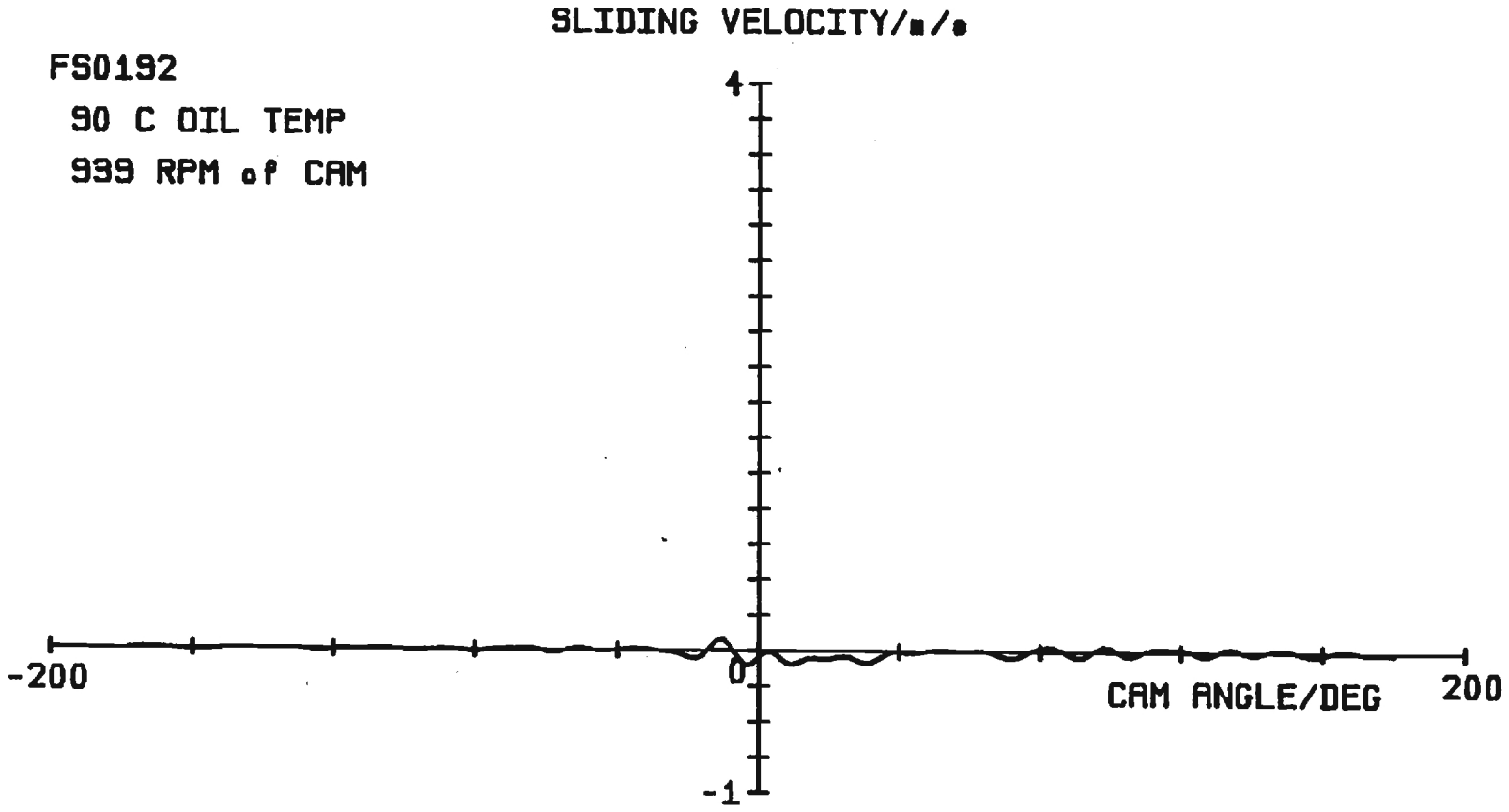
SLIDING VELOCITY/m/s
FS0192
90 C OIL TEMP
939 RPM of CAM
4
-200
0
200
CAM ANGLE/DEG
-1

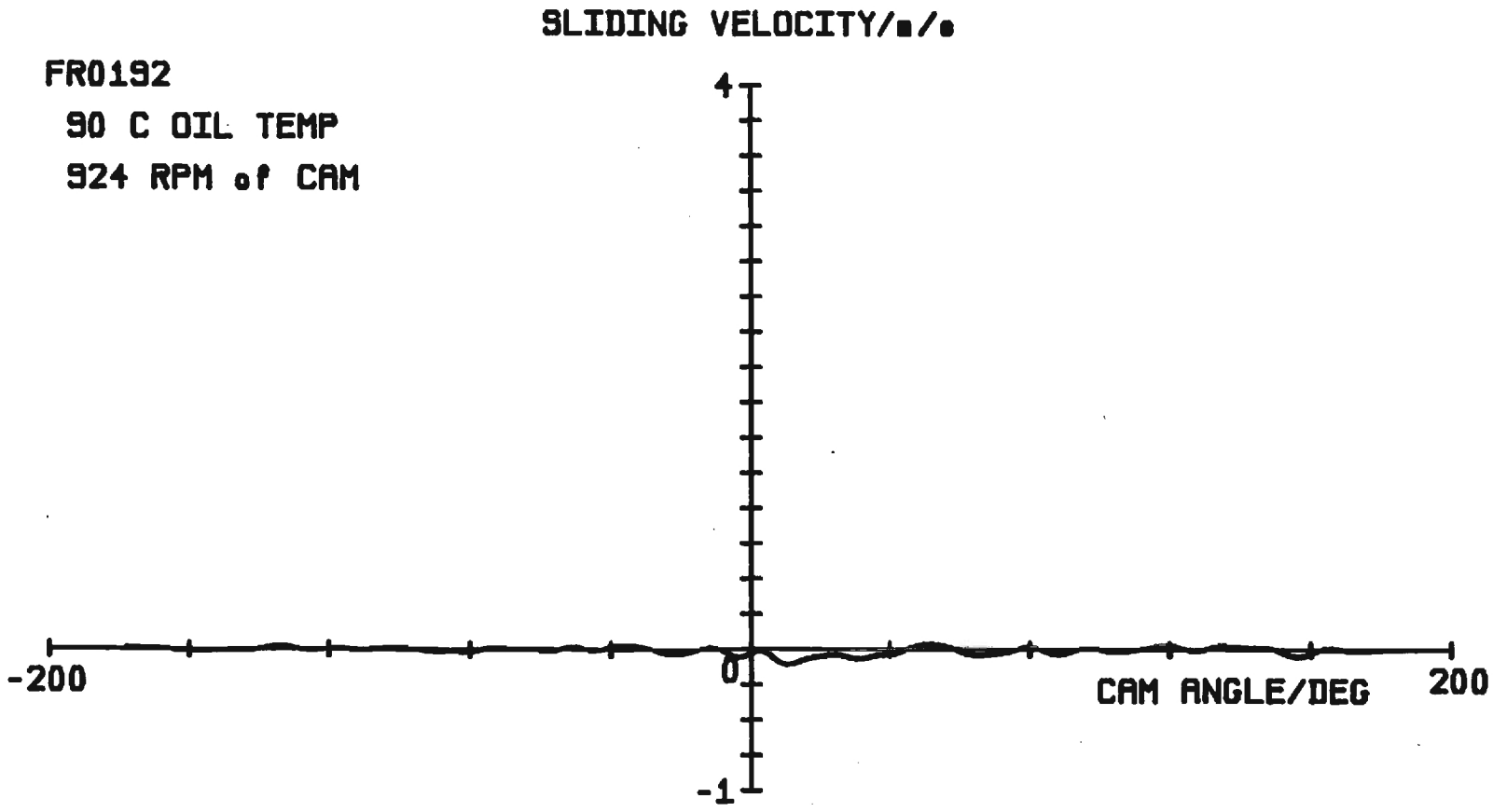
SLIDING VELOCITY/m/s
FR0192
90 C OIL TEMP
924 RPM of CAM
4
0
-1
-200
200
CAM ANGLE/DEG

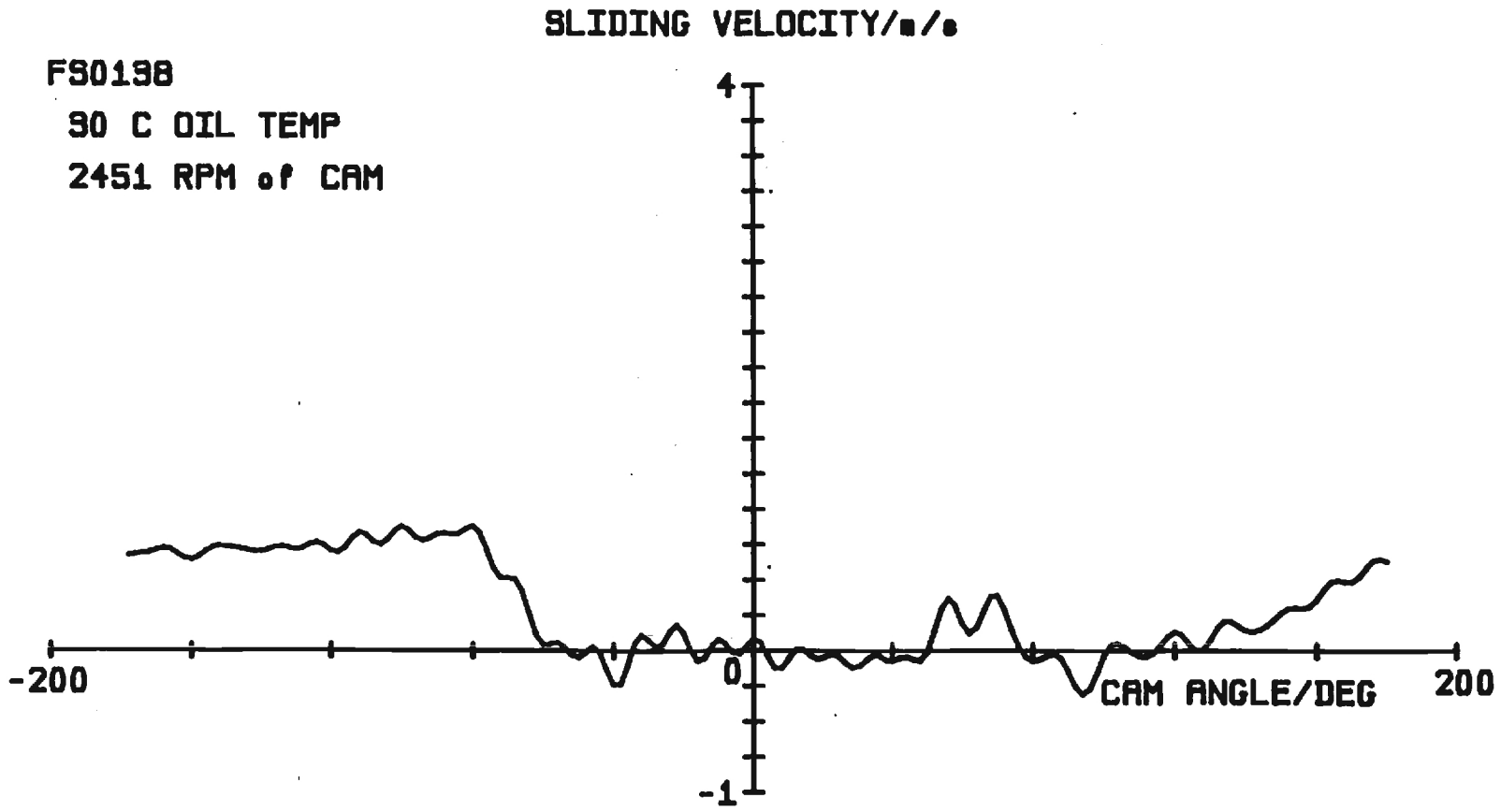
SLIDING VELOCITY/m/s
FS0198
90 C OIL TEMP
2451 RPM of CAM
4
-1
0
-200
200
CAM ANGLE/DEG

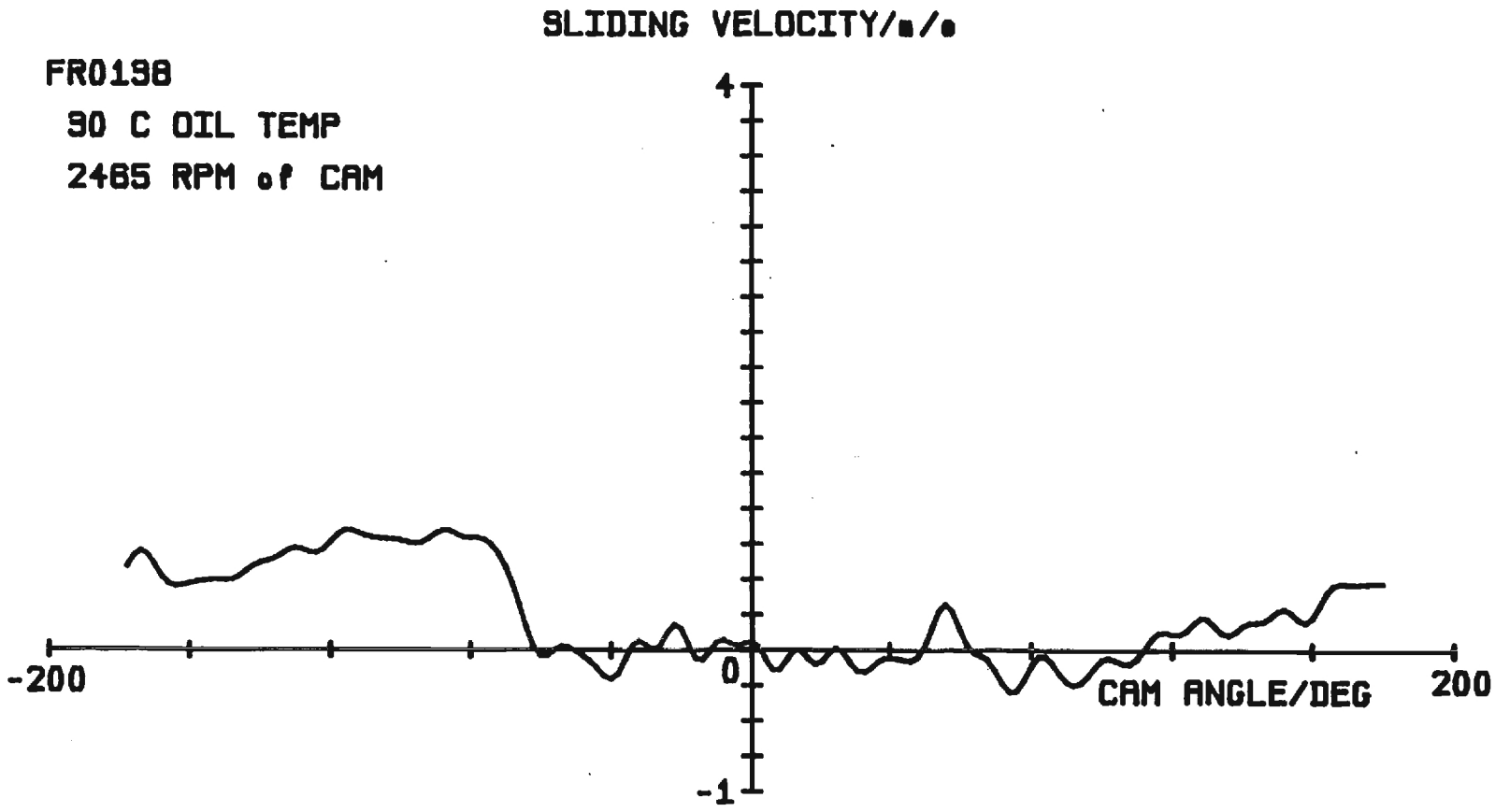
SLIDING VELOCITY/m/s
FR0198
90 C OIL TEMP
2465 RPM of CAM
4
-1
-200
0
200
CAM ANGLE/DEG

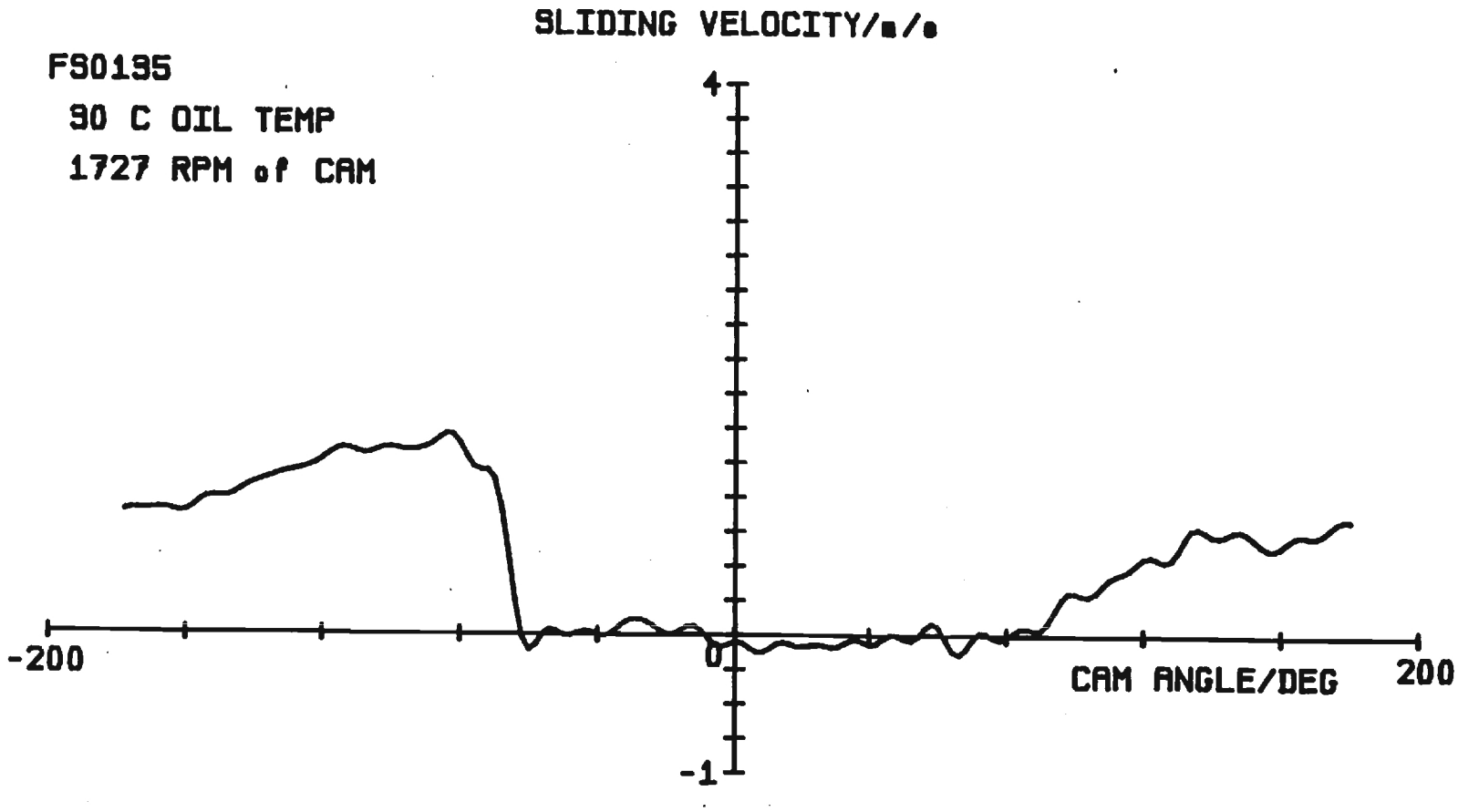
SLIDING VELOCITY/m/s
FS0135
90 C OIL TEMP
1727 RPM of CAM
4
-200
0
200
CAM ANGLE/DEG
-1

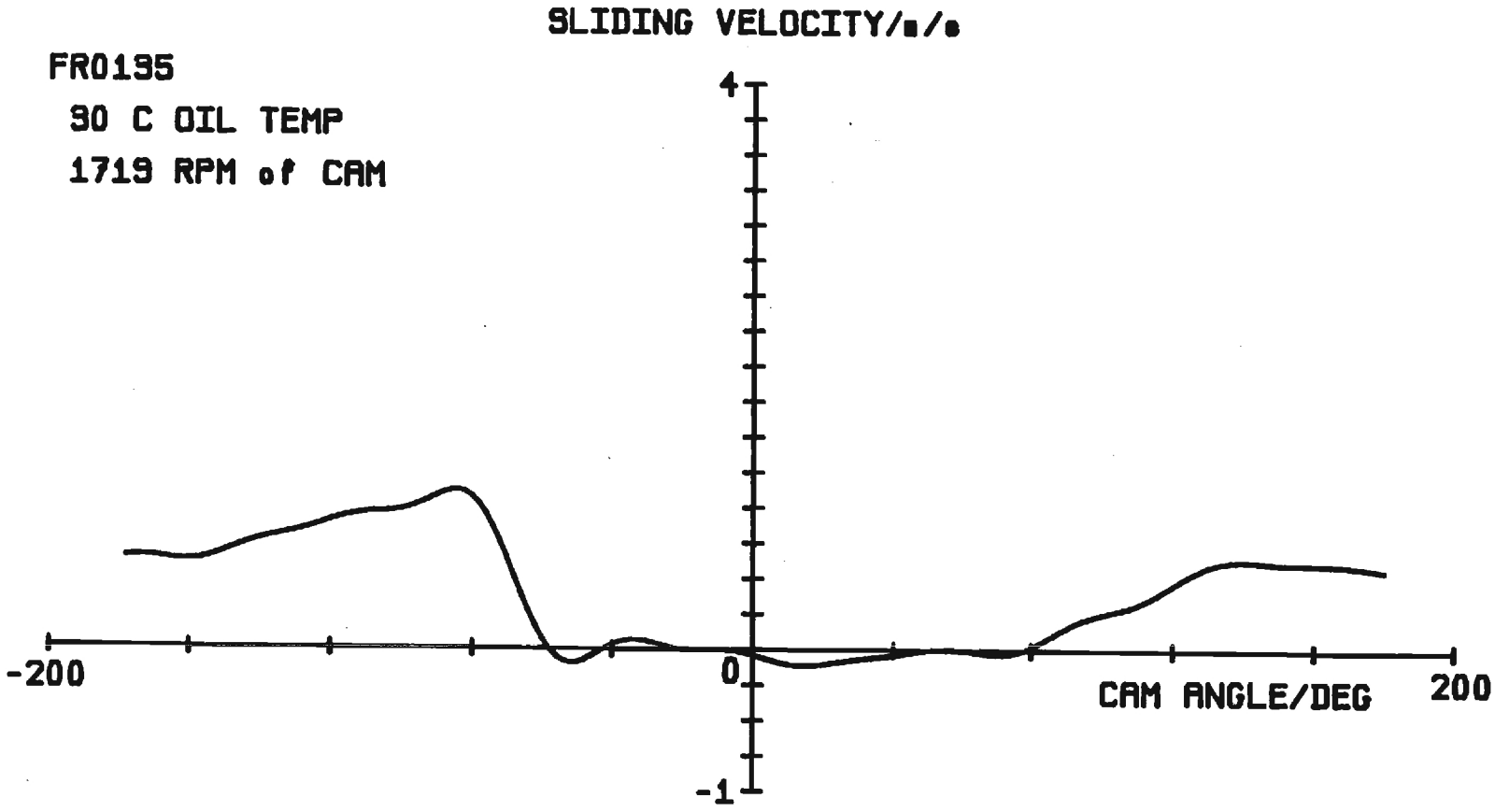
SLIDING VELOCITY/m/s
FR0135
90 C OIL TEMP
1719 RPM of CAM
4
-200
0
200
CAM ANGLE/DEG
-1

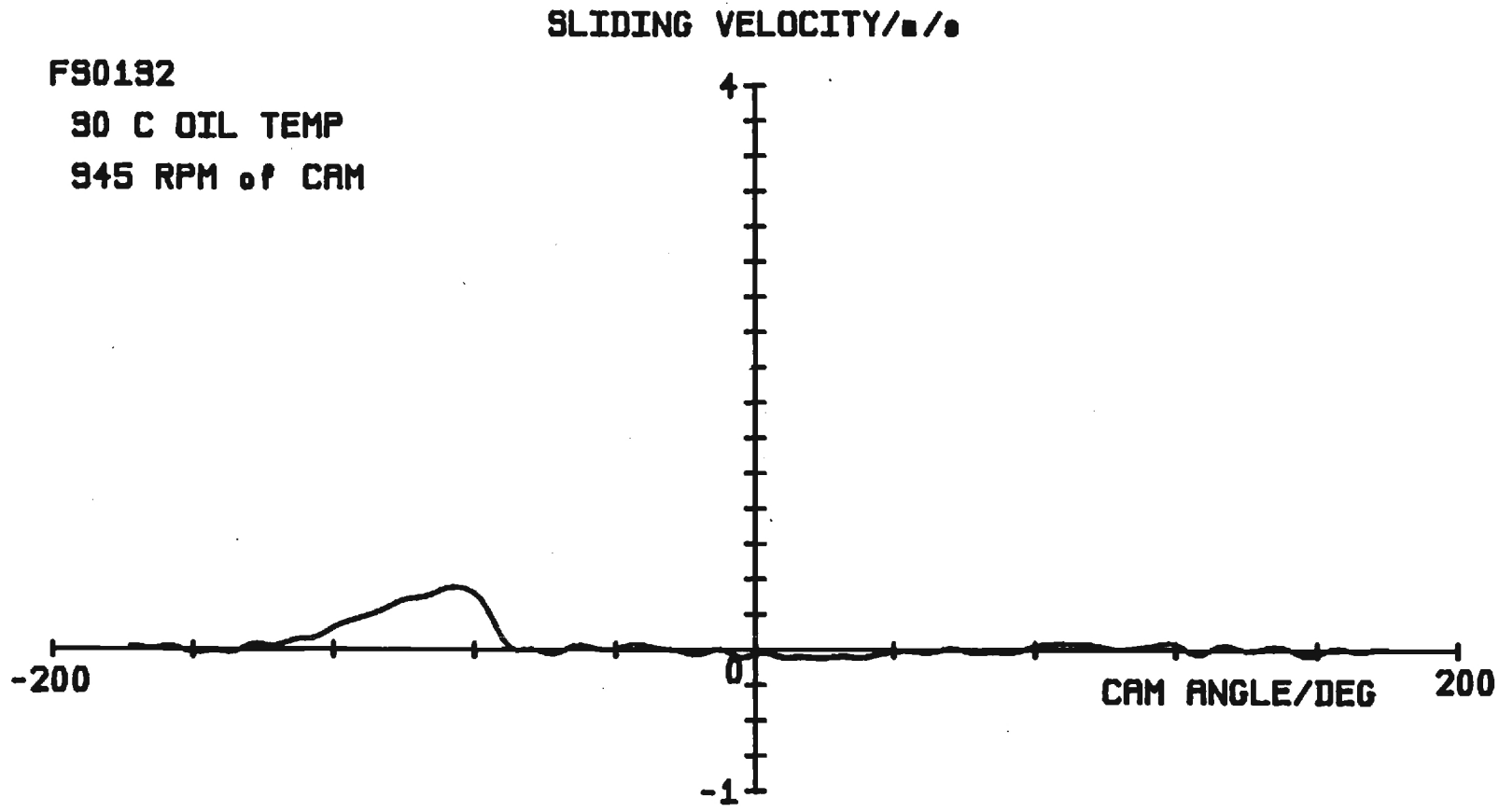
SLIDING VELOCITY/m/s
FS0132
90 C OIL TEMP
945 RPM of CAM
4
-200
0
CAM ANGLE/DEG
200
-1

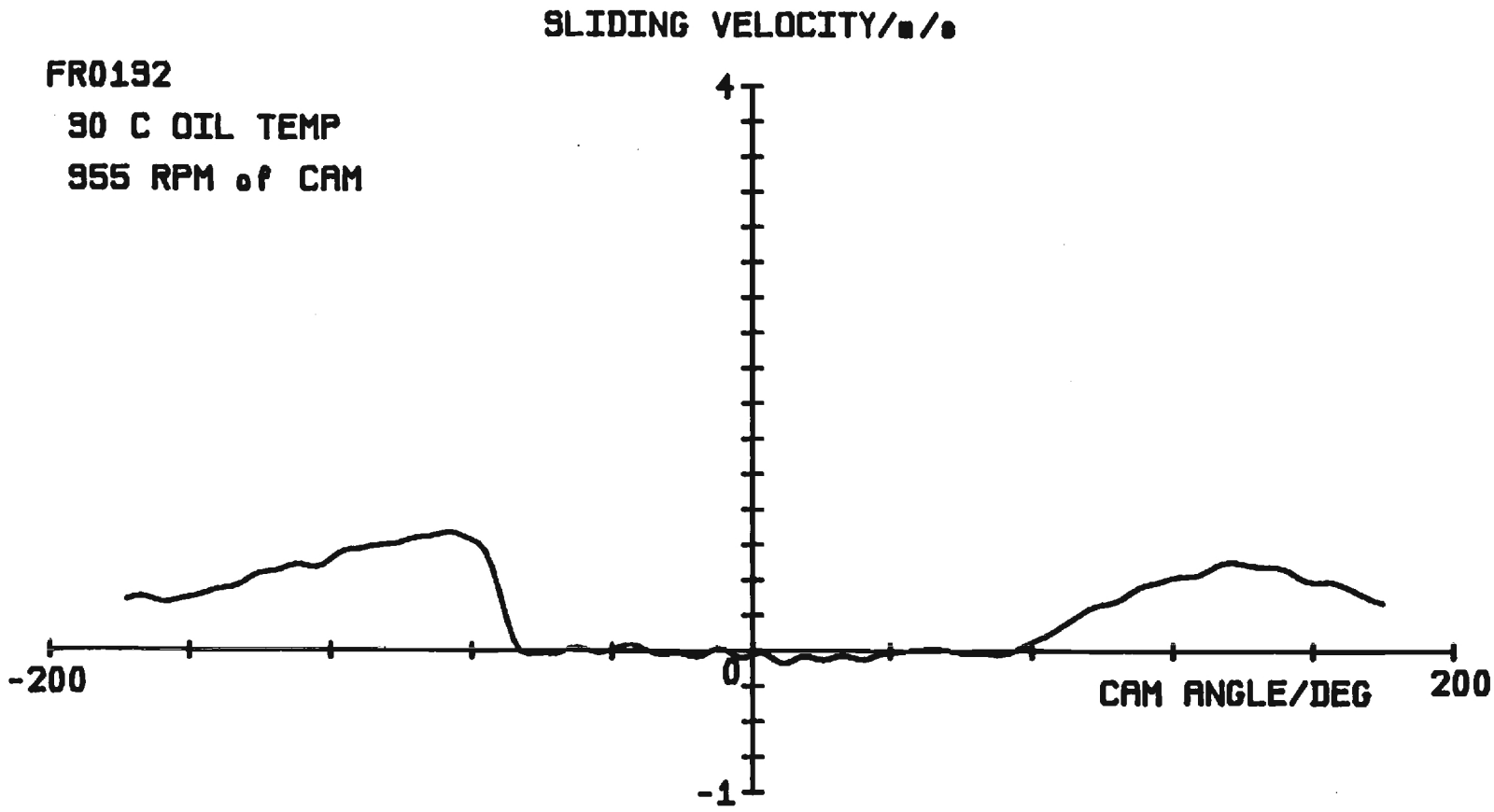
SLIDING VELOCITY/m/s
FR0192
90 C OIL TEMP
955 RPM of CAM
4
-200
0
200
CAM ANGLE/DEG
-1